DETERMINATION OF ALDICARB BY
GAS CHROMATOGRAPHY/MASS SPECTROMETRY
WITH SHORT CAPILLARY COLUMNS

By

MICHAEL LEE TREHY

A DISSERTATION PRESENTED TO THE GRADUATE SCHOOL
OF THE UNIVERSITY OF FLORIDA IN
PARTIAL FULFILLMENT OF THE REQUIREMENTS
FOR THE DEGREE OF DOCTOR OF PHILOSOPHY

UNIVERSITY OF FLORIDA

1984

ACKNOWLEDGEMENTS

I would like to express my gratitude to Dr. Richard A. Yost for his guidance with my research at the University of Florida. I would also like to acknowledge the assistance of Drs. Anna Brajter-Toth, Joseph J. Delfino, John G. Dorsey, Cemal Kemal, John J. McCreary, and J. Edward Singley.

I am grateful for the assistance of my fellow graduate students, especially Ted Britton, Mary Beth Budd, Sue Hummel, Jodie Johnson and Mike Lee for their support and assistance. In particular, I thank Jodie Johnson for his perseverance in the maintenance of the mass spectrometer and Mathew Monsees for his assistance in setting up the samples used in the degradation studies.

I would also like to express my sincere gratitude to another select group, whose support has made this work possible: Nan, Dan, Ben, Mary and Daniel.

TABLE OF CONTENTS

LIST OF TABLES

Table   Page

LIST OF FIGURES

Abstract of Dissertation Presented to the Graduate School
of the University of Florida in Partial Fulfillment of the
Requirements for the Degree of Doctor of Philosophy

DETERMINATION OF ALDICARB BY
GAS CHROMATOGRAPHY/MASS SPECTROMETRY
WITH SHORT CAPILLARY COLUMNS

By

Michael Lee Trehy

December, 1984

Chairman: Richard A. Yost
Major Department: Chemistry

   The rate of degradation of aldicarb in anaerobic

groundwater is determined in this study by a new, rapid gas

chromatographic/mass spectrometric method of analysis. The

ability to determine relatively non-volatile and thermally

labile compounds with short capillary columns operated with

the outlet at sub-atmospheric pressures is evaluated in

terms of the fundamental gas chromatographic (GC) equations.

This analysis indicates that short capillary columns offer

significant advantages in terms of speed of analysis,

particularly when operated with the column outlet at a

vacuum. The feasibility of analysis for the less-volatile

oxidation by-products of aldicarb, such as aldicarb sulfone,

by tandem mass spectrometry (MS/MS) of samples introduced by

the solids probe is shown. Aldicarb and aldicarb sulfone

are determined in orange juice spiked at a concentration of 36 ppb by extraction with methylene chloride, concentration of the extract by a factor of 50, and analysis of the extracts by MS/MS. The estimated limit of detection (LOD) is 0.4 ppm in the extract and 8 ppb in the orange juice.

The ability of tandem mass spectrometry to aid in the identification of ion structures is demonstrated. The 172^+ ion observed in the positive isobutane chemical ionization mass spectrum of aldicarb is found to be an isobutane adduct of aldicarb nitrile and is not due to the loss of water from aldicarb either on column or in the source. The effect of instrumental conditions on the sensitivity of MS/MS and for obtaining MS/MS library spectra is evaluated and discussed.

CHAPTER 1
INTRODUCTION

Background

Aldicarb is a highly toxic carbamate pesticide sold by
Union Carbide under the trademark Temik. More than 10% of
Florida orange groves are treated with Temik for control of
insects and nematodes (1). As a result of the detection of
trace quantities of aldicarb in agricultural wells in Long
Island, New York (2) in 1978 and in Florida (1) in 1982,
public concern has grown over the potential for widespread
contamination of Florida's water supplies with aldicarb.

In many areas of Florida, and in particular in South
Florida, the drinking water aquifers are close to the
surface and are not protected by intervening non-porous
layers. Thus, accidental spillage of toxic compounds that
degrade slowly in the environment pose significant health
hazards. In response to public concern over contamination
of Florida's drinking water supply by industrial
contaminants, the Florida Department of Environmental
Regulation (DER) sponsored a research project at the
University of Florida to study the "The Fate of Industrial
Organic Compounds in Drinking Water Aquifers." One of the
objectives of this study was to evaluate the rate of

1

degradation of aldicarb in groundwater and to determine its
degradation by-products. The findings on the rate of
degradation of aldicarb in groundwater will be summarized in
Chapter 2. The methods developed to carry out the analysis
of environmental samples for aldicarb and its degradation
by-products will be discussed in Chapter 4.

Degradation of Aldicarb

Degradation of aldicarb in soil (3-5), potato plants
(6), sugar beets (7), rats (8), cotton (9, 10) and insects
(9), and by soil fungi (11) has been studied. These studies
indicate that aldicarb (I), 2-methyl-2-(methylthio)propanal
O-[(methylamino)carbonyl]oxime, is oxidized rapidly with the
aid of microorganisms in soil or metabolized in plants and
animals to the toxic residue, aldicarb sulfoxide (II),
2-methyl-2-(methylsulfinyl)propanal O-[(methylamino)
carbonyl]oxime. Aldicarb sulfoxide then slowly hydrolyzes
to form the less toxic residue, aldicarb sulfoxide oxime
(III), 2-methyl-2-(methylsulfinyl)propanal oxime (below).

$$CH_3S-\underset{\underset{CH_3}{|}}{\overset{\overset{CH_3}{|}}{C}}CH=NO\overset{O}{\overset{||}{C}}NHCH_3 \qquad CH_3\overset{O}{\overset{||}{S}}-\underset{\underset{CH_3}{|}}{\overset{\overset{CH_3}{|}}{C}}CH=NO\overset{O}{\overset{||}{C}}NHCH_3 \qquad CH_3\overset{O}{\overset{||}{S}}-\underset{\underset{CH_3}{|}}{\overset{\overset{CH_3}{|}}{C}}CH=NOH$$
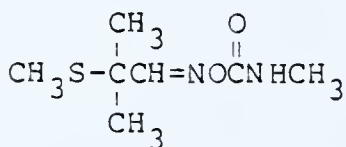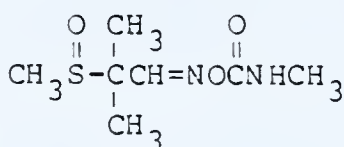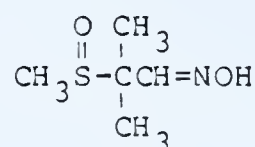
(I)   (II)   (III)

Since the rate of degradation of aldicarb is known to be
strongly influenced by microbiological conditions and pH,
the degradation of aldicarb is expected to be influenced by
the type of water. In order to model these widely varying
conditions, water samples were collected from two sources

and modified by the addition of either microorganisms or
alkaline reagents to represent different types of waters
likely to be encountered. In this study, aldicarb was
observed to degrade by hydrolysis in alkaline waters to form
aldicarb oxime (IV), 2-methyl-2-(methylthio)propanal oxime,
or, with the aid of anaerobic microorganisms in
microorganism-enriched water, to aldicarb nitrile (V),
2-methyl-2-(methylthio)propanenitrile, as shown below.

$$CH_3S-\underset{\underset{CH_3}{|}}{\overset{\overset{CH_3}{|}}{C}}-CH=NOH \qquad\qquad CH_3S-\underset{\underset{CH_3}{|}}{\overset{\overset{CH_3}{|}}{C}}-C\equiv N$$
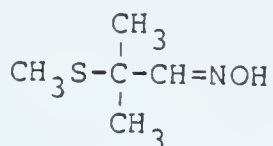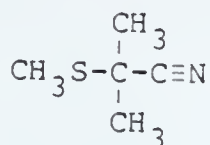
$$(IV) \qquad\qquad\qquad\qquad (V)$$

Selection of a Method of Analysis for Aldicarb

Since one of the concerns of the DER was the
determination of the major degradation by-products of
aldicarb in groundwater, it was desirable either to use an
existing method or to develop a new method of analysis for
aldicarb which was highly selective. Methods for the
analysis of aldicarb which have been reported include thin
layer chromatography (TLC) (8, 9); liquid chromatography
(LC) with various detectors [mass spectrometer (12),
ultraviolet detector (13), and post-column derivitization
and fluorometric detector (14, 15)]; and gas chromatography
(GC) with various detectors [Hall detector (5), mass
spectrometer (GC/MS) (16), flame ionization detector (2),
and esterification and detection with an electron capture
detector (17)]. Only the LC and TLC methods avoid

degradation of aldicarb. Aldicarb is thermally labile and rapidly degrades in the injection port or on the column in all the GC methods reported. The thermal degradation product of aldicarb has been identified as aldicarb nitrile by matching the retention time with that of a synthesized standard on a carbowax 20M packed column (8). Mass spectra obtained in this study for the thermal degradation of aldicarb observed on a 30 m carbowax 20M capillary column are consistent with this identification.

Liquid chromatography/mass spectrometry was not available nor did thin layer chromatography appear to be sufficiently selective and sensitive to fulfill the needs of this study. An alternative method of analysis would be one which employs short GC columns to facilitate faster analyses (18-25) and to avoid thermal degradation (26). Thermally labile Carbaryl residues in foods have been determined with a 1 m SE-30 packed column with some success (26). In this study it is found that rapid and sensitive analysis for aldicarb is made possible by the use of a short capillary column with mass spectrometric detection (27). This approach minimizes degradation of aldicarb and thus permits direct analysis for aldicarb.

A major drawback of previous GC methods for the analysis of aldicarb is that aldicarb not only degrades during the GC analysis to aldicarb nitrile, but may also degrade chemically in the environment to aldicarb nitrile. Thus, if aldicarb nitrile is not removed prior to GC

analysis by a florisil separation (28), this environmental degradation product will give a positive interference for aldicarb. The formation of aldicarb nitrile from aldicarb in environmental samples had been suspected (7), although only the oxidized forms of the nitrile had been detected in aerobic systems. It had also been found that from 3 to 12% of the aldicarb applied degrades to either 2-methyl-2-(methylsulphinyl)propanenitrile or 2-mesyl-2-methylpropanenitrile in potatoes (10%) (6), soils (5%) (3), sugar beets (5%) (7), and in aqueous cultures of soil fungi (3 to 11% depending on type of soil fungus) (11).

Gas Chromatography/Mass Spectrometry with Short Capillary Columns

Preliminary experiments in this laboratory with short capillary columns and mass spectrometric detection demonstrated efficient chromatographic separation. When capillary columns are directly coupled to a mass spectrometer, one might expect significant loss in chromatographic separation due to the large ratio of inlet to outlet pressures and the high gas velocities near the outlet. However, evaluation of the fundamental gas chromatographic equations reveals that the column's plate height is predicted to increase only to a small extent when operated at the optimum carrier gas velocity. The time necessary to perform a given separation, on the other hand, decreases as the column outlet pressure decreases. The increase in the speed of analysis is greater for short

columns than for long columns. Thus, the vacuum associated with the mass spectrometric detector is quite beneficial for rapid analysis, and in certain cases, permits analysis for compounds too thermally labile to pass through columns operated with the outlet at atmospheric pressure. The effect of greatly reduced outlet pressures in capillary gas chromatography will be discussed in Chapter 3.

Mass spectrometry provides both the selectivity and the sensitivity necessary for trace analysis. Frequently, however, separation of the analyte from its matrix is essential for quantization. The analysis of samples by the technique of GC/MS with selected ion monitoring (SIM) is particularly susceptible to positive interference, due to the possible existence of ions with the same nominal mass but originating from other components in the mixture which coelute with the analyte. Higher resolution chromatography is then necessary to provide additional separation of the analyte from the interfering components. Alternatively, tandem mass spectrometry can permit analysis for a single compound in a mixture, even though other compounds co-elute which ionize to form ions of the same mass. If the parent ions fragment to give different daughter ions, however, then analysis for the selected daughter ion may be performed without mass spectral interference. GC/MS/MS offers the advantage of more rapid analysis, because the added resolution found in tandem mass spectrometry does not

increase the analysis time, whereas enhanced chromatographic resolution frequently does.

Another source of potential interference is matrix effects. Even when the mass resolution of the analysis is adequate to prevent mass spectral interference, if the ionization process is altered by the presence of co-eluting components, then the signal is dependent on both the analyte and the matrix and a nonlinear response curve results. Both selected reaction monitoring (SRM) in tandem mass spectrometry and SIM are susceptible to this type of interference. In this case the matrix can greatly diminish sensitivity for the analyte, so that its concentration is either underestimated or not detected at all. In order to avoid these difficulties, a chromatographic separation step is generally employed. The time necessary to perform the chromatography is frequently the greatest restriction to rapid analysis.

An evaluation of gas chromatographic parameters with respect to analysis time and sensitivity is presented in Chapter 3. The application of short capillary columns for rapid analysis of trace components is evaluated in light of the developments in tandem mass spectrometric techniques.

Effect of Instrumental Parameters on Collision-Induced Dissociation Spectra

Tandem mass spectrometry (MS/MS) has become an accepted method for structure elucidation of ions. Examples of the use of MS/MS techniques for structure investigations include

analysis of drugs (29-32), peptides (33-36), isobaric ions formed in the source (37), and pesticides (27). Identification of ions formed by soft ionization techniques is aided by MS/MS (38). In the case of the structural isomers of octane, whose electron impact (EI) mass spectra are similar, the CID spectra have been found to be substantially different (39). The utility of MS/MS spectra in structural identification has led to an interest in developing CID reference library spectra. The objective of utilizing the CID spectra in a manner similar to that currently used for EI spectra in library matching algorithms requires that procedures be developed for standardization of collision-induced dissociation (CID) spectra. Standard procedures for the development of CID library spectra have been considered (40-42). In this report, the effects of collision pressure and collision energy are presented for the CID of aldicarb, aldicarb nitrile, and cyclohexene.

Investigations of CID processes at high collision energies (5 to 25 keV) in double-focussing sector instruments have shown that the CID spectra are generally independent of the ion's internal energy, with the exception of products formed through the process of lowest activation energy (43). CID spectra obtained from tandem quadrupole mass spectrometers, however, are strongly dependent on the target-gas density (44, 45) and collision energy (46, 47). At target-gas densities commonly employed for CID studies of ions in tandem quadrupole mass spectrometers, multiple

collisions are likely. Under multiple collision conditions, fragment ions of fragment ions formed from the parent ion in the collision cell can be observed (40). The effect of the internal energy of the parent ion on daughter ion ratios at pressures at which either single or multiple collisions dominate will also be discussed.

The thermal lability of aldicarb has resulted in some confusion over the identity of compounds which reach the detector and produce gas chromatographic peaks. In particular, it has been proposed that the 172^+ ion observed in the isobutane chemical ionization mass spectrum of aldicarb is due to a dehydration reaction producing the $(M-18)^+$ ion (16). The 172^+ ion is demonstrated by tandem mass spectrometry in this study, however, to be an isobutane adduct ion of aldicarb nitrile. The misidentification of this ion is of concern, since the supposition that it is formed as a dehydration product of aldicarb would be indicative of the presence of a toxic residue of aldicarb rather than the relatively non-toxic aldicarb nitrile. The application of CID spectra for the identification of ions requires an understanding of the effect of instrumental parameters on the spectra. The influence of these parameters on the CID spectra are evaluated and discussed in Chapter 5.

Significance of Results

The determination that the pesticide aldicarb degrades anaerobically to aldicarb nitrile is of significance to

environmental analysts, since this relatively non-toxic residue can result in a positive interference when samples are analyzed for aldicarb by previous GC methods. The investigations of the utility of short capillary columns indicate that analysis for thermally labile compounds such as aldicarb can be greatly aided by this approach. Further, tandem mass spectrometry is shown to be complementary to the use of short columns by providing an additional resolution element in the analysis which compensates for the chromatographic selectivity lost upon employing short capillary columns.

CHAPTER 2
SUMMARY OF DEGRADATION EXPERIMENTS FOR
ALDICARB IN GROUNDWATER

The rate of degradation of aldicarb (I) in groundwater
is strongly dependent on pH and on the microorganism
content. In anaerobic or aerobic water which is at neutral
pH and has a low microorganism content, aldicarb was found
to be quite stable. In three months, only approximately 10%
of the original aldicarb had degraded at pH 6.8. However,
aldicarb hydrolyzes to aldicarb oxime (IV) under anaerobic
conditions at pH 8.2 with a half-life of 43 days, as shown
in Figure 1. When anaerobic well water is enriched with
microorganisms or when ground limestone which has not been
sterilized is added, aldicarb degrades rapidly. In these
experiments, approximately 85% of the original aldicarb
degraded to aldicarb nitrile (V) in two weeks in those
samples which were enriched with microorganisms, or to which
limestone was added. The pathways determined for the
degradation of aldicarb in anaerobic groundwater are shown
below.

                        aldicarb
                          (I)
        hydrolysis   ↙   ↘   microorganisms/heat

        aldicarb oxime   aldicarb nitrile
            (IV)   (V)

11
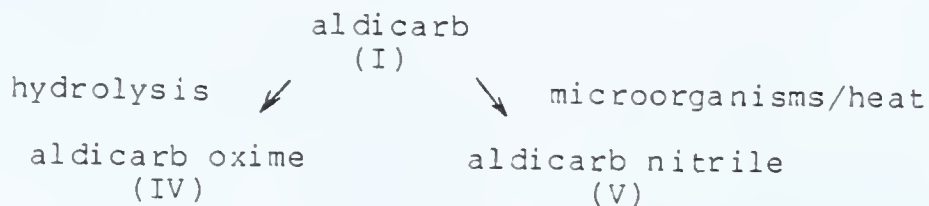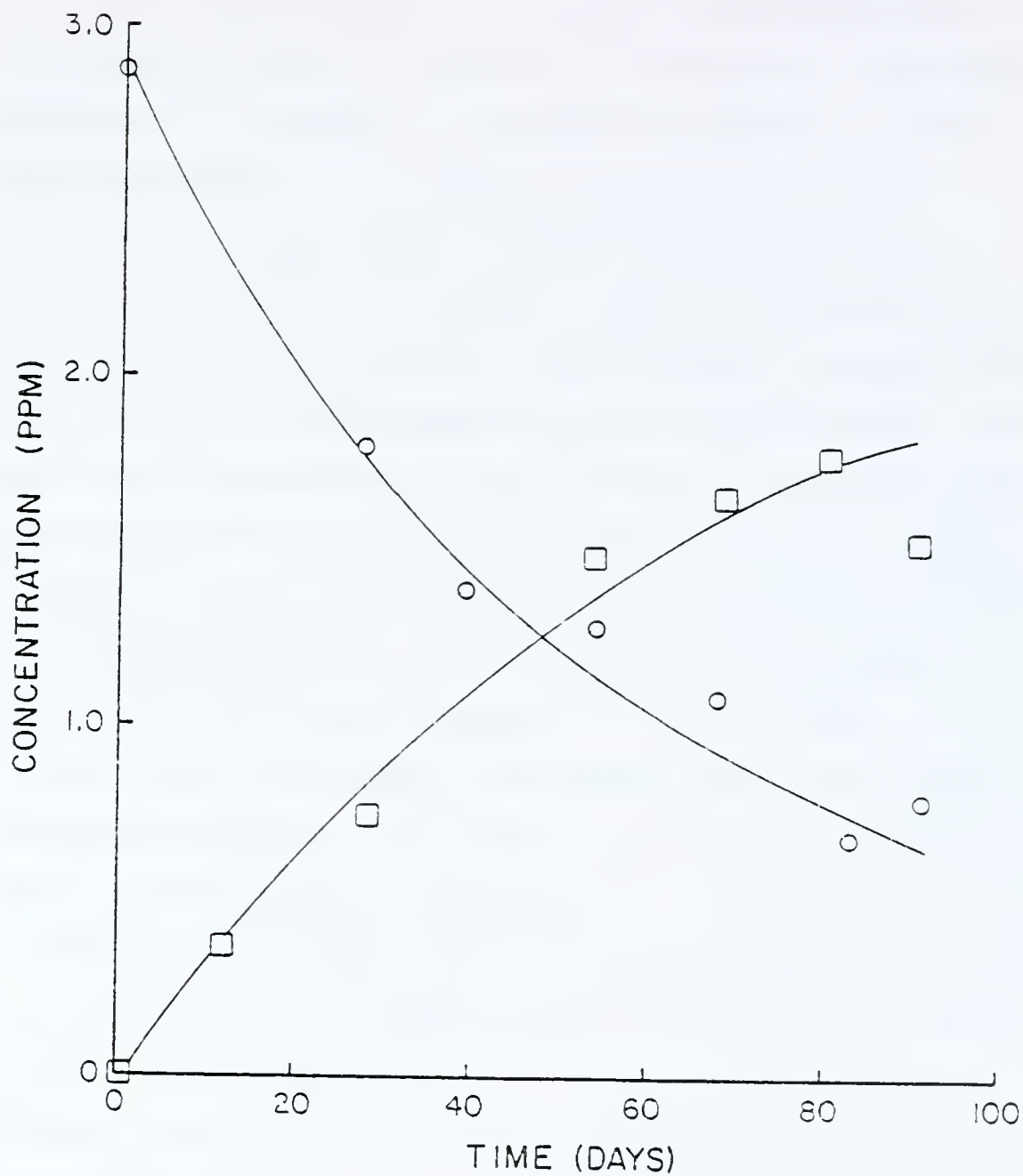
Figure 1. Hydrolysis of aldicarb, o, to aldicarb oxime, □, in sterile anaerobic groundwater at pH 8.3.

Experimental

Seven experiments were set up for the determination of the degradation rate for aldicarb. Two were for the aerobic degradation of aldicarb in groundwater at pH 5.5. These samples were set up by aseptically spiking aliquots of groundwater collected from a shallow aerobic well with aldicarb and storing the sample at ambient temperature in Teflon sealed septum bottles. Approximately 17 samples were prepared and two samples were analyzed every two weeks. The samples were extracted for thirty minutes in a rotary shaker after the addition of 10 mL of methylene chloride to the 100 mL sample. A portion of the methylene chloride extract was passed through anhydrous sodium sulfate and the dried extract was then stored in septum bottles for later analysis. Due to the need to maintain aerobic conditions, the water was used in its natural state without modification except for the addition of aldicarb.

The source of water for the anaerobic samples were wells at the Murphree water treatment plant. Water samples were collected aseptically at a header pipe prior to any treatment at the plant and with a minimum of agitation to avoid introduction of air. At the environmental engineering laboratory aliquots of the water were either sterilized for controls, spiked with microorganisms from an anaerobic digester, spiked with ground limestone, or used as obtained from the water treatment plant. All the sample bottles were spiked with resazurin in order to confirm the absence

of oxygen. All anaerobic samples were prepared inside an "atmos" bag, with a constant stream of nitrogen passing through the bag to avoid the the introduction of oxygen. Micronutrients were added to those samples which were spiked with microorganisms in accordance with a published procedure, in order to assure a good environment for microbiological growth (48). The samples were individually spiked with aldicarb and sealed while in the "atmos" bag in septum bottles with the rubber septum surface exposed to the water. The resazurin indicator became colorless and thus indicated the absence of oxygen. Samples were stored at room temperature. At two-week intervals, a set of samples was extracted following the same procedure used for the extraction of the aerobic samples.

Results and Discussion

Aerobic Degradation

The rate of degradation of aldicarb in aerobic groundwater water at pH 7 was quite slow, as shown in Table 1. The decrease in the concentration of aldicarb from the beginning of the experiment to the end was less than the experimental error calculated from the standard deviation of the slope and intercept of the calibration curve. The stability of aldicarb in water at neutral pH made it impossible to accurately determine the degradation rate during the 3 months these samples were incubated. The experimental data indicate that the rapid conversion of aldicarb to aldicarb sulfoxide which occurs in plants and

Table 1. Degradation of aldicarb in aerobic sterile groundwater at pH 5.5, SG, and in aerobic groundwater at pH 6, GW.

Sample	Time in days	Concentration mg/L in water*
Initial #1	0	2.0 ± 0.5
Initial #2	0	2.2 ± 0.5
Initial #3	0	2.0 ± 0.5
SG	13	2.0 ± 0.5
GW	13	2.2 ± 0.5
SG	29	2.2 ± 0.5
GW	29	2.0 ± 0.5
SG	43	1.9 ± 0.4
GW	43	1.7 ± 0.4
SG	59	1.5 ± 0.4
GW	59	2.0 ± 0.4

* Each concentration was measured only once. Standard deviation estimated from the standard deviation of the slope and intercept of the calibration curve.

animals (3-10) occurs much more slowly in natural waters removed from the ground.

Anaerobic Degradation

The rate of degradation of aldicarb in anaerobic groundwater at pH 7 was also quite slow, as shown in Table 2. The determination of small changes in concentrations in samples over an extended period was made more difficult by both possible variations in the precision of preparing fresh standards, and the instability of stock standard solutions. In order to improve the precision in the analysis, all the samples were analyzed a second time during one evening. The values shown in the tables are the results of the second analysis.

The rate of hydrolysis of aldicarb in sterile anaerobic groundwater at pH 8.2 and 11 was determined. The data are shown in Tables 3 and 4. The presence of aldicarb oxime was detected in this sample by GC/MS with both a 30 m Carbowax 20 Mcapillary column and a 3 m DB5 capillary column. The formation of aldicarb oxime from aldicarb at pH 8.2 was found to account for all the aldicarb that was lost by degradation. Aldicarb oxime formed by hydrolysis of aldicarb at pH 11 was found to be resistant to further hydrolysis. Since some surface waters and ground waters are slightly alkaline, degradation of aldicarb in these waters could occur by hydrolysis.

Table 2. Degradation of aldicarb in
anaerobic groundwater at pH 7.

Time in days	mg/L aldicarb*
initial	2.9 $\pm$ 0.7
12	2.8 $\pm$ 0.6
28	2.8 $\pm$ 0.6
39	2.9 $\pm$ 0.7
54	2.5 $\pm$ 0.6
68	2.5 $\pm$ 0.6
91	2.5 $\pm$ 0.6

* Each concentration measured only once.
Standard deviation estimated from
the standard deviation of the slope and
intercept of the calibration curve.

Table 3. Concentrations of aldicarb remaining and aldicarb oxime formed at pH 8.2 due to alkaline hydrolysis of aldicarb in sterile groundwater.

Time in days	mg/L aldicarb*	mg/L aldicarb oxime*
initial	2.9 ± 0.7	< 0.1
12	2.7 ± 0.6	0.25 ± 0.02
28	1.8 ± 0.5	0.63 ± 0.03
39	1.4 ± 0.5	not determined
54	1.3 ± 0.4	1.25 ± 0.05
68	1.1 ± 0.4	1.39 ± 0.05
83	0.7 ± 0.4	1.44 ± 0.05
91	0.8 ± 0.4	1.28 ± 0.05

* Each concentration measured only once. Standard deviation estimated from the standard deviation of the slope and intercept of the calibration curve.

Table 4. Concentrations of aldicarb remaining and aldicarb oxime formed at pH 11 due to alkaline hydrolysis of aldicarb in sterile groundwater.

Time in days	Concentration mg/L aldicarb*	Concentration mg/L aldicarb oxime*
1	< 0.2 ± 0.3	0.44 ± 0.02
5	< 0.2 ± 0.3	0.45 ± 0.02
33	< 0.2 ± 0.3	0.50 ± 0.02

* Each concentration measured only once. Standard deviation estimated from the standard deviation of the slope and intercept of the calibration curve.

In order to better evaluate the rate of degradation of aldicarb in the drinking water aquifers, aliquots of anaerobic groundwater were spiked with 10 g of 50/100 mesh limestone which had not been sterilized. The samples were then stirred twice a week for the following four weeks. After 13 days the concentration of aldicarb in the sample which had been spiked with limestone decreased by approximately 80%, while the groundwater control showed little change, as shown in Table 5. Aldicarb nitrile was determined to be present at a concentration of 0.7 ppm in the 13 day-old limestone-spiked sample, while it was absent in the earlier samples and in the groundwater controls.

The influence of the addition of microorganisms on the rate of degradation of aldicarb in groundwater was determined. When samples of anaerobic groundwater were spiked with microorganisms from either an anaerobic digester or a culture of groundwater microorganisms, aldicarb was found to degrade rapidly, as shown in Table 6. Aldicarb nitrile was found in these samples, but was not quantitated.

Summary

The rate of degradation determined in these experiments was for water spiked with aldicarb in the absence of soil or other materials. Since the rate of degradation was found to be strongly dependent on the microorganism content of the water, the rate of degradation of aldicarb in moist soil is anticipated to be greater than that observed here. However, if due to either application rates which exceed recommended

Table 5. Degradation of aldicarb in groundwater in the presence of pulverized limestone, GL, and in the absence of added limestone, GW.

Sample	Time in days	Concentration mg/L in water*	pH
Initial #1	0	1.3 ± 0.4	n.d.
Initial #2	0	1.3 ± 0.4	n.d.
GW	1	1.4 ± 0.4	7.4
GL	1	1.5 ± 0.4	7.35
GW	13	1.9 ± 0.5	7.45
GL**	13	0.2 ± 0.3	7.65

* Each concentration measured only once. Standard deviation estimated from the standard deviation of the slope and intercept of the calibration curve.
** Contained 0.7 mg/L of aldicarb nitrile.
n.d. = not determined

Table 6. Degradation of aldicarb in groundwater
that was enriched with microorganisms from an
anaerobic digester, DG, or with groundwater
microorgansims, GM.

Sample	Time in days	mg/L aldicarb*
initial	0	2.9 ± 0.7
GM	12	0.5 ± 0.4
DG	12	<0.4 ± 0.4
GM	28	<0.4 ± 0.4
DG	28	<0.4 ± 0.4

* Each concentration measured only once.
  Standard deviation estimated from the
  standard deviation of the slope and intercept
  of the calibration curve.

amounts or spillage aldicarb were to penetrate the upper

soil layers where microbial activity is high, then

contamination of the groundwater could be significant and

could persist for years.

In response to reports of problems associated with the

use of aldicarb, Union Carbide published a flier in which

the conditions are described under which aldicarb is likely

to persist in the environment (49). This informal report

states that aldicarb is likely to persist where

> a highly specific combination of environmental
> conditions including acid pH, sandy soil, cold
> temperatures, a general lack of soil microbial
> activity, a shallow water table and heavy rainfall
> occur at or shortly after the application of Temik.
> (p. 6)

The degradation experiments which are summarized in Table 7

indicate that it is not necessary for all of the above

conditions to exist simultaneously for aldicarb to

contaminate groundwater. The environmental conditions

should only be used as a guide with respect to the

advisability for applying aldicarb in a particular region.

Table 7. Aldicarb groundwater degradation experiment data summary.

Sample	Time in days	% aldicarb remaining
anaerobic		
limestone water	13	15
micronutrient enriched	12	17
groundwater pH 6.8	91	87
sterile groundwater pH 8.2	91	28
sterile groundwater pH 11	1	<10
aerobic		
sterile groundwater pH 6	59	75
groundwater pH 6	59	95

CHAPTER 3
GC/MS ANALYSIS WITH SHORT CAPILLARY COLUMNS

Short capillary columns can be used for rapid analysis of samples and for the determination of thermally labile compounds. In this chapter the effect of sub-atmospheric outlet pressures on the time for analysis and chromatographic resolution with GC/MS or GC/MS/MS is discussed. The selectivity available with MS and particularly with MS/MS methods of analysis is shown to provide sufficient selectivity to determine analytes in complex mixtures in spite of the column's short length. The theoretical equations for gas chromatography with respect to minimum time for analysis were evaluated by J. Calvin Giddings in 1962 (50). His derivations indicated that the optimum performance of gas chromatography with respect to minimum analysis time would be obtained when the outlet is connected to a vacuum. Giddings observed that the limiting factor in the time required for analysis was the term for mass transfer in the liquid phase.

Sources of Band Broadening

Due to improvements in the preparation of capillary columns, the liquid phase thickness of bonded phase columns is estimated to be approximately 0.0001 mm. Columns with an

25

inner diameter of 0.25 mm are standard. These improvements
significantly enhance the performance of capillary columns.
Band broadening with capillary columns and a mass
spectrometric detector is due to both column and
extra-column effects.

Column Effects

The dependence of the height of a theoretical plate
(HETP) on the average gas velocity, v, in capillary columns
is given by the Golay equation shown below.

$$HETP = B/v + Cv \qquad\qquad (3-1)$$

where B is the coefficient determined by the rate of
longitudinal diffusion, and C is the coefficient determined
by the rate of mass transfer (51). For illustration, Figure
2 shows the contribution of longitudinal diffusion, B/v, and
mass transfer, Cv, to the overall plate height, HETP. The
increase in the plate height that occurs at carrier gas
velocities beyond the optimum velocity prevents rapid
analysis from achieving maximum resolution.

Longitudinal diffusion. The contribution of
longitudinal diffusion to band broadening (52) is inversely
proportional to the average gas velocity. The magnitude of
the coefficient B in capillary columns is determined by the
diffusion coefficient, Dg, in the gas phase.

$$B = 2Dg \qquad\qquad (3-2)$$

The dependence of Dg on gas pressure can be derived from the
kinetic theory of gases (53), where η is the viscosity of

$$H = B/u + Cu$$
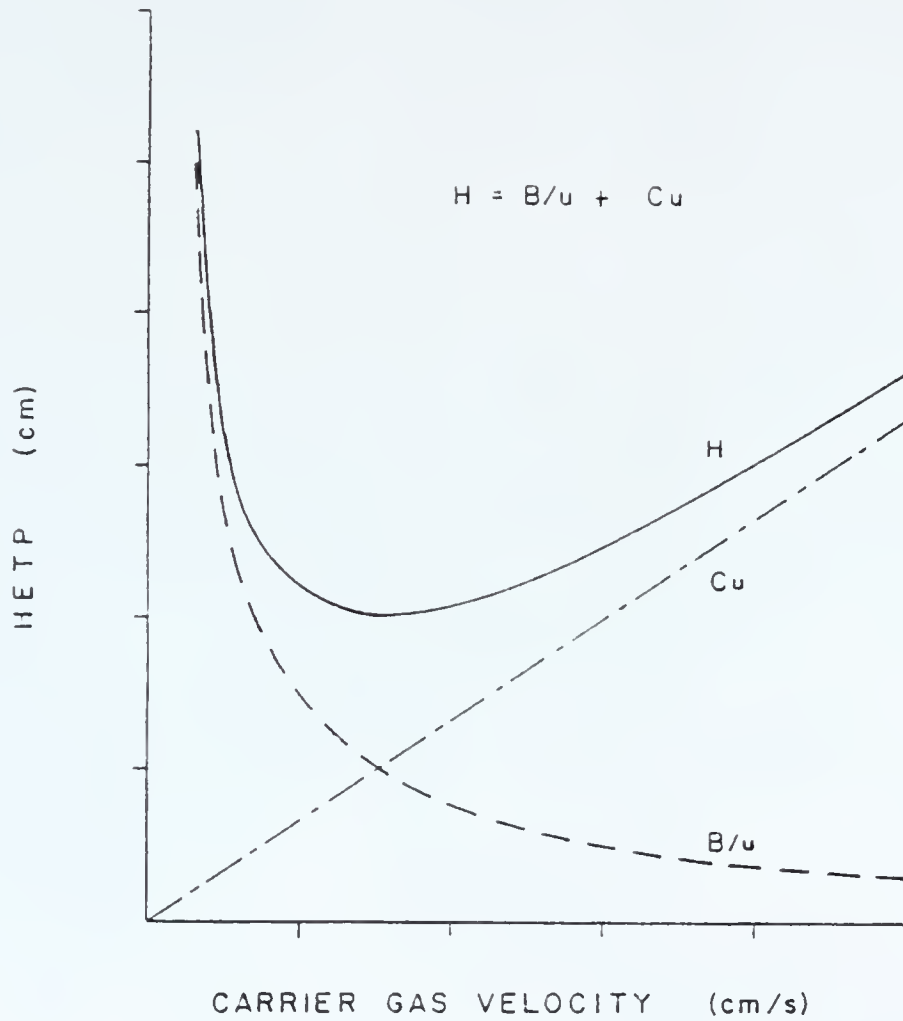
Figure 2. Plot of the height equivalent to a theoretical plate, HETP, vs average gas velocity for a capillary column according to the Golay equation.

the gas and ρ is the density of the gas, as shown below.

$$Dg = 6\eta/5\rho \qquad (3-3)$$

The density of the carrier gas is proportional to both its molecular weight and the pressure applied. Thus, a reduction in the average column pressure, or the selection of a carrier gas with a lower molecular weight, results in an increase in the gas diffusion coefficient, with a consequent increase in the B term. The increase in the B term shifts the optimum carrier velocity to a higher value, which shortens analysis time. This advantage of using light carrier gases such as helium or hydrogen has long been known. The advantage of operating at reduced column pressures (vacuum gas chromatography), however, has not yet been used to its full advantage due to the lack of gas chromatographs designed for this application.

Mass transfer. The effect of mass transfer on plate height is given by the C term in the Golay equation. The mass transfer term C has two components C_L, mass transfer in the liquid phase and C_G, mass transfer in the gas phase.

Mass transfer in the liquid phase generally dominates in packed columns and is given by the equation shown below (51):

$$C_L = \frac{(k)^3 r^2}{6 (1 + k)^2 K^2 D_L} \qquad (3-4)$$

where k is the capacity factor, K is the distribution coefficient, r is the column radius, and D_L is the

diffusion coefficient in the liquid phase. The effect of the thickness of the liquid phase on the mass transfer term has been shown to be given by equation 3-5, as shown below (54):

$$C_L = \frac{2 \ k \ d^2}{3 \ (1 + k)^2 \ D_L} \qquad (3-5)$$

where d is the thickness of the liquid phase. For packed columns with a reasonably thick film of approximately 0.005 mm, the mass transfer term in the Golay equation is dominated by C_L.

Capillary columns in current use, however have film thicknesses of approximately 0.0001 mm. With this film thickness, the mass transfer term due to the liquid phase is reduced by a factor of over 1000, and thus, mass transfer in the gas phase dominates. The coefficient for mass transfer in the gas phase is given by equation 3-6, shown below (51).

$$C_G = \frac{(1 + 6k + 11k^2) \ r^2}{24 \ (1 + k)^2 \ D_G} \qquad (3-6)$$

Thus, the use of lower gas densities (carrier gases either with lower molecular weights or at lower pressures) results in a decrease in the mass transfer term, C, in the Golay equation. As was the case with the B term, a reduction in the average column pressure shifts the optimum carrier gas velocity to higher values and permits shorter analysis time with minimal degradation in chromatographic resolution.

Extra-Column Effects

Band broadening which occurs as a result of operating parameters prior to introduction onto the column or after exiting the column are considered to be due to extra-column effects. The performance of a column can be significantly degraded by extra-column band broadening due to the detector response, data acquisition rate, or dead volume in the injection port or detector.

Detector response. The response time of the detector and recorder can limit resolution when recorders or detectors with long time constants are used. However, in the case of the data acquisition system with the Finnigan TSQ45 mass spectrometer, the time constant is small enough that no significant contribution is expected. The hardware used for data acquisition can acquire data at a rate of 40 kHz.

Data acquisition rate. The data acquisition rate significantly influences both the apparent peak shape and the peak area. Loss of chromatographic resolution results when the sampling interval is not adequate to separate adjacent peaks. The area calculated for the analyte will also be in error (55). If P data points are to be collected while scanning a peak, then the minimum data acquisition rate, Dt, in data points per s is given by equation 3-7 shown below:

$$Dt = \frac{P \, N^{1/2}}{t_R} \qquad (3-7)$$

where t_R is the retention time of the analyte and N is
the number of theoretical plates generated by the column.
Since both the retention time and the number of theoretical
plates are proportional to the column length, the minimum
data acquisition rate is inversely proportional to the
square root of the column length. The data acquisition rate
was calculated by equation 3-7 for columns with 2000, 10000,
and 100000 theoretical plates and is shown in Table 8. It
can be seen that rapid analysis with high efficiency columns
requires fast data acquisition systems.

Injection port. The introduction of a narrow
sample plug is more difficult with capillary columns than
with packed columns due to the lower gas flow rates and
small i.d. of capillary columns. The sample was introduced
into the column by vaporizing the sample in the pressurized
glass-lined injection port which was connected to the
capillary column. The glass insert used in the injection
port of the Finnigan 9610 GC has an internal volume of 0.7
ml. The injection of 1.5 μl of methylene chloride solvent
which contains the analyte into the 140 $^\circ$C injection
port results in a solvent gas volume of approximately 0.5
ml. In order to reduce band broadening in the injection
port, the gas exiting the injection port can be split
between the column and the splitter outlet. Thus, the flow
rate through the injection port can be much higher than
through the column. In Grob injection, the purging of the

Table 8. Data acquisition rate in data points per s for 10
data points per peak versus the retention time in s for a
column with the indicated number of theoretical plates.

t_R	Number of theoretical plates for column		
	2,000	10,000	100,000
10	45	100	333
30	14.9	33	111
60	7.5	16.7	53
120	3.7	8.3	26
300	1.5	3.3	11
600	0.75	1.7	5.3
1500	0.30	0.67	2.1
3000	0.22	0.33	1.1

inlet is momentarily interrupted to increase the amount of analyte entering the column with the carrier gas and solvent (56, 57). If the peak concentration profile from the injection port was characterized by plug flow without mixing, then in the absence of focussing effects on the column, the peak width (in time) would at least be equal to the inlet volume divided by the total gas flow rate. The improved sensitivity obtained by permitting the sample to enter the column for a longer time would increase the width of the peak by a corresponding amount, and the use of the Grob technique would result in a loss in resolution.

The contribution of the injection port to the observed band broadening was determined. The gas flow rates were measured at atmospheric pressure for various inlet gas pressures for 1.8 and 8.8 m long DB5 fused silica capillary columns (0.25 mm i.d.) connected directly to the mass spectrometer. The flow rates were determined at the mechanical pump outlet with a bubble flow meter and are shown in Table 9. The gas flow rate from the mass spectrometer in the absence of the carrier gas from the column was less than 0.2 ml/min. The flow rates through the columns are inversely proportional to the column length, as predicted by the Poiseuille equation shown below:

$$v = \frac{3 \ r^2 \ P_o \ (P^2 - 1)^2}{32 \ \eta \ L \ (P^3 - 1)} \tag{3-8}$$

where v is the average velocity in cm/s, r is the radius of the column in cm, P_o is the outlet pressure in

Table 9. Gas flow rate (mL/min) as measured at the outlet of the vacuum pump versus inlet pressure for a DB5 fused silica open tubular capillary column with the stated length.

inlet pressure	column length	
in psi*	1.86 m	8.8 m
17	10.1	1.70
19	11.3	1.94
21	13.5	n.d.
23	16.2	3.35
25	19.7	n.d.
29	n.d.	6.25
39	n.d.	11.8

n.d. = not determined

* pressure with respect to the column outlet

dynes/cm^2, η is the viscosity in poise, L is the length of the column in cm, and P is the ratio of inlet pressure to outlet pressure. The flow rates are approximately 5 times greater with the shorter column. At the higher gas flow rate, the injector volume is flushed in approximately 6 s in the absence of splitting. If a 1:10 split ratio is used, the volume is replaced in 0.6 s. However, in the case of the longer 8.8 m column, which is still shorter than commonly used, the inlet volume is replaced in approximately 30 s in the absence of splitting, and in 3.0 s with a 1:10 split ratio. In the absence of focussing effects, the minimum peak widths would correspond to the time intervals required to flush the injector. Thus, band broadening effects due to the injection port are anticipated to be greater for columns with lower gas flow rates.

The peak widths are experimentally found to be narrower than predicted by the gas flow rates. Solvent effects and cold trapping at the head of the column appear to considerably reduce the width of the peaks. The improvement in the peak widths has been reported to be largely due to solvent effects when volatile analytes are determined (58). In the case of ethyl benzoate, which at ambient temperature has a retention time of 76 s and a peak width of 1.2 s, little opportunity exists for thermal focussing. The peak width of 1.2 s is considerably less than the injection band width, 6 s. It has been postulated (55) that the high concentration of solvent which is adsorbed initially at the

head of the column acts as a very thick film, greatly retarding the movement of the analytes through the column. Once the solvent front has passed, the analytes then interact with the thin-film liquid phase in the column, and the analytes pass more rapidly through the column.

Analysis Time

The retention time of an analyte is inversely proportional to the average gas velocity of the carrier gas. When GC is performed with the outlet connected to a vacuum, the high gas velocities near the outlet greatly decrease the retention time of the analyte. In this section the effect of the lower gas pressures and greater carrier gas velocities will be evaluated.

Outlet Pressure

When the outlet of the capillary column is below atmospheric pressure, the optimum carrier gas velocity is shifted to higher values than when the outlet is at atmospheric pressure, due to the increase in the gas phase diffusion coefficient. The optimum inlet gas pressure can be calculated (59) by equation 3-9 shown below:

$$P_{i,opt} = \frac{64 \ P_1 \ N \ f_{1,opt} \ \eta \ D_{m,1} + P_o}{r^2} \qquad (3-9)$$

where P_1 is atmospheric pressure in dynes/cm^2, $D_{m,1}$ is the diffusion coefficient at atmospheric pressure, and f_1 is the Gidding's correction factor, as shown below.

$$f_1 = \frac{9 \ (P^4 - 1) \ (P^2 - 1)}{8 \ (P^3 - 1)^2} \qquad (3-10)$$

The optimum gas velocity under vacuum outlet conditions for thin-film columns (59) operated at the optimum inlet pressure is given by equation 3-11.

$$v_{opt,vac} = \frac{[P_1 \, 3 \, (1 + k)^2 \, D_{m,1}]^{1/2}}{[2 \, N \, (11k^2 + 6k + 1) \, \eta]^{1/2}} \qquad (3-11)$$

Since the number of theoretical plates for a column is equal to the length of the column divided by the plate height, the optimum gas velocity for capillary columns is inversely proportional to the square root of the column length. The retention time of compounds on short columns will be less not only due to the column being physically shorter but also due to the higher optimum carrier gas velocities for shorter columns. For comparison, the optimum gas velocity with atmospheric outlet pressure (59) is given by the equation 3-12 shown below.

$$v_{opt} = \frac{4 \, D_{m,o} \, f_{2,opt} [3(1 + k)^2]^{1/2}}{r \, [11k^2 + 6k + 1]^{1/2}} \qquad (3-12)$$

where $f_{2,opt}$ is the Martin-James correction factor for the pressure gradient across the column (60) given by equation 3-13 shown below.

$$f_2 = \frac{3(P^2 - 1)}{2(P^3 - 1)} \qquad (3-13)$$

In this case, the optimum gas velocity is also dependent on the column length; however, the dependence of the optimum gas velocity on column length is less for columns with the outlet at atmospheric pressure. In Table 10, the optimum

Table 10. Comparison of vacuum outlet versus atmospheric pressure outlet gas chromatography with a 0.25 mm i.d. DB5 fused silica capillary column with 2000 theoretical plates per m. Optimum velocity in cm/s with helium at 70 $^{\circ}$C.

Length (cm)	Atmospheric Outlet P inlet torr	Atmospheric optimum velocity	Vacuum Outlet P inlet torr	Vacuum optimum velocity	Ratio V(vac)/V(atm)
100	799	45.4	174	303	6.7
200	836	44.4	214	246	4.8
500	942	41.5	390	136	3.3
1000	1090	37.9	551	96	2.5
1500	1220	35.1	675	78	2.2
3000	1540	29.5	955	55	1.9
6000	2040	23.6	1350	39	1.7

carrier gas velocities calculated from equation 3-11 and
3-12 are shown with the associated optimum inlet pressures
for columns ranging from 1 to 60 m in length. The greatest
gain in optimum carrier gas velocity occurs with shorter
columns due to the lower carrier gas density. A 2 m column
has an optimum carrier gas velocity approximately 5 times
greater with vacuum-outlet conditions than with atmospheric
outlet conditions. It is also notable that a 2 m column has
an optimum carrier gas velocity which is 3 times greater
than a 15 m column when they are both operated at their
optimum inlet pressures and the outlets are connected to a
vacuum. Thus, the use of a 2 m column at its optimum inlet
gas pressure will decrease the retention time of the analyte
by a factor of 24 compared to a 15 m column with vacuum
outlet, and by a factor of 52 when compared to the same 15 m
column with an atmospheric outlet pressure. For example,
the retention time for aldicarb on a 2 m column was
determined, and the corresponding retention time for
aldicarb on the 15 m column was calculated. Aldicarb has a
retention time of approximately 2 min on the 2 m column,
while with the 15 m column and the outlet at atmospheric
pressure, the retention time would be nearly 2 h, and the
peak width would be so broad that the peak would be
difficult to detect.

Gas chromatographic analyses are commonly performed not
at the optimum carrier gas velocity, but rather at the
optimum "practical" carrier gas velocity (61), in order to

minimize analysis time. It has been observed that there is an increase in the calculated number of theoretical plates per m when a column is divided into shorter pieces (62, 63). It has been suggested that either no real improvement in the chromatography actually occurs (62), or that the improvement that does occur is due to greater uniformity in the carrier gas velocity with shorter columns (63).

However, a more tenable explanation can be obtained by evaluating the chromatographic equations with respect to the rate of change expected in the height of a theoretical plate versus flow rate for two columns of widely differing length. The C_G mass transfer term, which determines the slope of the Golay plot in the region beyond the optimum carrier gas velocity, is proportional to the average gas pressure on the column. Since shorter columns are operated at lower gas pressures, particularly when the outlet is connected to a vacuum, the rate of change in the Golay plot in the region beyond the optimum carrier gas velocity is lower for shorter columns. Hence, when the optimum carrier gas velocity is increased, the increase in the HETP for a 1.8 m column will be less than that for an 8.8 m column.

The observed increase in the number of theoretical plates per m upon dividing capillary columns can therefore be readily explained. When the number of theoretical plates is measured at velocities greater than the optimum, shorter columns will have more theoretical plates/m due to the smaller C term in the Golay equation at the lower operating
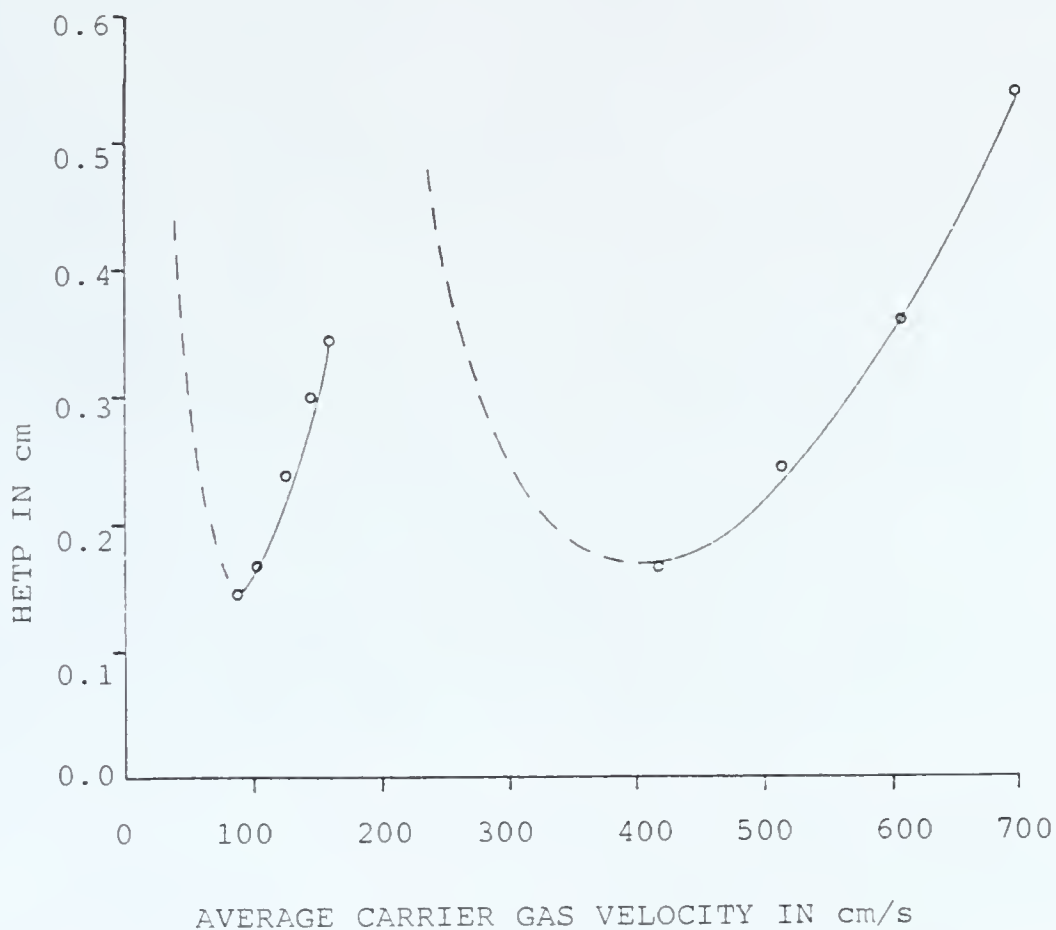
Figure 3. The experimenatlly determined dependence of the height equivalent to a theoretical plate, HETP, vs the average helium carrier gas velocity on 8.8 m and 1.8 m DB5 capillary columns operated with the outlet connected to a vacuum. Values calculated by fitting the data to an equation with three variables are shown by the dashed lines.

pressures used with short columns. In Figure 3, an
experimentally determined Golay plot is shown for 1.8 and
8.8 m DB5 fused silica capillary columns. The difference in
the rate of change in the HETP versus the average gas
velocity is apparent. An increase in the carrier gas
velocity from 415 cm/s to 465 cm/s with the 1.8 m column
increased the HETP from 0.017 cm to 0.020 cm while for the
8.8 m column a similar increase in velocity from 100 cm/s to
150 cm/s increased the HETP from 0.017 cm to 0.030 cm. The
HETP for the 1.8 m column increases more slowly than with
the 8.8 m column. It also can be seen both from the
experimental data shown in Figure 3 and from equation 3-6
that, since the HETP is a function both of the average
velocity and the average column pressure, a linear
relationship between HETP and the average velocity is not
expected even at higher average carrier gas velocities. The
Golay equation predicts a linear increase in the HETP beyond
the optimum carrier gas velocity. This will occur when mass
transfer is limited by the liquid phase mass transfer term,
or in applications where the column pressure does not change
significantly.

Temperature Effects

The fundamental resolution equation shown below
describes the relationship between: N, the number of
theoretical plates; α, the alpha value (equation 3-15);
k_2, the capacity factor for the later eluting component;
and R_s, the resolution between the two components.

$$R_s = \frac{N^{1/2} \ (\alpha - 1) \ (k_2)}{4 \ (\alpha) \ (1 + k_2)} \qquad (3-14)$$

Short columns can be used for the analysis of thermally labile compounds because these columns do not retain the analyte beyond a reasonably useful retention time at the lower temperatures necessary to avoid thermal degradation. The reduction in temperature not only avoids thermal degradation but is also expected to influence the separation process as well. A reduction in the column length by a factor of 4 will reduce the number of theoretical plates by a factor of 4, and the resolution will be decreased by a factor of 2. However, when lower temperatures are used the alpha value will also change. Alpha is given by equation 3-15 shown below:

$$\alpha = \frac{k_i}{k_j} = \frac{V_{g,i}}{V_{g,j}} \qquad (3-15)$$

where k is the capacity factor $[k = (t_R - t_o)/t_o]$ and Vg is the corrected retention volume. In Figure 4 is shown a plot of ln(Vg) versus 1/T for aldicarb, methyl benzoate and ethyl benzoate on 1.8 and 8.8 m DB5 capillary columns. The retention volume for each component was determined from the retention time and the carrier gas flow rate measured at atmospheric pressure. The slope of the plot of ln(Vg) vs 1/T (T is in degrees Kelvin) is equal to -Ha/R where Ha is the heat of adsorption and R is the gas constant (64). The heats of adsorption for aldicarb, methyl benzoate, and ethyl
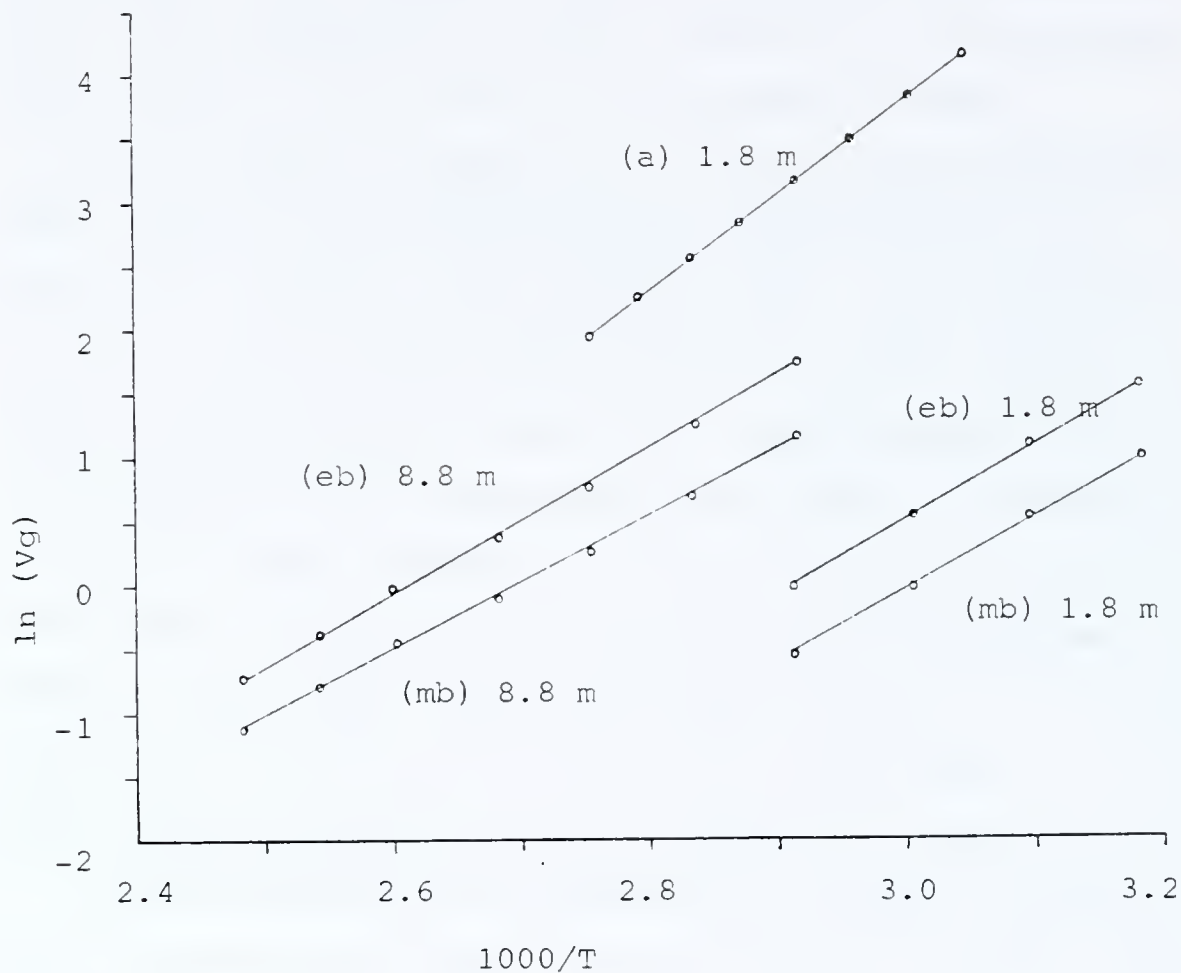
Figure 4. The natural log of the corrected retention volume, Vg, for methyl benzoate (mb), ethyl benzoate (eb), and aldicarb (a) vs 1000/T where T is the temperature in degrees Kelvin. Data are shown for both the 8.8 m and the 1.8 m columns.

benzoate are calculated from the slopes on the 8.8 m column to be -14.9 kcal, -10.3 kcal and -11.2 kcal, respectively. The retention volume at other temperatures may then be calculated. The corrected retention volumes calculated for these three compounds are shown in Table 11. The calculated alpha values at 50 $^{\circ}$C and 120 $^{\circ}$C are shown in Table 12. The decrease in temperature increases the corresponding alpha values for the ethyl benzoate, methyl benzoate pair and for the aldicarb, ethyl benzoate pair. The increase in the alpha values improves the resolution. Thus, when the column is shortened by a factor of 4 and the analysis is carried out at a lower temperature, the loss in resolution is only 32% rather than 50%, due to the increase in the alpha value. In Table 13, the experimentally determined retention times, peak widths, and resolutions at temperatures from 41.5 $^{\circ}$C to 130 $^{\circ}$C for methyl and ethyl benzoate on 1.8 m and 8.8 m columns are shown.

Thermal focussing of aldicarb can be readily achieved due to its relatively large heat of adsorption. Since, with the 1.8 m column, the injection volume is swept out in 6 s at a flow rate of 0.17 ml/s, if plug flow occurs, then the greatest possible volume the aldicarb peak could initially occupy is 1.02 ml. If the column is initially at 30 $^{\circ}$C, the retention volume of aldicarb on the 1.8 m column will be 421 ml. The distance travelled by the aldicarb peak in the initial 6 s can be calculated based on the average flow rate and the previously determined retention volume. Based on

Table 11. Calculated retention volume in mL for
methyl benzoate, ethyl benzoate and aldicarb at
50 $^{\circ}$C and 120 $^{\circ}$C on a 1.8 m DB5 capillary
column.

	Vg at 50 $^{\circ}$C	Vg at 120 $^{\circ}$C
methyl benzoate	7.78	0.448
ethyl benzoate	14.9	0.671
aldicarb	90.7	1.45

Table 12. Calculated alpha values for pairs of compounds;
mb, methyl benzoate; eb, ethyl benzoate and a, aldicarb at
50 $^{\circ}$C and 120 $^{\circ}$C on a 1.8 m DB5 capillary column.

	alpha$_{eb,mb}$	alpha$_{a,mb}$	alpha$_{a,eb}$
50° C	1.91	11.7	6.11
120° C	1.50	3.23	2.16

Table 13. The effect of column temperature in $^{\circ}C$ on peak width (s), resolution, and retention times (s) of methyl and ethyl benzoate on a 1.8 m and 8.8 m DB5 capillary column.

T	column length	methyl benzoate t_R	width	ethyl benzoate t_R	width	resolution
70	8.8	103	5.49	181	10.1	10.0
80	8.8	67	3.55	114	5.2	10.7
90	8.8	44	2.69	73	4.2	8.4
100	8.8	31	2.36	49	3.0	6.7
110	8.8	23	1.92	35	2.3	5.7
120	8.8	16	1.77	24	1.9	4.4
130	8.8	12	1.73	18	2.0	4.4
41	1.8	17	2.06	32	4.4	4.6
50	1.8	11	2.13	20	4.0	3.0
60	1.8	7	1.32	11	1.9	3.0
70	1.8	4	1.53	7	1.7	1.7

these calculations the aldicarb peak will have been trapped in the first 0.43 cm of the column. On raising the column temperature to 80 $^{\circ}$C, the retention volume will be reduced to 12.7 ml and the aldicarb peak will flow through the column with a velocity of 2.43 cm/s. At this velocity, aldicarb would have a band width of 0.18 s due to the band broadening in the injection port. When temperature programming was used, with a one minute hold at 30 $^{\circ}$C followed by a temperature ramp of 30 $^{\circ}$C/min to 85 $^{\circ}$C, aldicarb eluted at a retention time of 160 s with a peak width of 5.5 s. The peak width is much greater than the peak width contribution due to band broadening in the injection port.

The experimentally determined number of theoretical plates when temperature programming with an initial hold period was higher than expected. In order to demonstrate that the hold time artifically increases the number of theoretical plates while the resolution remains essentially unchanged, the hold time was varied and the number of theoretical plates for aldicarb determined as shown in Table 14. The number of theoretical plates increases as the hold time is increased. A sample containing p-hydroxyacetophenone and diethyl phthalate was analyzed with different hold times as, shown in Table 15. The data indicate that, even though the calculated number of theoretical plates increases, the resolution remains essentially unchanged.

Table 14. Effect of hold time at room temperature prior to ramping at 30 ^{o}C/min to 85 ^{o}C on the calculated number of theoretical plates, N, for p-hydroxyacetophenone on a 1.8 m DB5 capillary column with an i.d. of 0.25 mm and an inlet pressure of 4 psig. The peak widths and times are given in s.

Hold Time	t_R	w_b	N	peak ht. (counts/1000)
30	131	6.0	477	293
60	161	5.5	857	276
90	191	6.6	837	293
120	220	6.4	1180	313
180	279	6.4	1900	282
240	338	6.1	3070	261
300	397	6.4	3850	300
420	516	6.1	7200	252
600	693	6.4	11700	220

Table 15. Resolution and number of theoretical plates versus hold time at ambient temperature for 1.8 m DB5 capillary column with an i.d. of 0.25 mm. Peak widths and retention times are in s.

| Hold Time | p-hydroxyacetophenone | | | diethyl phthalate | | | resolution |
	t_R	w_b	N	t_R	w_b	N	
60	195	14.4	183	219	7.3	920	2.3
120	257	16.6	240	278	7.8	1300	1.7
300	442	12.9	1170	466	8.1	3350	2.3
600	753	16.8	2000	773	8.7	7900	1.6

Sensitivity

The value of short columns lies not only in the potential for rapid analysis, but in the increased sensitivity obtained as well. The sample concentration in the detector is greater for shorter columns than for longer columns when the columns are operated at their optimum gas velocity. The higher concentration is due to the narrower peaks with shorter columns. The width of a peak is given by equation 3-16 shown below.

$$w_b = \frac{t_R}{(N)^{1/2}} \tag{3-16}$$

The retention time of a compound is given by equation 3-17 shown below.

$$t_R = \frac{L(1 + k)}{v_{opt}} \tag{3-17}$$

The dependence of the width of the peak, w_b, on the column length, L, can therefore be shown to be given by equation 3-18 shown below.

$$w_b = \frac{L(1 + k)}{v_{opt} (L/H)^{1/2}} = \frac{(L\ H)^{1/2}(1 + k)}{v_{opt}} \tag{3-18}$$

The peak width increases in proportion to the square root of the column length, while the concentration of the analyte is decreasing in proportion to the width of the peak. Since the response of the detector is proportional to the concentration of the analyte, the signal intensity per unit time is greater for the shorter columns. A 1.5 m column will have a signal intensity approximately 3 times greater

than that of a 15 m column with the same amount of sample.
The increased signal intensity should improve the limit of
detection (LOD) for the 1.5 m column vs the 15 column by a
factor of 3 as well.

The minimum plate height, $H_{min,vac}$, for capillary
columns with a column radius, r, when the outlet is
connected to a vacuum (59) is given by equation 3-19 shown
below.

$$H_{min,vac} = \frac{9 \ r \ [11k^2 + 6k + 1]^{1/2}}{8 \ [3 \ (1 + k)^2]^{1/2}} \qquad (3-19)$$

Since the column plate height is directly proportional to
the column radius, the use of smaller diameter columns
improves the LOD obtainable for trace components. Thus, the
net improvement in the LOD upon employing a 1.5 m capillary
column with an i.d. of 0.25 mm over the use of a 30 m
capillary column with an i.d. of 0.32 mm is a factor of 5.
However, in the case of vacuum outlet capillary
chromatography, for this improvement to be realized the
inlet pressure needs to be maintained below atmospheric
pressure, as shown in Table 10. Currently, most gas
chromatographs are not equipped to perform vacuum inlet
chromatography, and therefore this benefit is not fully
utilized. It should be noted that, while obtaining a gain
in sensitivity of a factor of 5, the analysis time would be
reduced by a factor of more than 140.

Selected Reaction Monitoring vs Selected
Ion Monitoring

Selected reaction monitoring (SRM) refers to the tandem mass spectrometry technique of passing a selected parent ion through the first quadrupole mass analyzer, fragmenting this ion by collision with a neutral target gas in the second quadrupole, and subsequently analyzing for a particular daughter ion in the third quadrupole. This technique is illustrated and compared with that of selected ion monitoring (SIM), in Figure 5. In the method of selected ion monitoring, all ions formed in the source are passed by the first two quadrupoles, and the third quadrupole is set to pass the selected ion. The use of two mass analyzers to select both the parent and the daughter ion mass in SRM greatly improves the selectivity, so that analysis of complex samples with minimal separation is possible.

An example of the enhanced selectivity obtained with SRM compared to that with SIM can be seen in the analysis of aldicarb in positive chemical ionization (CI) mode. In the positive CI mass spectrum of aldicarb, the major ions are 116^+ and 89^+. When aldicarb is extracted with methylene chloride from clean water samples, the chemical background consists primarily of solvent ions from methylene chloride which do not interfere, and SRM does not improve the limit of detection (LOD) compared with SIM. However, when aldicarb is extracted from a spiked sample of orange juice the added selectivity of SRM provides considerable improvement in the LOD. This extract contains numerous
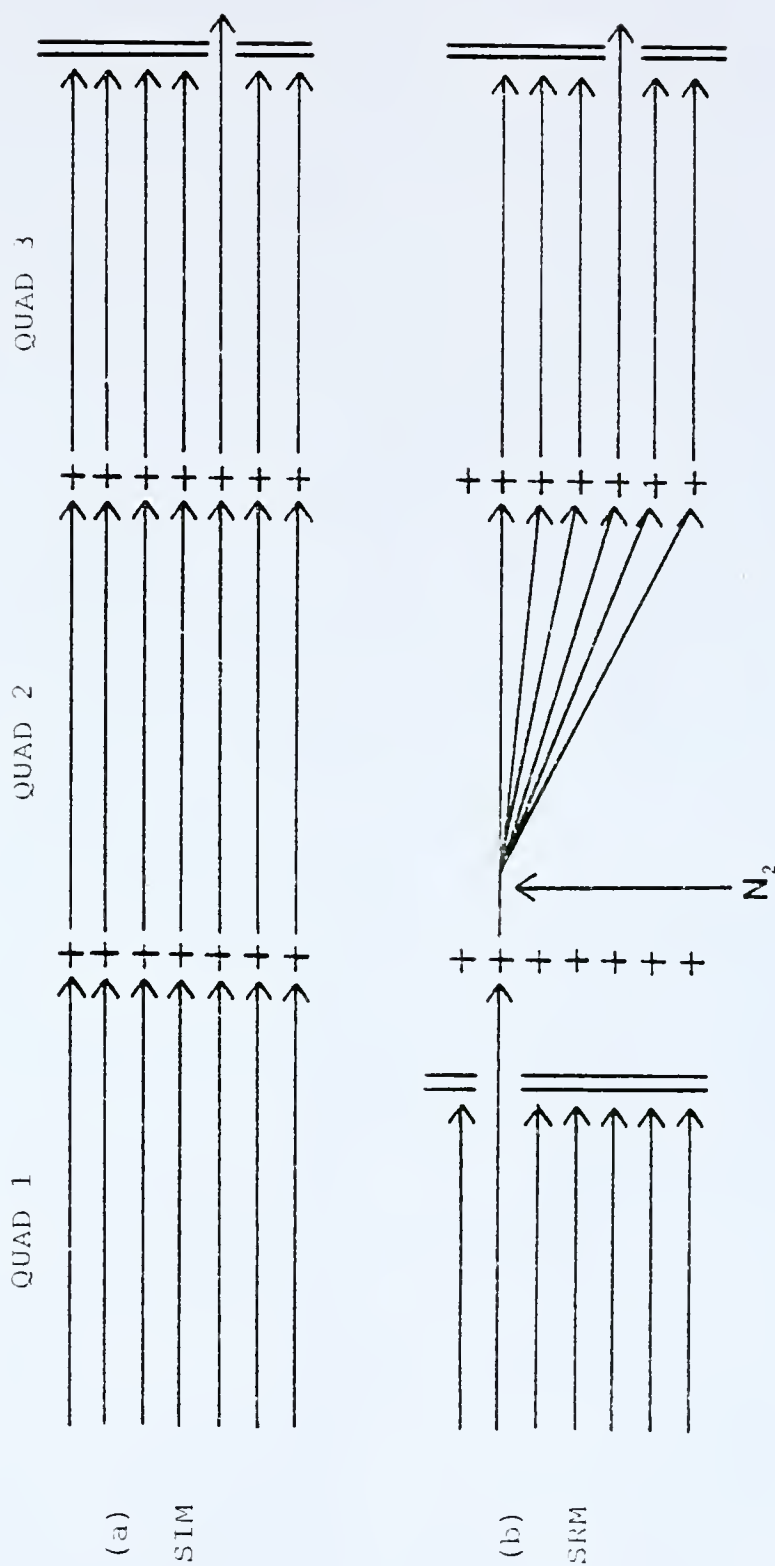
Figure 5. Illustration depicting the Finnigan TSQ45 mass spectrometer operated in (a) selected ion monitoring mode (SIM) and (b) selected reaction monitoring mode (SRM).

compounds which produce ions of the same m/z ratio as aldicarb, which then interfere in SIM. In Figure 6, a chromatogram obtained by SIM of aldicarb in a sample of orange juice spiked with 36 ppb of aldicarb is compared to that obtained by SRM. The presence of aldicarb in the sample is apparent when the sample is analyzed by SRM; however when SIM for the m/z 89, 116 or 191 ions is used, aldicarb is not detected due to the high chemical background signal. The concentration of aldicarb in the sample was determined from the standard curve to be 29 ppb. The standard curve obtained using SRM (m/z 116 fragmenting to give m/z 89) is shown in Figure 7. In Figure 8 is shown a logarithmic calibration for SRM demonstrating linearity of the response obtained. However, the repeated injection of samples which contain a high concentration of relatively non-volatile components contaminate the injection port and the column. This contamination adversely affects analyses by increasing the retention time and peak width.

Resolution Requirements

The technique of MS/MS is well suited to rapid analysis by short column chromatography, because the enhanced selectivity of MS/MS compensates for the reduced chromatographic resolution. In addition, the added sensitivity obtainable with the shorter column is beneficial for analysis by MS/MS, since this technique is inherently less sensitive than is MS alone. The method of SRM has poorer sensitivity than SIM due to the inefficiency of CID
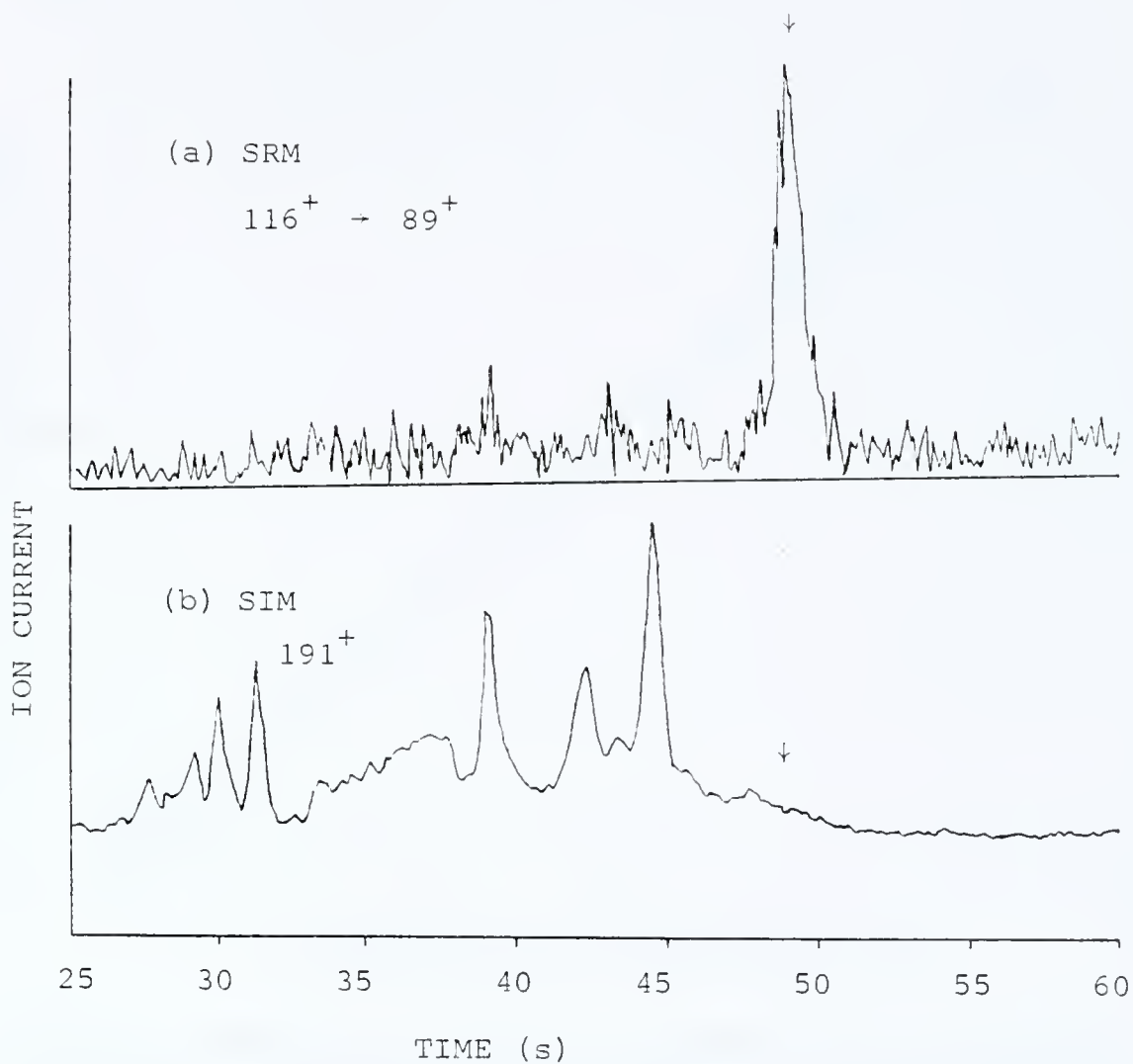
Figure 6. Ion current for the determination of aldicarb in a sample of orange juice spiked with 36 ppb of aldicarb by (a) SRM and (b) SIM. The arrows point to the aldicarb peak. Selected ion monitoring for the m/z 89, 116, and 191 ions did not detect the presence of aldicarb.
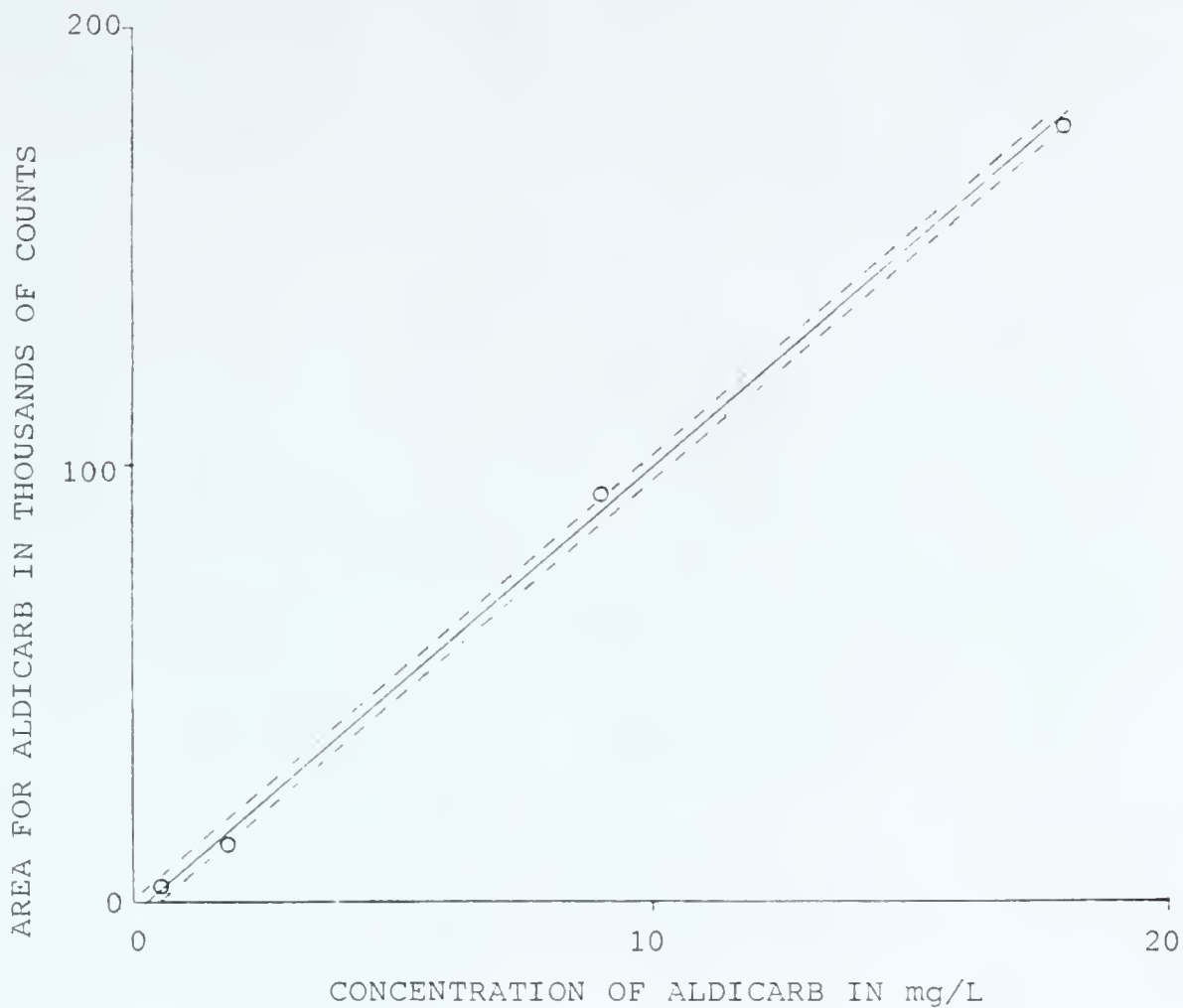
Figure 7. Response plot for the determination of aldicarb in methylene chloride by SRM of the m/z 116 ion fragmenting to form the m/z 89 ion. The correlation coefficient is 0.999. The dashed line shows the range calculated for one standard deviation.
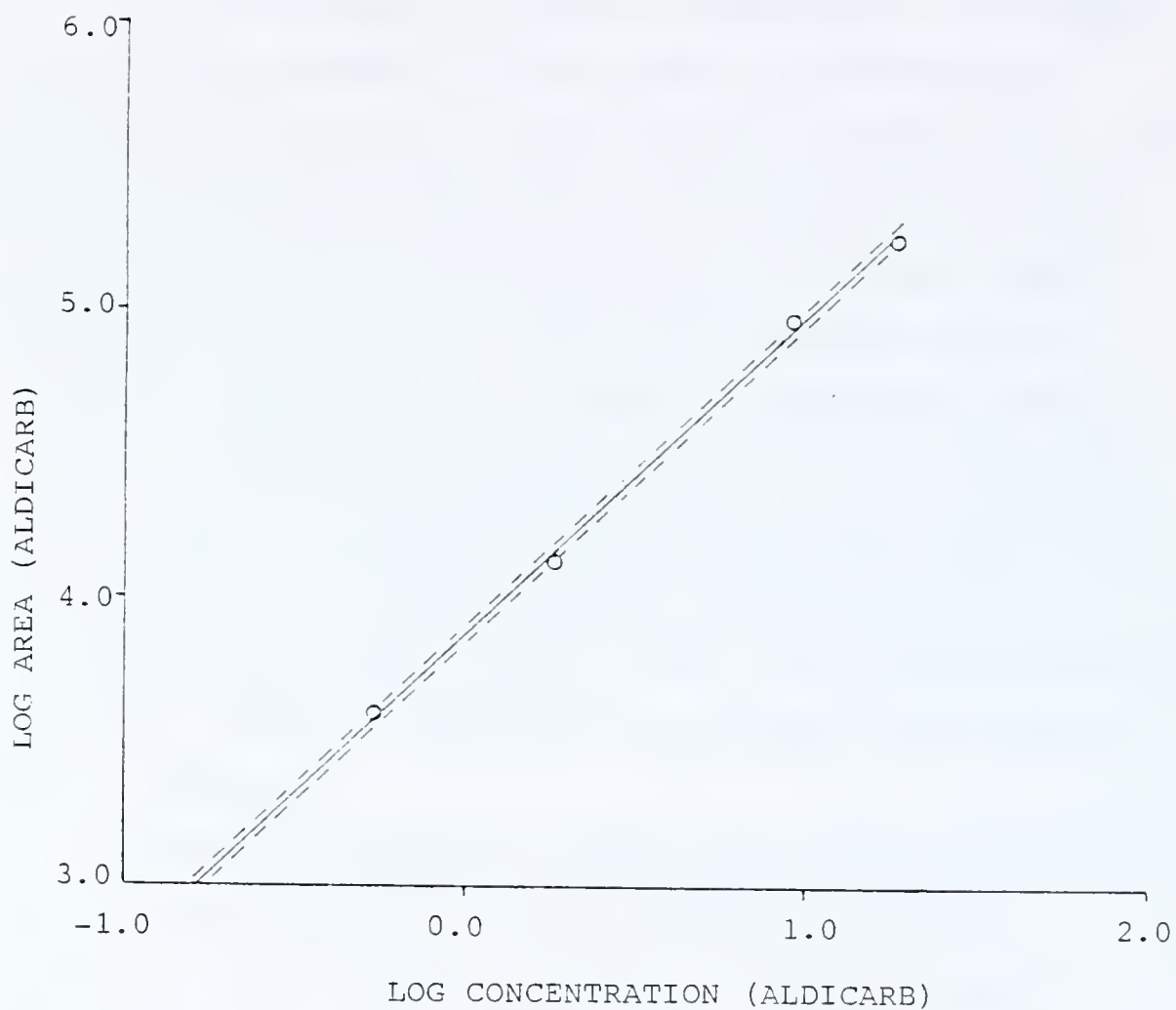
Figure 8. Log of the response for aldicarb by SRM vs the
log of the concentration of aldicarb in methylene chloride.
The correlation coefficient is 0.999 with a slope of 1.1.
The dashed line shows the range calculated for one standard
deviation.

and the second stage of mass analysis in MS/MS, but is less susceptible to chemical interference, when short columns are used.

Selectivity in SRM vs SIM

The selectivity of a method is dependent on the number of resolution elements in the method, and the degree of selectivity obtainable by each resolution element (65). The Finnigan TSQ45 mass spectrometer, when operated in the SIM mode, has unit mass resolution and a mass range of 1000. Thus, with SIM one out of 1000 possible masses may be selected. Since the mass resolution elements are directly coupled in SRM, the analyst may select one of 1000 possible parent ions, P, and then fragment the selected parent ion to form one of P - 1 possible daughter ions for a total of 499,500 possible combinations. Thus, SRM is inherently 500 times more selective than SIM, if the entire mass range of 1000 is employed.

The added selectivity of SRM can be used to compensate for the lost resolution in the application of short capillary columns for the analysis of thermally labile compounds or for rapid analysis. The number of peaks that could be detected, each with a resolution of 1, was calculated. A short computer program was used to calculate the number of peaks possible both for a short column with 2000 theoretical plates and an analysis time from 30 s to 240 s, and for a longer column with 100,000 theoretical plates and an analysis time from 180 s to 1800 s. When

these conditions are used, 730 peaks can be determined with the long column, while 95 peaks could be determined with the short column.

In spite of the lower chromatographic resolution, the use of MS/MS in combination with a short column provides greater selectivity by a factor of 65 than does MS in combination with a long column (499,500 x 95 / 1000 x 730). The enhanced selectivity obtainable with SRM permits rapid analysis without loss of confidence in the selectivity of the analysis. The effect of the fragmentation process on selectivity will be discussed in Chapters 4 and 5.

Summary

Analysis of complex samples for thermally labile compounds by GC/MS or GC/MS/MS can be performed more rapidly and with greater sensitivity when short capillary columns are used. The minimum analysis time was shown to occur when the capillary column is operated with a vacuum outlet. The combination of the shorter column length and the higher carrier gas velocities decreased the time required for analysis of aldicarb from 2 h with a 15 m column to 2 min with a 2 m column. The LOD for an analyte was also shown to be improved by a factor of 5 when a 1.5 m column with an i.d. of 0.25 mm is compared to a 30 m column with an i.d. of 0.35 mm. Thus, short capillary columns offer significant advantages for rapid analysis of compounds present at low concentrations.

CHAPTER 4
DETERMINATION OF ALDICARB, ALDICARB OXIME AND ALDICARB NITRILE IN WATER BY GAS CHROMATOGRAPHY/MASS SPECTROMETRY

The gas chromatographic/mass spectrometric method for the determination of aldicarb in water developed in this research greatly aided the determination of the degradation by-products of aldicarb. The development of this method required investigations not only of the chromatographic process, but also of the extraction, sample introduction, and mass spectrometric processes as well. In this chapter the experimental parameters used in the analysis for aldicarb and its degradation by-products are presented and discussed.

Experimental

Apparatus. A Finnigan gas chromatograph/triple-stage quadrupole mass spectrometer/data system was used in this study. Electron energies of 70 and 100 eV were used for electron ionization (EI) and chemical ionization (CI), respectively. The chemical ionization reagent gas was methane or isobutane at an ionizer pressure of 0.8 torr. The mass spectrometer was tuned with FC43 (perfluorotri-butylamine). The EI spectra for aldicarb and aldicarb oxime were similar to those in the NBS library. Nitrogen collision gas was introduced at 1.7 mtorr and collision

energies were 10-20 eV for collision-induced dissociation (CID) spectra. The continuous dynode electron multiplier was operated at 850-900 V, with the conversion dynodes at $\pm$3000 V. The preamplifier gain was set for 10^8 V/A. Selected ion monitoring for the 9 positive ions (m/z 86, 89, 116, 134, 150, 151, 202, 207, and 223) in a total scan time of 0.273 s was used for quantitative analysis. The capillary columns were inserted directly into the ion source.

Reagents and standard compounds. Standards of aldicarb, aldicarb oxime, aldicarb sulfoxide, aldicarb oxime sulfoxide, and aldicarb sulfone were obtained from the U.S.E.P.A. Pesticides & Industrial Chemicals Repository (MD-8), Research Triangle Park, NC 27711 USA. Stock solutions were prepared in methylene chloride and stored at 4 $^{\circ}$C.

Aldicarb nitrile was synthesized using a published procedure (66). Temik (416 g) was extracted with 2 successive aliquots of methanol (400 mL and 300 mL). The combined methanol extract was concentrated to 200 mL and then added slowly to 300 mL of distilled water. The precipitated white aldicarb crystals (17.8 g) were collected on a Buchner funnel and washed with 20 mL of distilled water. Then 17 g of the extracted aldicarb was refluxed in a 250 mL round bottom flask in 50 mL of cyclohexene for 67 h. The cyclohexene was separated from a lower layer of

viscous oil and concentrated by passing a stream of air over the surface. The liquid residue was distilled under vacuum to obtain aldicarb nitrile, which had a boiling point of 71 $^{\circ}$C at 39 torr.

Gas chromatographic conditions. [1] A 2.6 m fused silica bonded phase capillary column (J & W DB5, SE54 equivalent) was operated at 2 psig (pounds per square inch gauge) or 860 torr with respect to the column outlet. Helium was used as the carrier gas for analysis of samples for aldicarb and aldicarb oxime. Splitless injection was used with the sweep off for 30 s. The injection port was operated at 130 $^{\circ}$C and a clean silanized glass insert was used to minimize loss of sample due to degradation and adsorption. The interface temperature was 135 $^{\circ}$C and the column temperature was programmed from 40 $^{\circ}$C to 100 $^{\circ}$C at a rate of 20 $^{\circ}$C/min after a hold of 1 min. Aldicarb oxime eluted after 64 s, while aldicarb eluted after 207 s. Ethyl benzoate, used as an internal standard, had a retention time of 76 s.

[2] A 9 m section of the fused silica DB5 capillary column was necessary to separate aldicarb nitrile from the solvent peak. Analysis for aldicarb nitrile was performed with the injection port at 60 $^{\circ}$C and the interface at 100 $^{\circ}$C. Splitless injection was used with the sweep off for 12 s. The column was programmed from 30 $^{\circ}$C to 100 $^{\circ}$C at 20 $^{\circ}$C/min after a hold of 1 min. Helium was used as

the carrier gas at a pressure of 4 psig (960 torr).
Aldicarb nitrile had a retention time of 120 s.

[3] A 30 m carbowax 20M fused silica capillary column
was employed for the evaluation of the thermal degradation
products of aldicarb. Splitless injection was used with the
sweep off for 30 s. The injection port was operated at
250 $^{\circ}$C while the interface was maintained at 200 $^{\circ}$C.
The column temperature was programmed from 40 $^{\circ}$C to 180 $^{\circ}$C
at 25 $^{\circ}$C/min, with an initial hold of 2.5 min and a
final hold at 180 $^{\circ}$C for 6 min. The helium carrier
pressure was 14 psig (1500 torr). The retention time of
aldicarb nitrile was 385 s.

Extraction efficiencies. Aldicarb, aldicarb oxime,
aldicarb sulfoxide, aldicarb oxime sulfoxide, and aldicarb
sulfone were separately spiked into pH 5.7 buffered water at
10 to 30 ppm concentrations. Each aqueous sample was
extracted with methylene chloride after vigorous shaking for
2 min in a 250 ml separatory funnel. The concentration of
each compound in the aqueous layer was then determined by
its UV absorption. Extraction efficiencies for aldicarb,
aldicarb oxime and aldicarb oxime sulfoxide were also
evaluated on the basis of their concentrations in the
organic layer as determined by GC/MS. Aldicarb sulfoxide
and aldicarb sulfone were also evaluated using MS with
direct probe sample introduction.

Aldicarb nitrile did not absorb in the spectral range
from 220 nm to 800 nm. The extraction efficiency for

aldicarb nitrile was therefore determined by GC/MS analysis of spiked methylene chloride samples before and after partitioning with deionized water. The relative standard deviation for the analysis was 2.5%.

Results and Discussion

Partition Coefficients

The partition coefficients obtained for the extraction of aqueous samples with methylene chloride are compared with those reported with chloroform (9) in Table 16. The partition coefficients for the two different solvents were found to parallel one another closely. However, the extraction efficiency obtained for aldicarb sulfoxide using a single extraction of spiked water with a 1:11.5 ratio of methylene chloride to water was considerably lower than that reported for two consecutive extractions with methylene chloride using a 1:10 ratio (12). Efficient extraction of aldicarb sulfoxide has been reported for four consecutive extractions of water with chloroform if a ratio of 1:2 chloroform to water is used (5). In our experiments, for a single extraction with methylene chloride of water in a ratio of 1:11.5, aldicarb, aldicarb nitrile and aldicarb oxime were extracted with 99%, 102%, and 44% extraction efficiencies, respectively.

Chromatography

A small portion of the aldicarb injected degrades to aldicarb nitrile when an injection port temperature of 130 $^{\circ}$C is used. As a result, aldicarb gives a positive

Table 16. Comparison of the partition coefficients determined for aldicarb and five of its degradation by-products for extraction of water samples with methylene chloride (this study) with that obtained using chloroform (9).

compound	methylene chloride	chloroform
aldicarb	140	25.8
aldicarb oxime	12	1.66
aldicarb sulfoxide	1.0	0.95
aldicarb oxime sulfoxide	0.047	0.15
aldicarb sulfone	5.2	3.45
aldicarb nitrile	>190	n.d.

n.d. = not determined.

interference for aldicarb nitrile. However, aldicarb nitrile does not interfere with the analysis for aldicarb because, unlike in previous GC methods, in this procedure the analysis is carried out for the intact aldicarb molecule. The presence of the intact molecule is demonstrated by the appearance of the MH^+ ion in methane and isobutane CI, and by matching the EI spectrum obtained with that of standard aldicarb introduced by direct probe insertion. The mass spectra for aldicarb, aldicarb nitrile and aldicarb oxime are shown in Figures 9, 10, and 11, respectively.

Analysis for the intact aldicarb molecule (as opposed to a thermal degradation product) is of distinct advantage, since it is possible to differentiate between aldicarb and aldicarb nitrile without the florisil clean-up procedure commonly used. The 3 m DB5 capillary column was found to provide greater sensitivity and reproducibility in the analysis for aldicarb than the 9 m DB5 capillary column, since aldicarb elutes at a lower temperature on the short column. A representative gas chromatogram is shown in Figure 12. Figure 13 shows the standard curve for aldicarb with the 3 m DB5 capillary column. The use of on-column injection techniques in conjunction with the use of short capillary columns would quite likely improve the sensitivity of the technique. On the longer columns normally used for GC/MS analysis, aldicarb does not elute in a reasonable time at temperatures low enough to avoid thermal degradation.
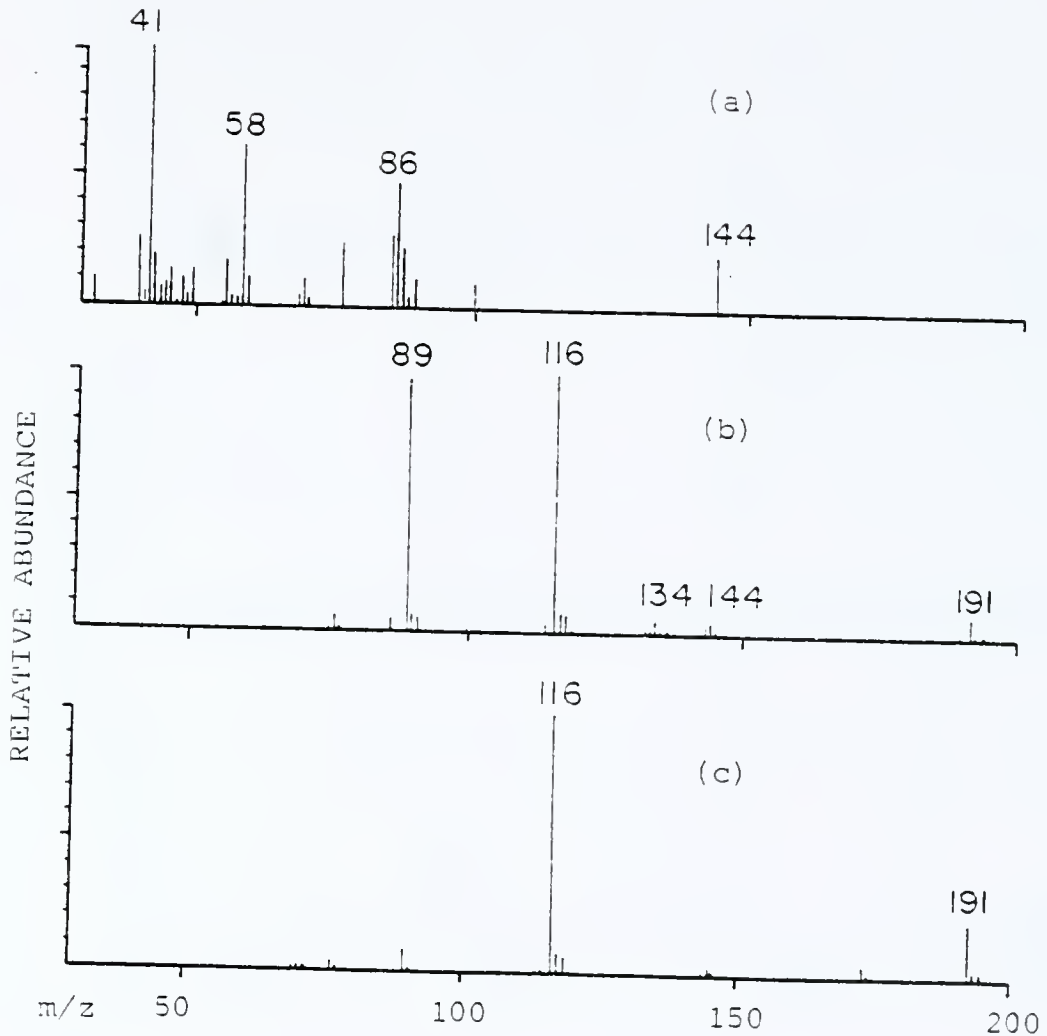
Figure 9. The mass spectra for aldicarb (molecular weight 190) with the source temperature at 100 $^{\circ}$C by (a) electron impact, (b) positive methane CI, and (c) positive isobutane CI.
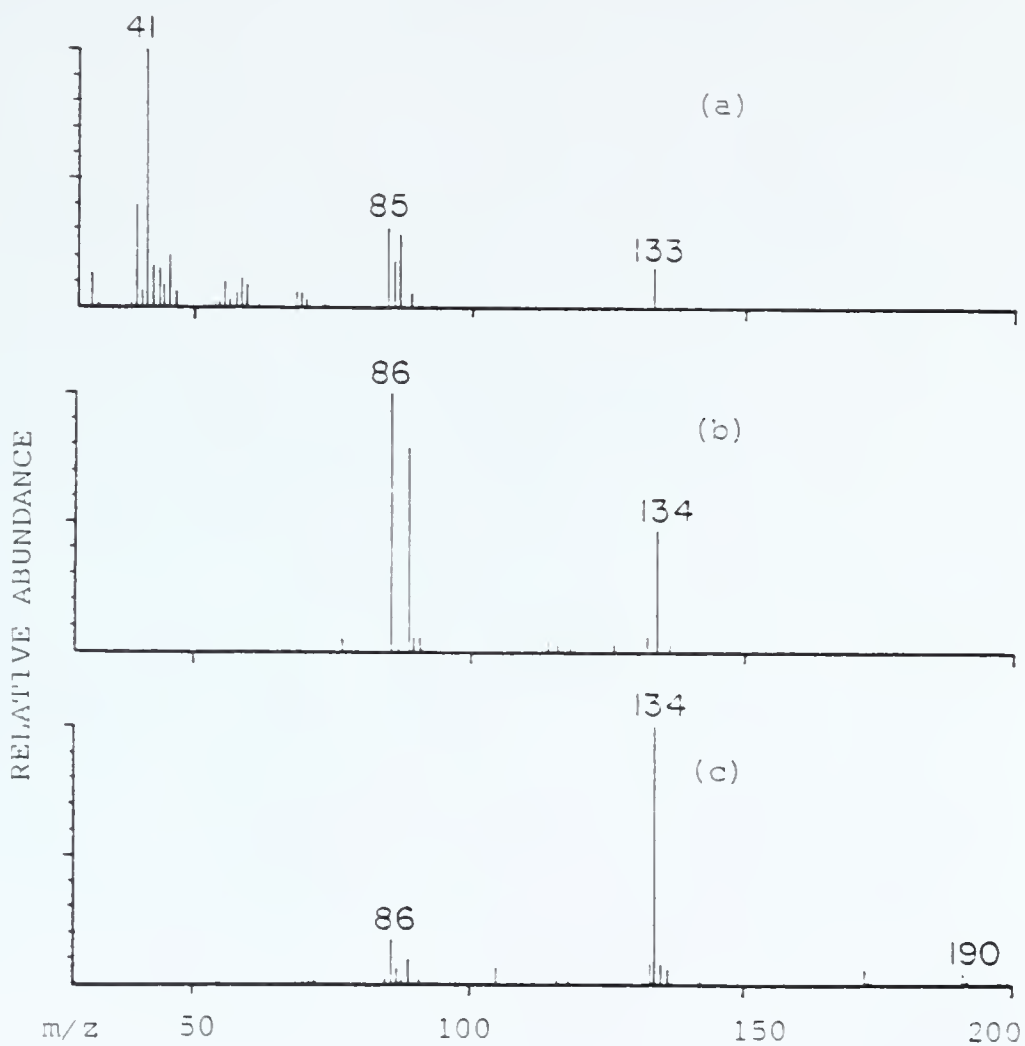
Figure 10. The mass spectra for aldicarb oxime (molecular weight 133) with the source at 100 $^{\circ}$C by (a) electron impact, (b) positive methane CI, and (c) positive isobutane CI.
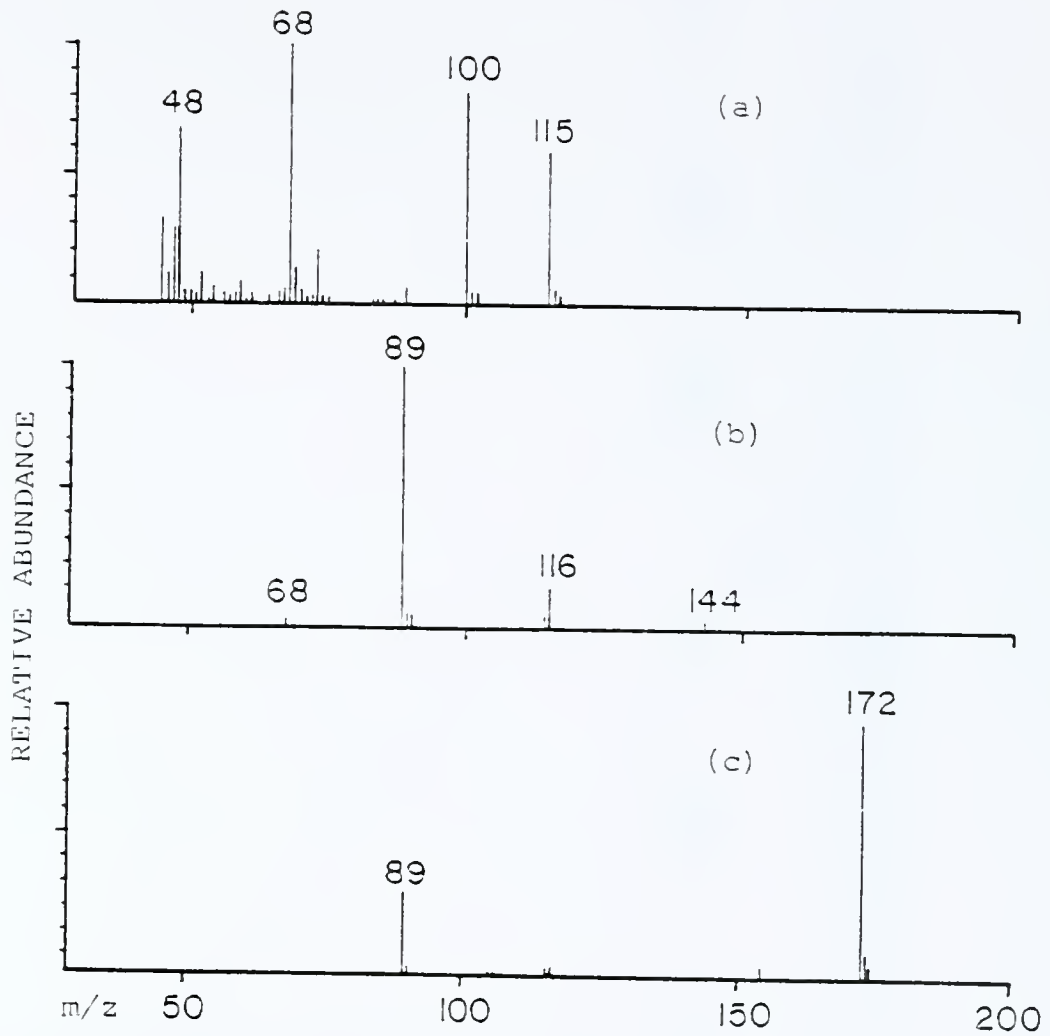
Figure 11. The mass spectra for aldicarb nitrile (molecular weight 115) with the source at 100 $^{\circ}$C by (a) electron impact, (b) positive methane CI, and (c) positive isobutane CI.
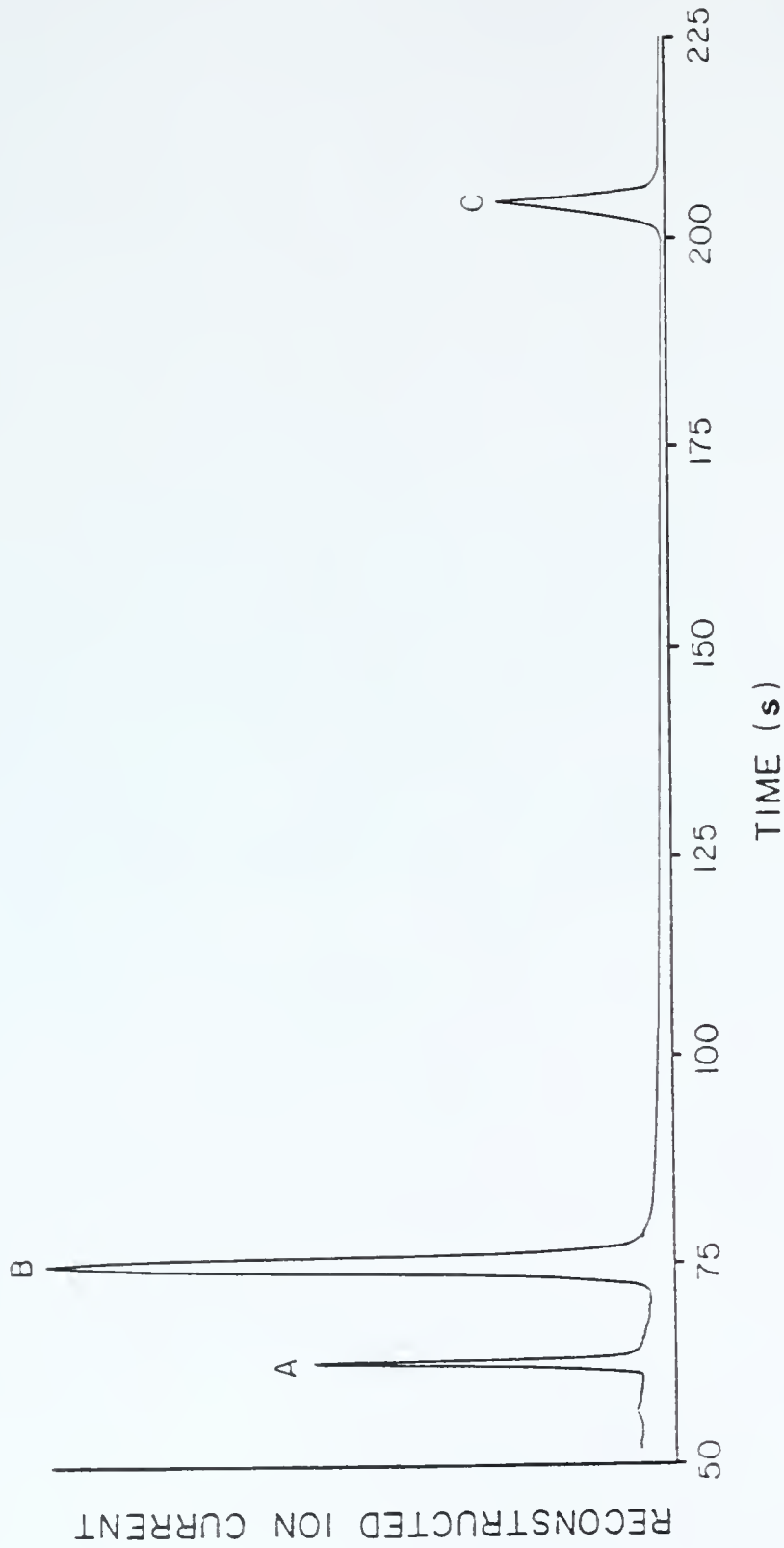
Figure 12. Reconstructed ion current (RIC) for (a) aldicarb oxime, (b) ethyl benzoate, and (c) aldicarb in methylene chloride with a 2.5 m DB5 capillary column.
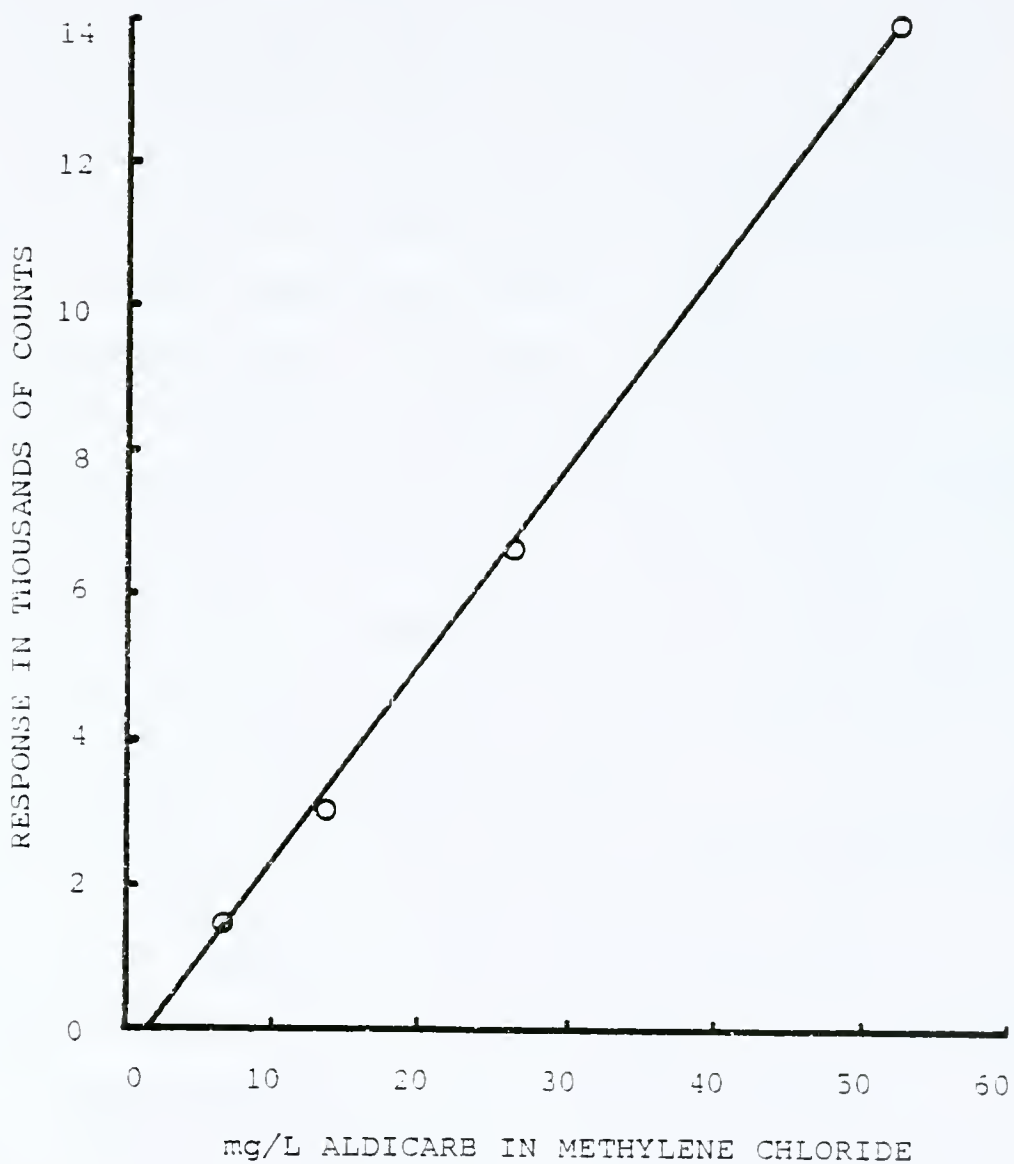
Figure 13. Response in counts vs concentration of aldicarb in methylene chloride with a 2.5 m DB5 capillary column.

The use of a short SE54 capillary column produced poorer limits of detection for aldicarb than did the "equivalent" bonded phase DB5 column, possibly due to adsorption on the column. It was also observed that the condition of the injection port had considerable influence on the sensitivity and linearity of the aldicarb analysis. A clean silanized glass insert was necessary to obtain a linear response from 1.5 ng to 150 ng injected. The limit of detection for aldicarb was 0.3 ng at a S/N ratio of 3 when the 2.6 m DB5 capillary column was used.

Aldicarb oxime does not thermally degrade even with an injection port temperature of 350 $^\circ$C (9). The narrow peak width of aldicarb oxime necessitated the use of a fast scan repetition rate (0.27 s/scan) in order to obtain sufficient data points to quantitate the 1.5 s wide peak. Aldicarb oxime was found to have a linear response from 1.2 ng to 150 ng, with a LOD of 1.2 ng.

The analysis for aldicarb nitrile is complicated by the formation of aldicarb nitrile from aldicarb in a hot injection port. Aldicarb nitrile can be selectively determined, however, if the injection port is maintained at 60 $^\circ$C. A sample containing 1.28×10^3 mg/L aldicarb produces a response corresponding to 1.3 mg/L of aldicarb nitrile due to its formation in the injection port. The variation in the observed responses for aldicarb nitrile and aldicarb as the temperature of the injection port is increased is shown in Table 17. The linear dynamic range

Table 17. Response for aldicarb (I) and aldicarb nitrile (II) in thousands of counts vs temperature of the injection port when aldicarb is injected at a concentration of 1.28 mg/mL.

Temperature °C	area for (I)	area for (II)	Ratio of (II/I)
60	142	1.08	0.0076
100	2850	10.0	0.0035
140	8100	104.	0.0130
180	4368	359.	0.0821
220	1531	862.	0.563

for aldicarb nitrile was found to be from 0.15 ng to 150 ng with a LOD of 0.05 ng.

The determination of aldicarb sulfoxide and aldicarb sulfone was not possible using the 2.6 m capillary column. Aldicarb sulfoxide is less volatile than aldicarb and appears to be even more thermally labile. Since these compounds can be analyzed by direct probe insertion, the use of even shorter capillary columns might provide a means for their analysis.

Mass Spectrometry

Analysis by Direct Probe Insertion

Direct probe insertion is an effective method of analysis for compounds which are not volatile at room temperature. If a tandem mass cpectrometric technique is not used then in order for quantitative analysis to be practical, the analyte must either ionize to form a unique ion or a pre-separation process is necessary. Figure 14 shows the standard curve obtained for the determination of aldicarb sulfoxide by direct probe insertion. Positive isobutane CI was used with SIM for the MH^+ ion. Carbaryl (1-Naphthalenol methylcarbamate) was used as the internal standard. It is notable that non-linear response curves were obtained for aldicarb, aldicarb sulfoxide and aldicarb sulfoxide oxime with this method. Only aldicarb sulfone was found to have a linear response plot.

76
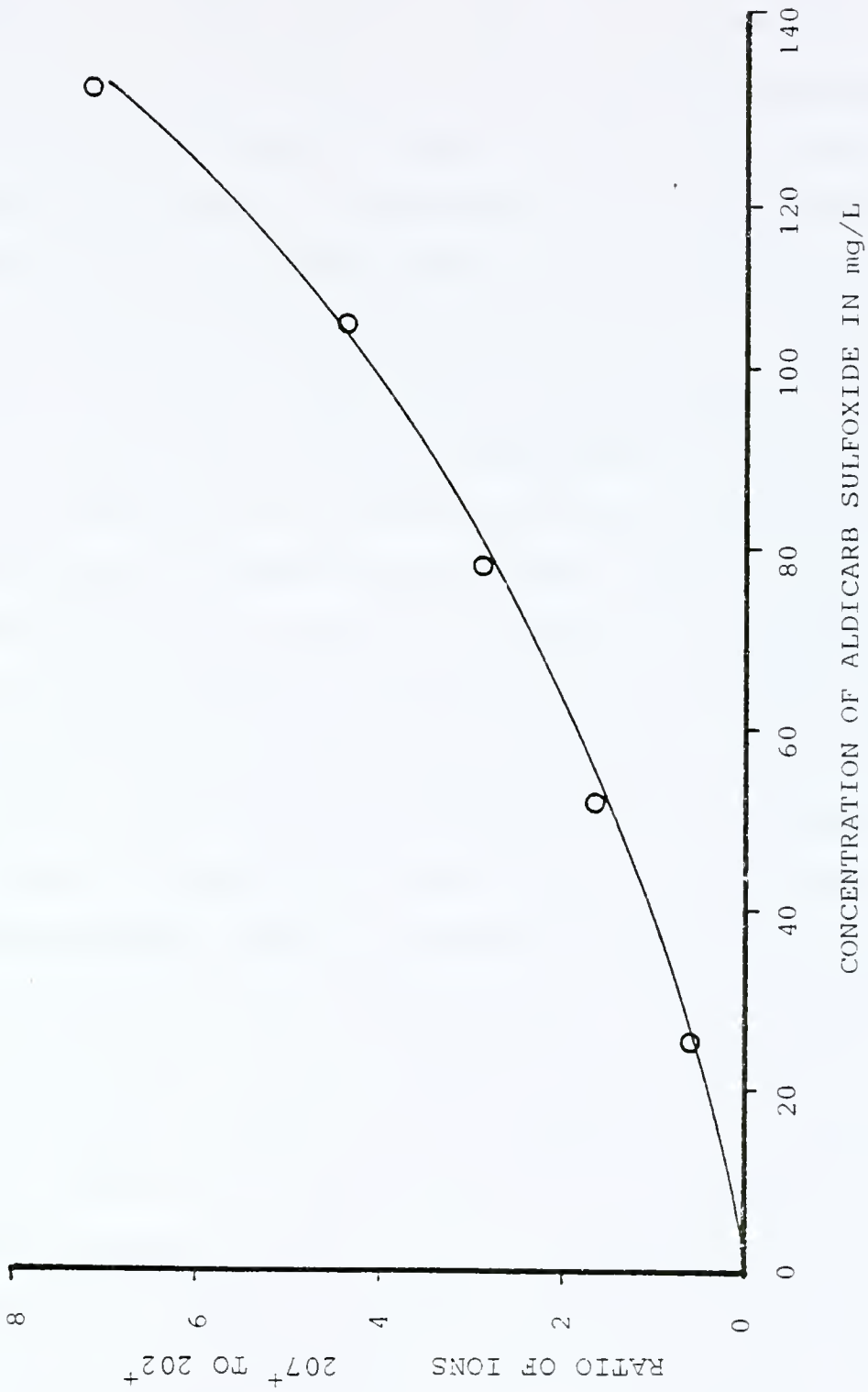
Figure 14. Response vs concentration of aldicarb sulfoxide by SIM of standards introduced by the solids probe. The ratio of the intensity for the aldicarb sulfoxide m/z 207 ion to the internal standard, carbaryl, m/z 202 ion is plotted vs the concentration of aldicarb sulfoxide in the sample.

As discussed in the previous chapter, the mass resolution capabilities of tandem mass spectrometry, MS/MS, can be used to replace or enhance the chromatographic resolution obtained with GC/MS or LC/MS. An alternative method of analysis for compounds that are difficult to determine by gas chromatography is to introduce the samples with the solids probe and analyze by SRM. If there are two compounds present, then spectral interference can occur. If it is assumed that the other component can fragment with equal probability of forming any of the ions that can be determined by the mass spectrometer, then an estimate of the selectivity of the method can be made. The selectivity of this method should be proportional to the probability of randomly selecting the parent and daughter ions used in the analysis. The lower the probability for coincidental overlap, the greater the selectivity of the method. Unlike chromatography, where an individual compound can result in only one peak, in mass spectrometry a single compound often ionizes to form numerous ions of varying intensity. If we assume that the parent ion, P, fragments in the source to form a total of 20 ions, and that each of these ions can further fragment in CID to form 5 daughter ions, then the selectivity of SRM for samples introduced by direct probe insertion can be estimated. The probability of a second component forming the same parent ion selected for fragmentation is 0.02 (20 ions/1000 possible ions) when a mass spectrometer with unit mass resolution and a mass range

of 1000 is used. SRM contains an additional mass resolution step. If the same parent ion were chosen as that of the second component, then the probability for the parent ion of the second component to fragment with the formation of the same selected daughter ion may be estimated. The number of possible daughter ions is one less than the mass of the parent ion, P, so that the probability is $5/(P-1)$. Since the probability for spectral interference is dependent on the mass of the parent ion, the probability for all possible parent ions from m/z 1 to 1000 was calculated and averaged. The average probability for spectral interferece was calculated to be 0.025. The probability of randomly selecting a given parent ion and daughter ion is given by the product of the two probabilities or 0.0005.

For comparison, the selectivity of SIM in combination with gas chromatography can be estimated. A column that has 100,000 theoretical plates could resolve approximately 1000 compounds in an hour. If the selectivity of the SIM process is once again 0.02, then the probability of two compounds detected on the column having overlapping retention times and ionizing with the formation of the same ion is 0.00002. Thus, GC/MS with selected ion monitoring and a capillary column with 100,000 theoretical plates can be estimated to be 25 times more selective than analysis by direct probe insertion with SRM. However, analysis by the direct probe insertion technique only requires a few minutes, while analysis by GC/MS would require an hour. SRM could be used

as a rapid screening technique, since its selectivity is still adequate to avoid frequent false positives.

The positive isobutane CI mass spectra for 2 of aldicarb's degradation by-products, aldicarb sulfoxide oxime and aldicarb sulfone, are shown in Figures 15(a) and 16(a). The daughter spectra for the corresponding MH^+ ions are shown in Figures 15(b) and 16(b), respectively. The MH^+ ions formed could be used for analysis of aldicarb's thermally labile by-products by SRM. In order to demonstrate the potential for SRM with direct probe insertion, a sample of orange juice was extracted with methylene chloride and the concentrated extract was then spiked with aldicarb sulfone. The extract contained 1.8 ppm of aldicarb sulfone. Selected reaction monitoring for 223^+ fragmenting to form 166^+ produced the reconstructed ion chromatogram shown in Figure 17. The presence of aldicarb sulfone can be clearly seen in 17(b), while no apparent signal was observed in the analysis of an extract which did not contain aldicarb sulfone 17(a). This technique could provide a means for rapid screening of crops or food products suspected to contain aldicarb or its degradation by-products. An additional advantage of analysis by direct probe insertion is the avoidance of contamination of the capillary column and injection port with non-volatile components, which could adversely affect the chromatographic separation of subsequent samples. Contamination of the source can also cause significant
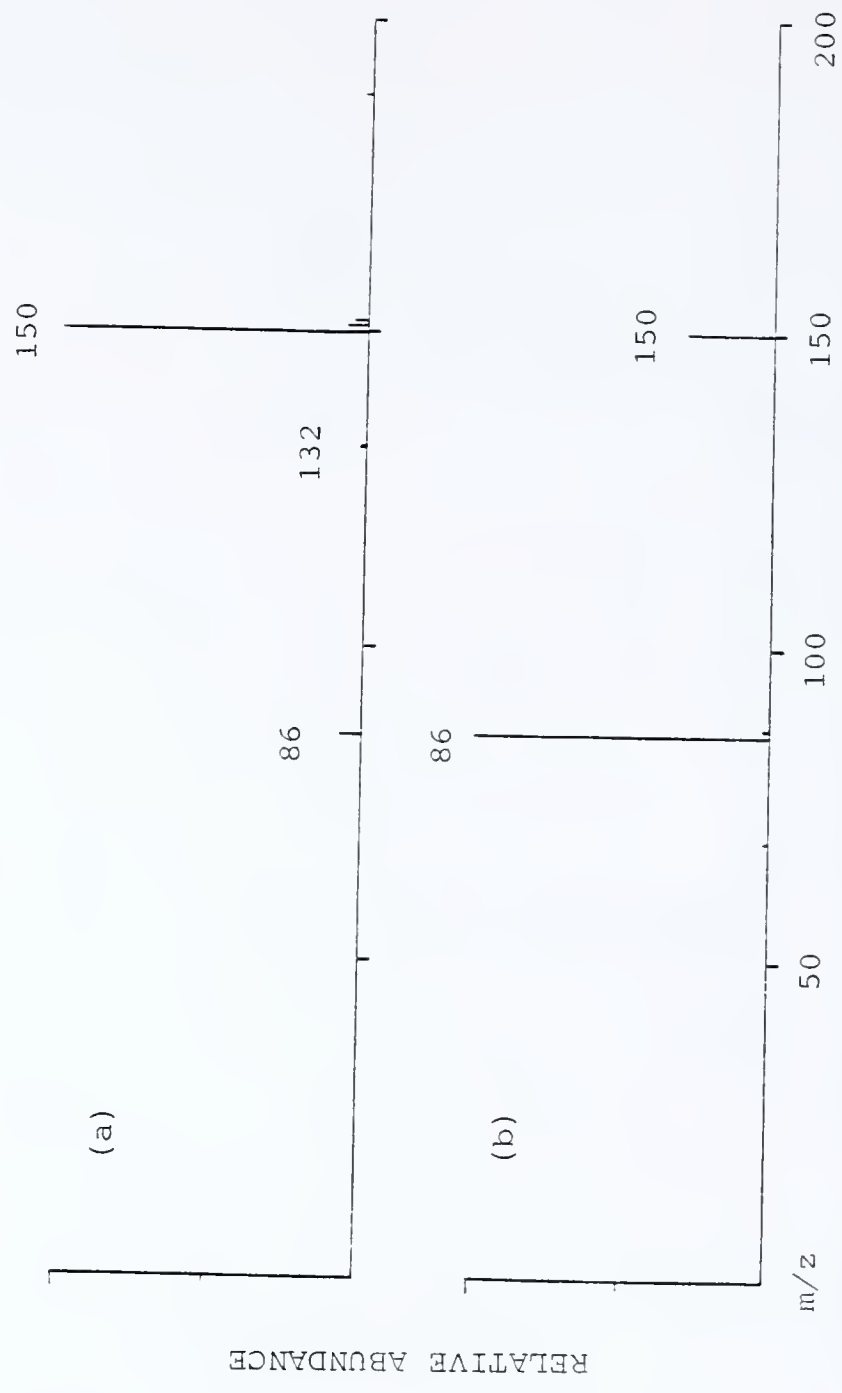
Figure 15. The positive isobutane CI mass spectrum for aldicarb sulfoxide oxime is shown in (a) while the daughter spectrum of the MH$^+$ ion, m/z 150, formed in positive isobutane CI is shown in (b).
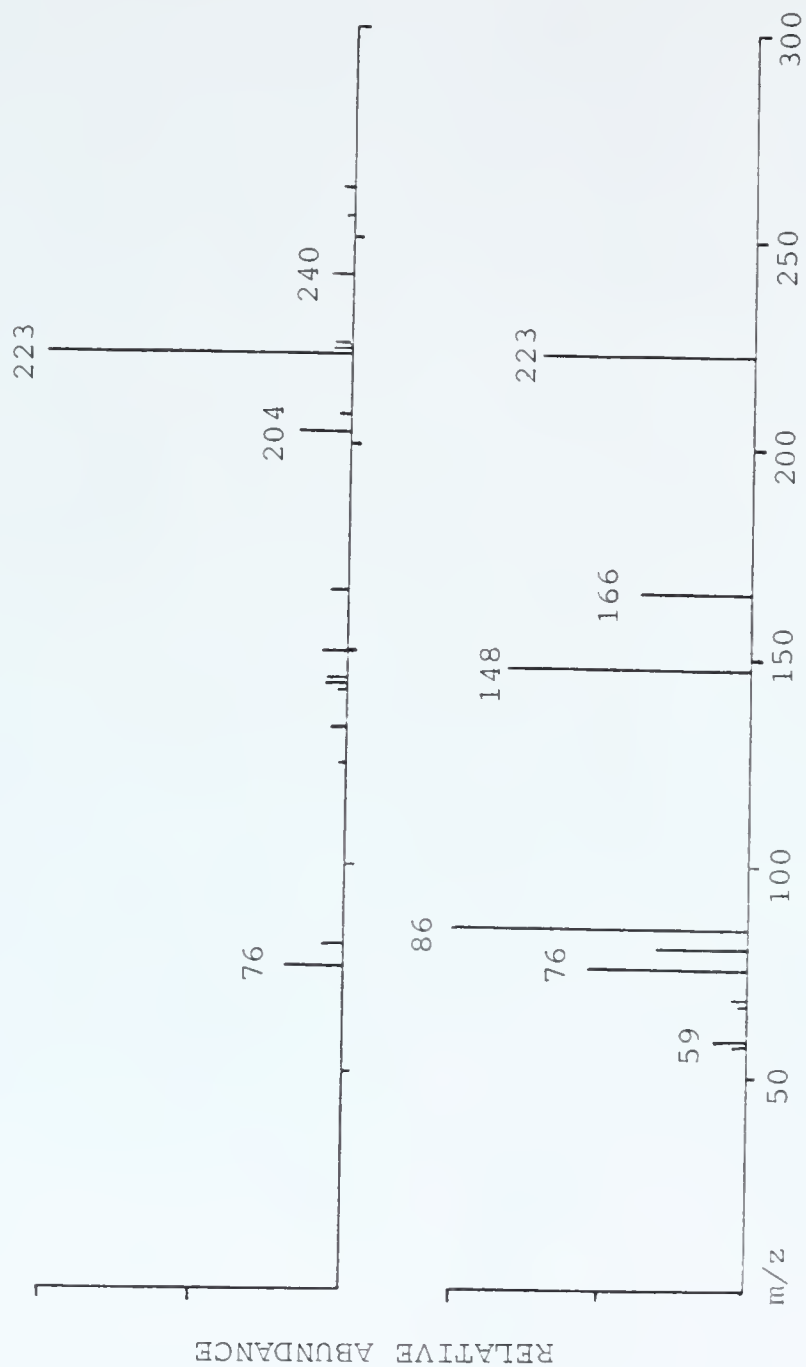
Figure 16. The positive isobutane CI mass spectrum for aldicarb sulfone is shown in (a) while the daughter spectrum of the MH^+, m/z 223 ion, formed in positive isobutane CI is shown in (b).
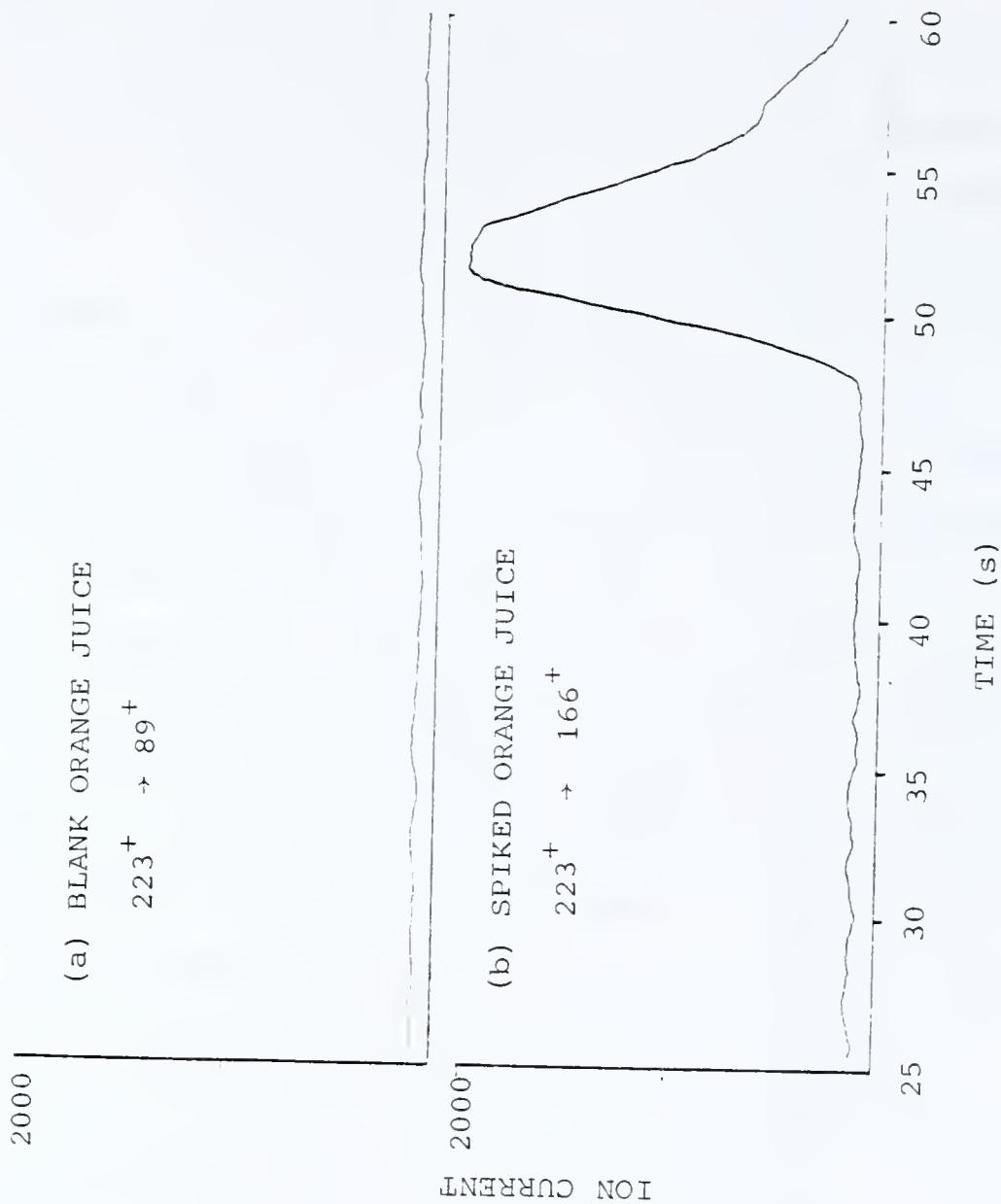
Figure 17. Analysis of an extract from (a) a blank sample of orange juice and (b) a sample of the same extract with 1.8 mg/L of aldicarb sulfone in the concentrated methylene chloride extract.

difficulties, but can be reduced by frequent replacement of the ion volume in the source.

Mass Spectra

The CI sensitivity obtained with methane was 4 times greater than that obtained with isobutane; however, this gain in sensitivity was offset by the higher chemical background due to greater ionization of the methylene chloride solvent with methane. In addition to the MH^+ ion, m/z 116, for aldicarb nitrile, the isobutane spectra for aldicarb nitrile (Figure 11c)contains a twenty-times more intense $(M+57)^+$ ion, m/z 172, corresponding to the addition of isobutane ion to the aldicarb nitrile molecule. The methane CI spectrum for aldicarb nitrile contains the MH^+ ion plus the less intense $(M+29)^+$ and $(M+41)^+$ ions (Figure 11b). The EI spectrum for aldicarb nitrile is characterized by the presence of an abundant molecular ion, 115^+ (Figure 11a). It has been reported that aldicarb dehydrates on a 2% OV-17 column, based on the presence of a m/z 172 ion $(M-18)^+$ in the isobutane CI spectrum (16). Our data suggest that this corresponds instead to the $(M+57)^+$ ion of the nitrile. In order to confirm that the m/z 172 ion in the isobutane CI spectrum of aldicarb nitrile was indeed the $(M+C_4H_9)^+$ ion, a CID daughter spectrum was acquired. This configuration of the tandem mass spectrometer is illustrated in Figure 18. The major fragments were: m/z 57, $(C_4H_7)^+$; m/z 89, $(C_4H_9S)^+$; and m/z 116, $(172-C_4H_8)^+$, as shown in Figure 19a.
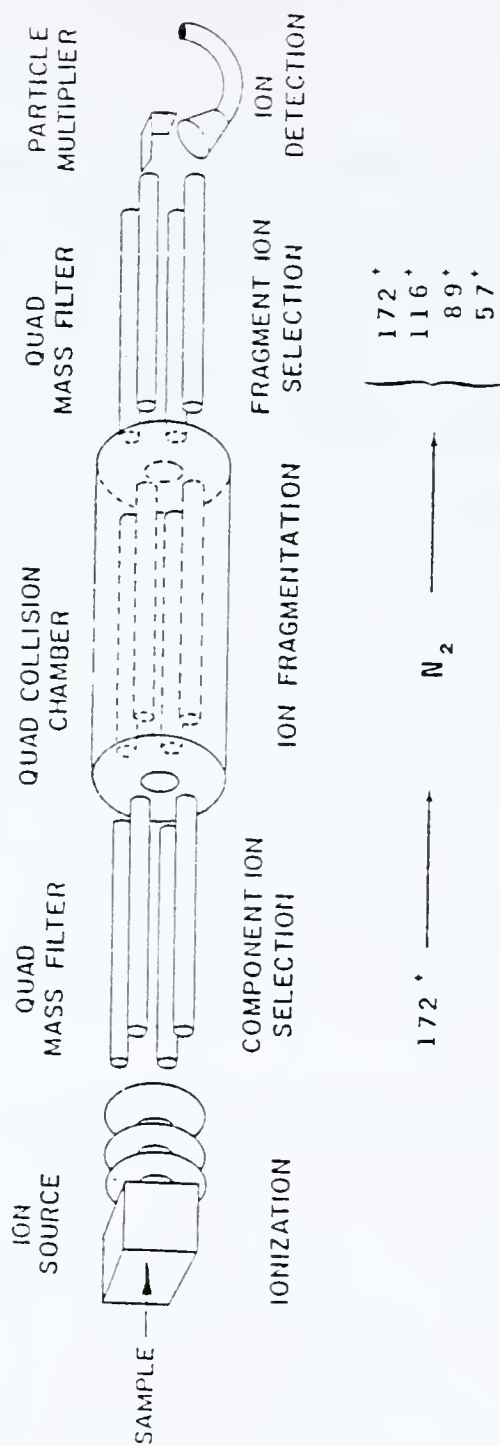
Figure 18. Configuration of the Finnigan TSQ45 mass spectrometer for CID spectra. The fragmentation of the m/z 172 is illustrated and the expected daughters ions are shown.

In contrast, the CID daughter spectrum of the MH^+ ion m/z 191 of aldicarb does not yield a 57^+ ion or a $(191-C_4H_8)^+$ ion, as shown in Figure 19b.

Precision

The temperature and pressure dependence of the isobutane positive CI spectrum of aldicarb was determined. The maximum sensitivity can be seen to occur when the uncorrected isobutane pressure in the source is approximately 0.8 torr (corrected pressure 0.22 torr), as shown in Figure 20. The relative standard deviation in the analysis for aldicarb with positive CI SIM was found to be 25%, while with EI, the relative standard deviation was only 10%. The considerably greater standard deviation in CI is likely attributable to changes in the CI gas pressure. The use of an internal standard with a retention time closer to that of aldicarb, such as a deuterated analog of aldicarb, would be expected to improve the precision and sensitivity (67).

The temperature dependence of the CI spectrum of aldicarb is shown in Figure 21. The change in the intensity of the signal for a given ion is relatively small with respect to the temperature fluctuations likely to occur in the source, and would be expected to have only a minor impact on the observed response during analysis. However, the selection of the temperature to use for the analysis could significantly influence the observed sensitivity. The signal intensity for the m/z 116 ion decreases by a factor
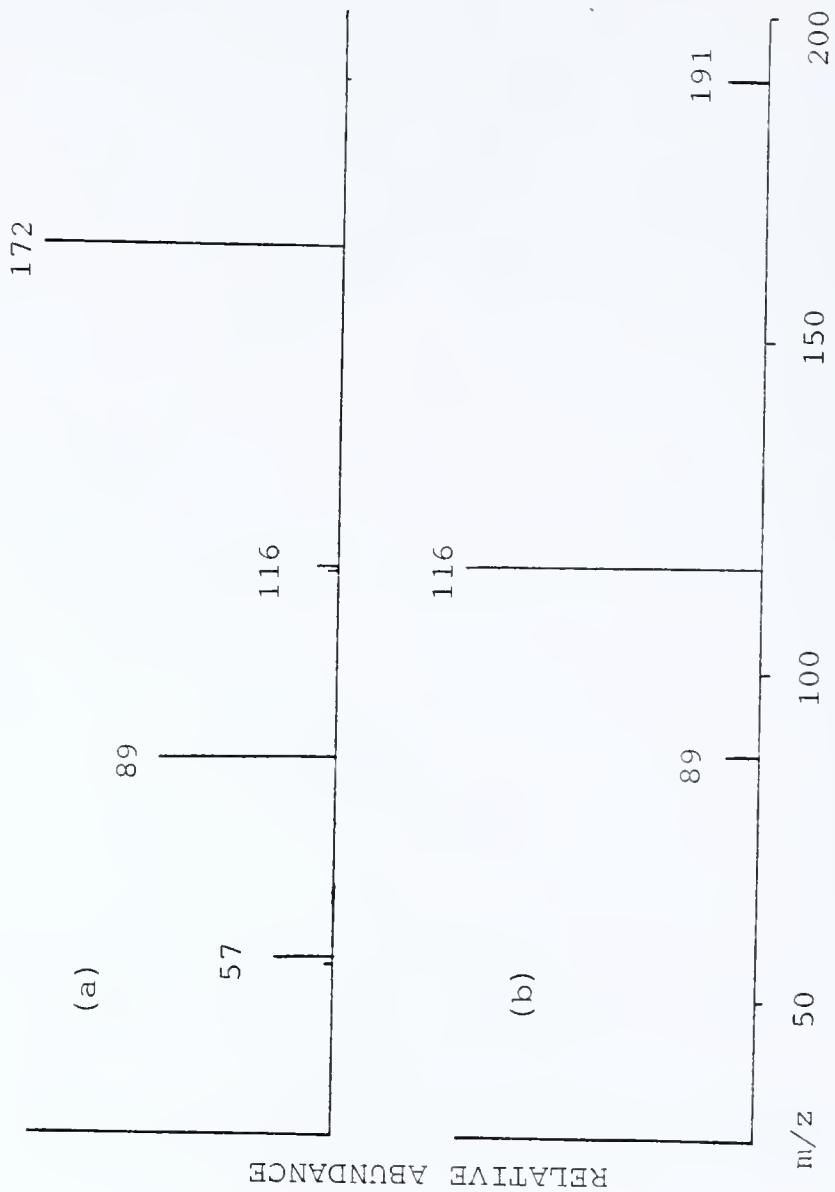
Figure 19. The daughter spectrum of the m/z 172 ion is shown in (a) and that of the m/z 191 ion in (b). The m/z 172 ion fragments to yield the m/z 57 ion indicating that the m/z 172 ion is actually an adduct ion of aldicarb nitrile, mass 115, with the isobutane reagent gas ion, mass 57.
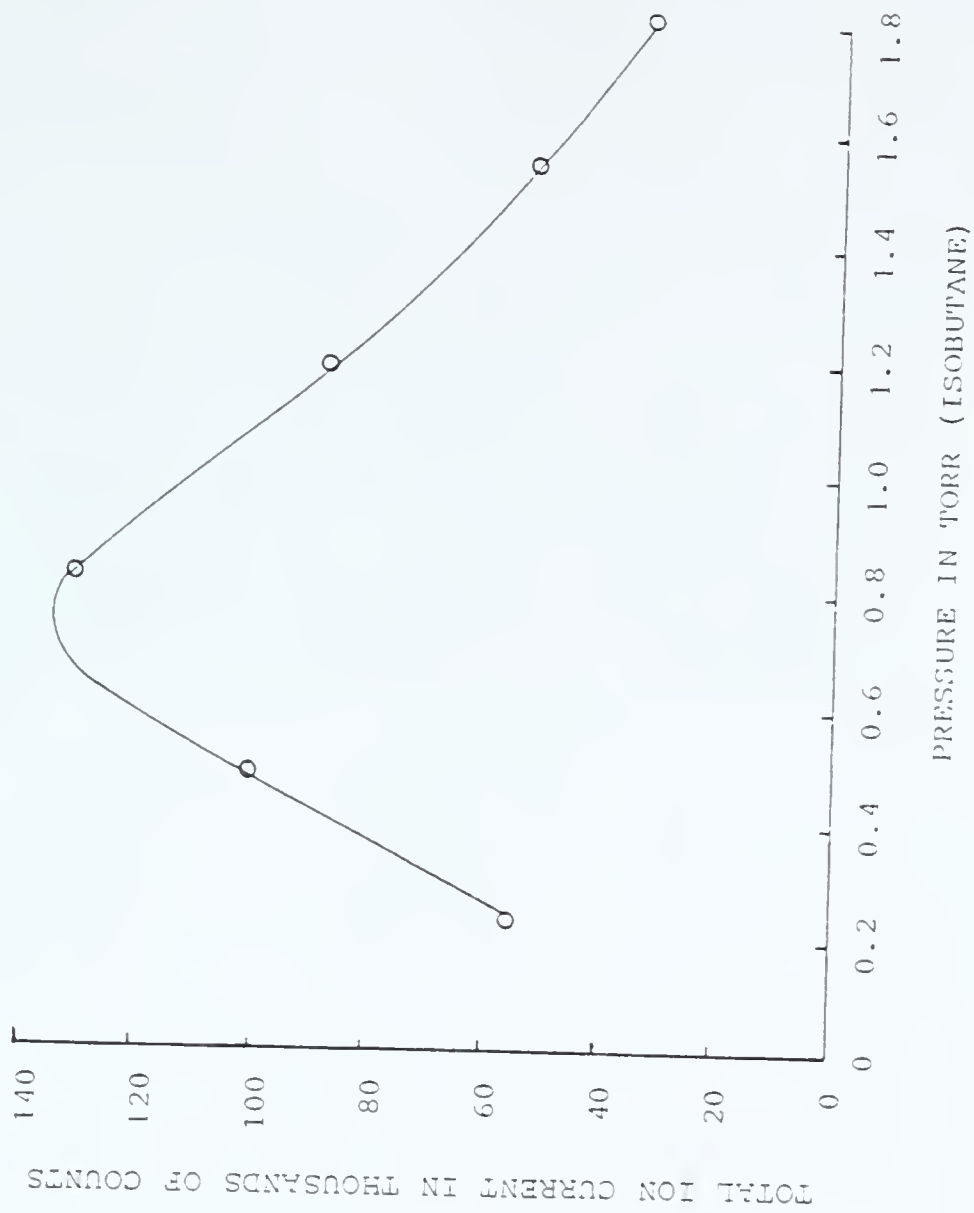
Figure 20. Response obtained for aldicarb vs isobutane CI reagent gas pressure.
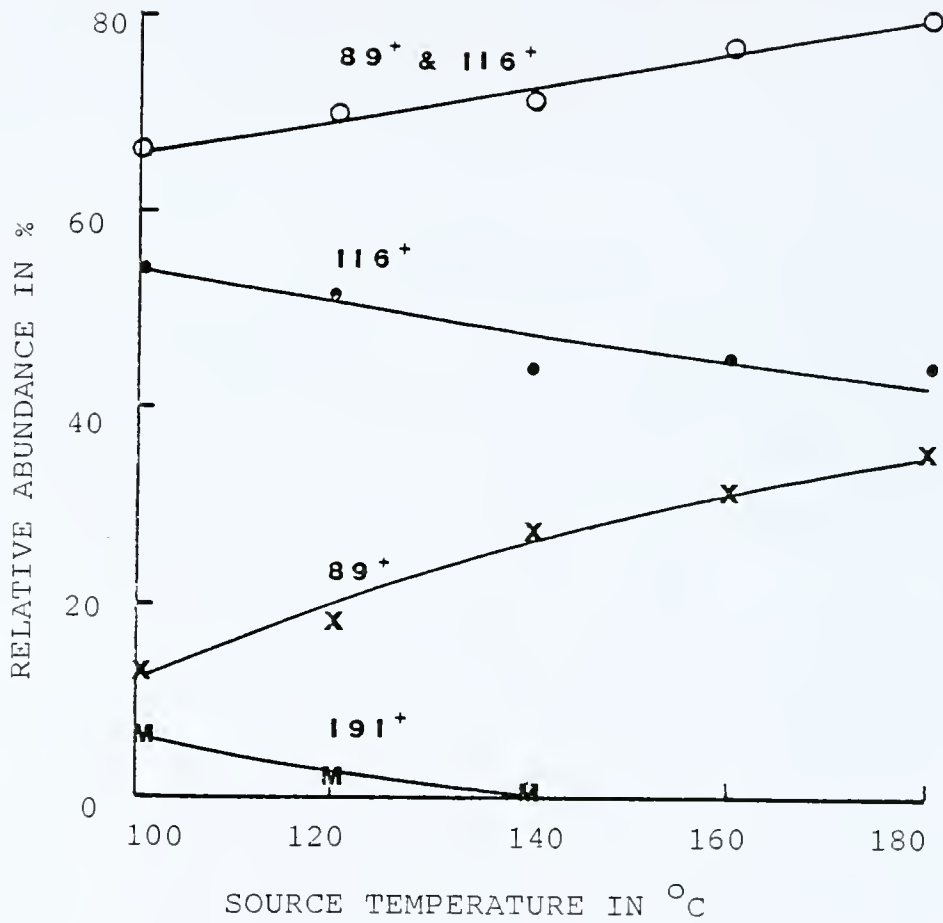
Figure 21. Relative abundance vs source temperature for the m/z 89, 116, and 191 ions in the positive isobutane CI of aldicarb.

of approximately 20%, while the sensitivity for the m/z 89 ion increases by a factor of 200%, as the temperature of the source is changed from 100 $^{\circ}$C to 180 $^{\circ}$C.

Quantitation was performed using selected ion monitoring (SIM) with ethyl benzoate as an internal standard. In order to obtain greater precision in the data, all the samples were run in a single day. The samples that had been previously extracted with methylene chloride and stored in sealed septum bottles at 4 $^{\circ}$C were analyzed at a rate of 6/h.

Conclusions

The half-life for aldicarb at pH 8.2 in sterile anaerobic water was 43 d. Essentially all of the degraded aldicarb could be accounted for by the formation of aldicarb oxime. Aldicarb oxime was found to be stable in alkaline conditions as high as pH 11 for 2 weeks.

In the presence of a high concentration of microorganisms or in the presence of ground limestone under anaerobic conditions, aldicarb degraded rapidly with the formation of aldicarb nitrile. In these samples, 85% of the original aldicarb had degraded in less than two weeks. Aldicarb nitrile was found in these samples to account for 100% of the degraded aldicarb. This is of particular interest since aldicarb nitrile gives a positive interference for aldicarb when conventional GC methods are used. A florisil clean-up procedure is not necessary with

the short column method employed in this study, because the intact aldicarb molecule itself is determined.

The conversion of aldicarb to aldicarb nitrile probably involves an intramolecular rearrangement both in the gas phase for thermal degradation in the injection port, and in aqueous solutions in the presence of microorganisms or ground limestone. This pathway has been suggested as the mechanism for the synthesis of aldicarb nitrile from aldicarb employed in this study (62). Aldicarb, I, thermally degrades to aldicarb nitrile, V, and N-methylaminomethanoic acid, VI.

$$CH_3-S-\underset{\underset{CH_3}{|}}{\overset{\overset{CH_3}{|}}{C}}-CH=N-O-\overset{\overset{O}{\|}}{C}-NH-CH_3 \rightarrow CH_3-S-\underset{\underset{CH_3}{|}}{\overset{\overset{CH_3}{|}}{C}}-C\equiv N + HO-\overset{\overset{O}{\|}}{C}-NH-CH_3$$

$$(I) \qquad\qquad\qquad (V) \qquad\qquad (VI)$$
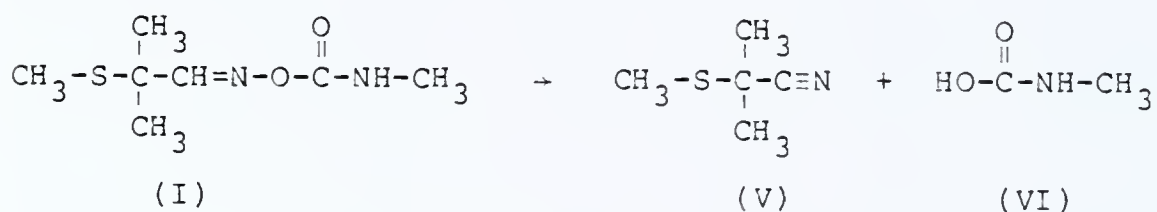
The base peak in the CID daughter spectra of the MH^+ ion for aldicarb is the m/z 116 ion, which corresponds to the aldicarb nitrile MH^+ ion. The base peak in the electron capture negative methane CI spectra for aldicarb is 74^-, which is presumably the N-methylaminomethanoate ion.

CHAPTER 5
EFFECT OF INSTRUMENTAL PARAMETERS ON THE COLLISION-INDUCED DISSOCIATION OF ALDICARB

The added resolution provided by tandem mass spectrometry (MS/MS) for the determination of aldicarb in complex mixtures was shown in Chapter 3 to enhance the LOD, while the added structural information provided by CID spectra was shown in Chapter 4 to be of value in the identification of ions formed in the source. Application of MS/MS techniques such as these could be further improved by evaluating the effect of the mass spectrometric parameters such as source temperature (ion internal energy), collision energy, collision gas, and collision gas pressure, which are under the control of the analyst. The choice of operating conditions is important for optimization of tandem mass spectrometric conditions. For example, the selectivity of the SRM process can be seen to be dependent on the number of fragment ions formed in the CID process. As the number of fragment ions increases for both the analyte and the contaminant, the selectivity of SRM is expected to decrease due to spectral interference.

This increased fragmentation, while detrimental to the selectivity of SRM, is desirable for the generation of CID library spectra, because the information content of the spectra increases rapidly as the number of fragment ions

increases. The number of possible combinations of n objects taken r at a time (68) is given by the equation shown below.

$$\# \text{ of combinations} = \frac{n!}{(n-r)! \; r!} \qquad (5\text{-}1)$$

From this simple calculation, one can estimate that, for an ion with a m/z of 150 with unit mass resolution, the possible number of unique CID spectra for 1, 2, 3, 4 and 5 fragment ions formed on CID is 150, 1.1×10^4, 5.5×10^5, 2.0×10^7 and 5.9×10^8, respectively. Clearly, CID spectra offer greater potential for the identification of ions when the parent ion fragments to form more ions.

For CID spectra to be of value for the identification of trace components, the spectra should be obtained under conditions of maximum sensitivity, while still retaining significant fragmentation for interpretation. In addition, since CID spectra are strongly influenced by the instrumental conditions used, standard conditions for CID spectra should be selected, so that interchange of library spectra are possible. In this chapter, the influence of temperature, target gas density and collision energy on CID will be evaluated.

<u>Experimental</u>

<u>Apparatus</u>

A Finnigan TSQ45 triple-stage quadrupole mass spectrometer/data system was used in this study. The electron energy was 100 eV for chemical ionization. The

chemical ionization reagent gas was methane or isobutane. The mass spectrometer was tuned with FC43 (perfluorotributylamine). The continuous dynode electron multiplier was operated at 850-1000 V with the conversion dynodes at ±3000 V. The preamplifier gain was set for 10^8 V/A. Aldicarb was introduced by direct probe insertion, while aldicarb nitrile was introduced by direct leak. For studies involving CID at pressures from 3.5×10^{-5} torr to 5.2×10^{-5} torr [corrected ion gauge pressures, (69)] in the collision chamber, the pressure in the collision cell was varied by changing the CI reagent gas pressure from 0.5 to 1.0 torr (0.3 to 0.6 torr corrected Pirani gauge readings). Experiments with higher collision pressures were done with nitrogen or argon as the collision gas.

<div align="center">Effect of Source Temperature</div>

Ion Internal Energy

Reactions that are observed in tandem mass spectrometry occur during the microsecond time span that ions are in the quadrupoles. The unimolecular reaction of the protonated aldicarb ion (I) to form the protonated aldicarb nitrile ion (V) and methylaminomethanoic acid (VI) is likely to occur by way of the intramolecular rearrangement shown below.

$$CH_3S-\overset{\overset{\displaystyle CH_3}{|}}{\underset{\underset{\displaystyle CH_3}{|}}{C}}-CH=N\overset{+}{\diagdown}\overset{H}{\underset{O}{\diagup}}\overset{O}{\underset{\diagdown}{\overset{\|}{C}}}NHCH_3 \quad \rightarrow \quad CH_3S-\overset{\overset{\displaystyle CH_3}{|}}{\underset{\underset{\displaystyle CH_3}{|}}{C}}-\overset{+}{C}\equiv NH \quad + \quad HO\overset{\overset{\displaystyle O}{\|}}{C}NHCH_3$$

<div align="center">(I)   (V)   (VI)</div>
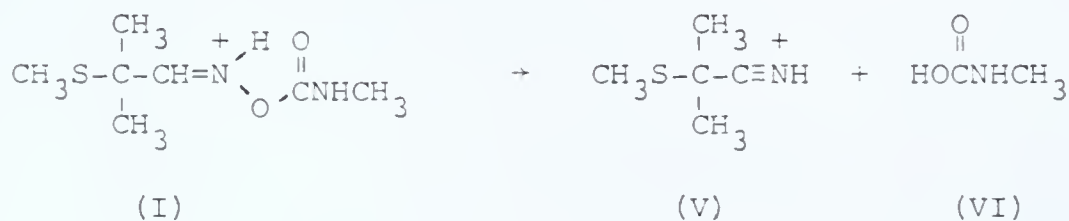
<div align="center">Scheme II</div>

This reaction has a low critical energy and high critical entropy requirement, which is characteristic of metastable ion reactions observed in double-focussing mass spectrometers (70). The low energy pathways for the dissociation of these ions increase the likelihood of observing internal energy effects in their CID spectra. The collision conditions were varied in order to determine if the internal energy of the protonated aldicarb ion significantly influences its CID spectrum, and to determine the energy of activation for the unimolecular dissociation of this ion.

Detection of Metastable Ions

The fragmentation of aldicarb as a function of collision pressure was investigated in order to determine the rate of unimolecular dissociation of the protonated aldicarb molecule in the absence of CID. Aldicarb is known to undergo thermally an intramolecular rearrangement to form aldicarb nitrile (66). The intramolecular pathway for the dissociation of aldicarb was anticipated to increase the likelihood of observing internal energy effects in the low energy collisions of the protonated aldicarb ion. Methane and isobutane chemical ionization (CI) were used for ionization of aldicarb samples introduced by direct probe insertion. In order to observe the unimolecular dissociation, the tandem quadrupole mass spectrometer was tuned to pass the m/z 191 ion (MH$^+$) through the first quadrupole with a kinetic energy of 6 eV. In the second

quadrupole, which serves as a collision chamber, the m/z 191 ion was decelerated to 1 eV (LAB) where E_{LAB} is the collision energy in the laboratory frame of reference. This increases the time for unimolecular dissociation, so that the products formed by dissociation of metastable ions can be more easily detected (71). In the last quadrupole, the parent ion and its daughter ions were determined. A plot of ln(P/Po) versus target gas density (P and Po are the parent ion intensities at the specified target gas densities and in the absence of the target gas, respectively.) is shown in Figure 22 for the protonated aldicarb ion at two source temperatures, 120 ^{O}C and 160 ^{O}C. The contribution of unimolecular dissociation to net observed fragmentation at each temperature may be determined from the y-intercept of the plot. The internal energy acquired by the ion in the source influences both the unimolecular rate constant and the effective collision diameter determined from the slope of the plot. Approximately 6.4% and 7.7% of the protonated aldicarb ions formed at 120 ^{O}C and 160 ^{O}C, respectively, dissociate unimolecularly in the second quadrupole. The effective cross sections for the CID of the protonated aldicarb ion were found to be 5.1 x 10^{-15} and 7.6 x 10^{-15} cm^{2}/molecule at 120 ^{O}C and 160 ^{O}C, respectively.

The unimolecular dissociation of the aldicarb nitrile MH^{+} ion (m/z 116) was also investigated. Aldicarb nitrile was introduced by a direct leak into the source, and its protonated molecular ion was generated by methane CI. The

Figure 22. Plot of ln(P/Po) vs collision gas pressure for aldicarb with the source at 120 $^{\circ}$C and 160 $^{\circ}$C for positive methane CI. The parent ion intensity at zero pressure is represented by Po, while the parent ion intensity at higher pressures is given by P. The standard deviation in the intercept is shown (-0.0667 + 0.0026 at 120 $^{\circ}$C and -0.0807 + 0.0080 at 160 $^{\circ}$C).

aldicarb nitrile MH$^+$ ion fragments by CID to form the same CID spectrum as does the aldicarb m/z 116 ion which is formed in the source during CI of aldicarb. Thus, the protonated aldicarb nitrile ion is quite likely to be identical to the m/z 116 ion of aldicarb and provides a means to investigate the sequential dissociation of the protonated aldicarb ion. The unimolecular dissociation was studied at 130 ^{O}C and 180 ^{O}C. A plot of ln(P/Po) vs pressure is shown in Figure 23. Only 0.53% and 0.86% of the aldicarb nitrile dissociated unimolecularly during the time the 116$^+$ ion was in the second quadrupole at 130 ^{O}C and 180 ^{O}C, respectively. The effective cross sections were determined by this method to be 6.5 x 10^{-16} and 7.9 x 10^{-16} cm^2/molecule, with a collision energy of 0.9 eV and the source at 130 ^{O}C and 180 ^{O}C, respectively.

These experiments show that the internal energy of the ions influences both the y-intercept, which corresponds to the unimolecular rate constant, and the slope, which corresponds to the effective cross section for CID.

Rate Constants for Unimolecular Dissociation

Unimolecular reactions occur both in the source and during the time the ions are passing from the source to the detector. The rates for the unimolecular dissociation of the MH$^+$ ions of aldicarb and aldicarb nitrile were determined both in the source and while in the center quadrupole. The difference in the rate constants was anticipated to be indicative of the degree to which ions
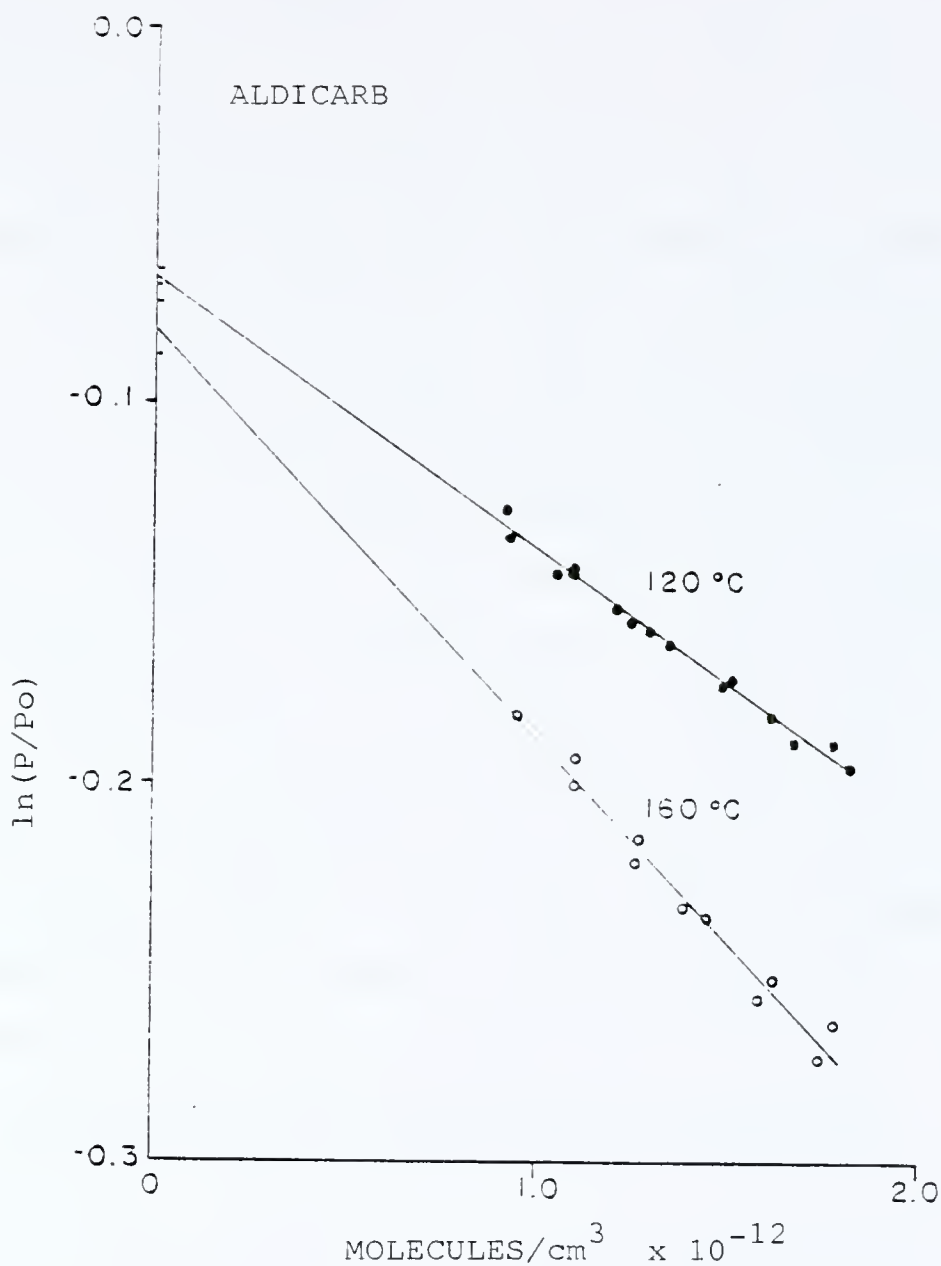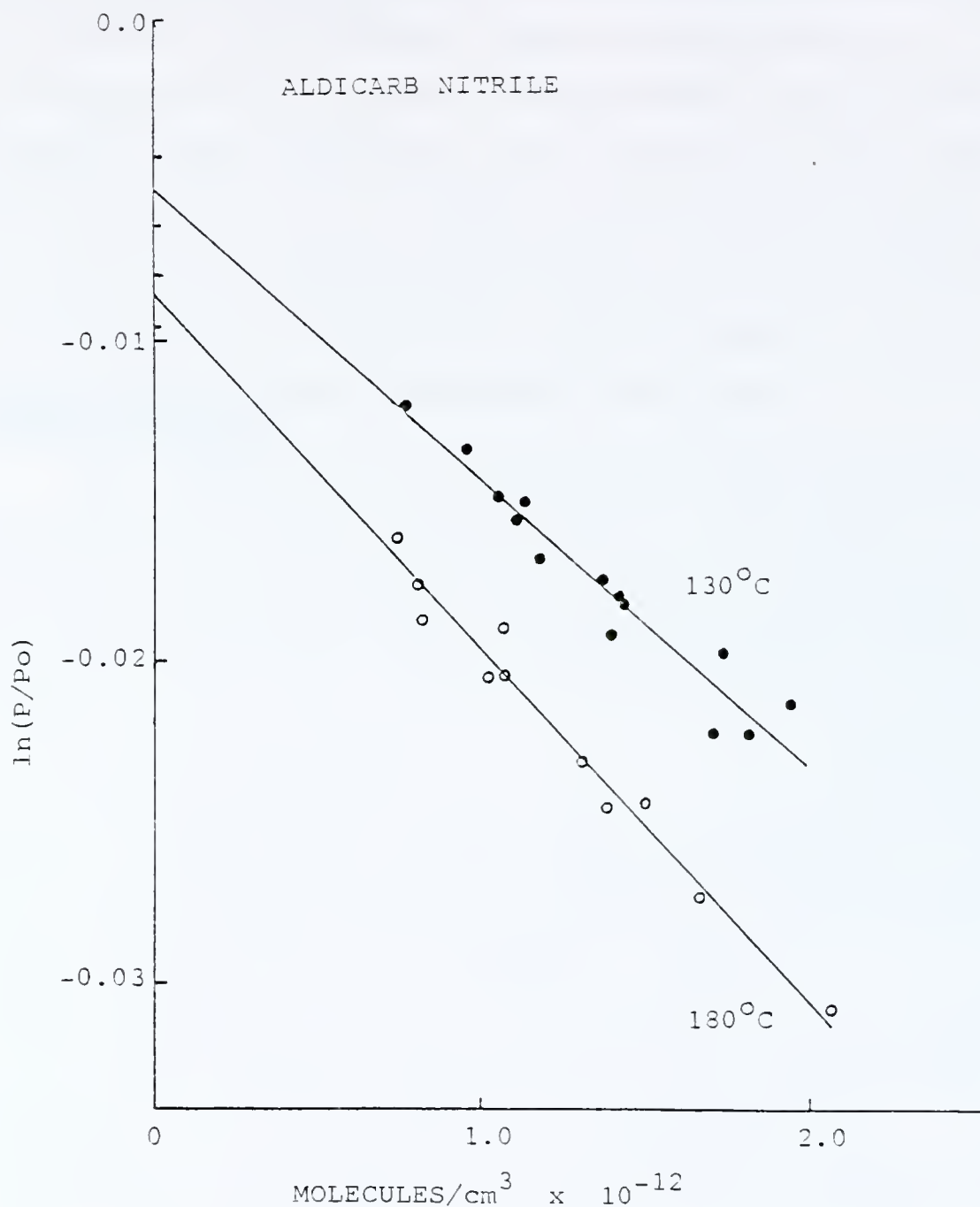
Figure 23. Plot of ln(P/Po) vs collision gas pressure for aldicarb nitrile with the source at 130 °C and 180 °C for positive methane CI. The parent ion intensity at zero pressure is represented by Po, while the parent ion intensity at higher pressures is given by P. The y-intercepts and the standard deviation in the intercepts are -0.0053 ± 0.0010 at 130 °C and -0.0086 ± 0.0007 at 180 °C.

which undergo CID had lost internal energy gained while in the source. Ions initially formed in the source are anticipated to have greater internal energy than ions which reach the center quadrupole, due to loss of internal energy by collisions in the ion volume, radiative energy losses, and rapid dissociation of ions which have internal energies in excess of that necessary for breaking bonds.

Rate of Dissociation of Metastable Ions in the Second Quadrupole

Rate constants for the unimolecular dissociation of metastable ions which dissociate while in the second quadrupole can be estimated, since the time the ions are in the second quadrupole region is given by equation 5-2 shown below:

$$t = L \, [m/(2eV)]^{1/2} \qquad\qquad (5-2)$$

where t is time in s, L is the length of collision cell in cm, m is the mass of the ion in g/molecule, and eV is the kinetic energy $(1.6 \times 10^{-12}$ erg/eV). When the kinetic energy is 0.9 and 1.1 eV, the 191^+ and 116^+ ions are in the second quadrupole for 147 and 104 μs, respectively. Assuming first order kinetics, the calculated rate constants for the unimolecular dissociation of aldicarb are 450 s^{-1} and 550 s^{-1} at 120 $^\circ$C and 160 $^\circ$C, respectively. For aldicarb nitrile, the rate constants are 51 s^{-1} and 83 s^{-1} at 130 $^\circ$C and 180 $^\circ$C, respectively. These rate constants are for ions which either did not have sufficient energy to dissociate while in the source or in the first

quadrupole, or have a preexponential factor in the Arrhenius equation sufficiently small that the rate of dissociation is slow. The steric requirement for the intramolecular rearrangement of aldicarb slows the reaction, so that the ions which reach the second quadrupole retain a portion of the internal energy they acquired in the source. However, the observed unimolecular reaction is quite likely skewed due to loss by fragmentation of the more energetic ions in the first quadrupole. The greater the internal energy of the parent ion, the more likely that the ion will dissociate prior to entering the second quadrupole. This loss due to unimolecular dissociation in the first quadrupole is of interest, since it should result in a leveling effect on the range of internal energies that ions have upon entering the collision cell. CID spectra obtained with lower accelerating potentials in the first quadrupole are therefore not expected to be as sensitive to the mode of formation of the ion and its internal energy in the source.

Rate of Unimolecular Dissociation in the Source

In order to investigate the internal energy of ions in the source vs those which reach the second quadrupole region, the rate for the unimolecular dissociation of aldicarb in the source was determined.

Residence time of ions in the CI source. The half-life for the reagent gas in the CI ion volume is calculated to be approximately 0.7 ms for a gas flow of 0.122 ml/s at 760 torr, a CI reagent gas pressure of 0.48

torr (corrected) in the source, and a CI volume of 0.2 ml. The source for the generation of ions is operated at ground potential. Due to the closed design of the ion volume and the application of low potentials on the extraction lens, -1 to -2 V, the ions are not likely to experience a significant potential gradient while in the ion volume.

Rate constants for the unimolecular dissociation of aldicarb and aldicarb nitrile can be estimated from the rate of fragmentation of the parent ions in the CI ion source (72). The reaction of the protonated parent ion in the source is analogous to that in a stirred-flow reactor. For first order kinetics, the rate constant can be determined from the relationship (73) shown below:

$$k \ (a-x) = (u/V) \ x \qquad\qquad (5-3)$$

where k is the rate constant, u is the flow rate, V is the volume of cell, a is the initial concentration, and x is the the steady state concentration of the fragment ions.

The rate constants for the dissociation of aldicarb in isobutane CI at 70, 90, 110, 132, 150, and 170 $^{\circ}$C are estimated to be 4.5×10^3, 7.0×10^3, 1.1×10^4, 2.4×10^4, 4.4×10^4, and 1.15×10^5 s^{-1}, respectively. These rate constants are 200 times greater than those estimated from the rate for the unimolecular dissociation of the protonated aldicarb ions in the second quadrupole. The considerable difference in the observed rate constants for dissociation in the source versus that observed in the collision cell can be attributed to the loss of the more energetic ions by

fragmentation or deactivation either through low energy collisions or radiative processes in the source or in the first quadrupole (74).

Effective Cross Section

The ratio of the effective cross section to the maximum effective cross section for the CID of protonated aldicarb and aldicarb nitrile ions were determined. The maximum effective cross section was calculated from the loss of the parent ion at higher collision energies, with the contribution of unimolecular dissociation subtracted. Figures 24 and 25 show the effect of collision energy on the transmission of the parent ions, 191^+ and 116^+, for aldicarb and aldicarb nitrile, respectively. The effective cross section for aldicarb, obtained from the slope of the plot of ln(Po/Po) vs target-gas density (in molecules per cm^3), was 7.6×10^{-15} cm^2/molecule at 160 $^{\circ}$C. This was equal to the maximum collision diameter determined from the variation in transmission of the parent ion vs collision energy with the source at 160 $^{\circ}$C, as shown in Figure 24. The effective collision diameter for aldicarb nitrile was estimated to be 4.3×10^{-15} cm^2/molecule from the variation of the transmission efficiency vs collision energy, as shown in Figure 25. The fraction of parent ions fragmenting continues to increase with increasing collision energy in the case of aldicarb nitrile, while the yield for aldicarb levels off at approximately 12 eV (LAB). The effective collision diameter determined by this method for
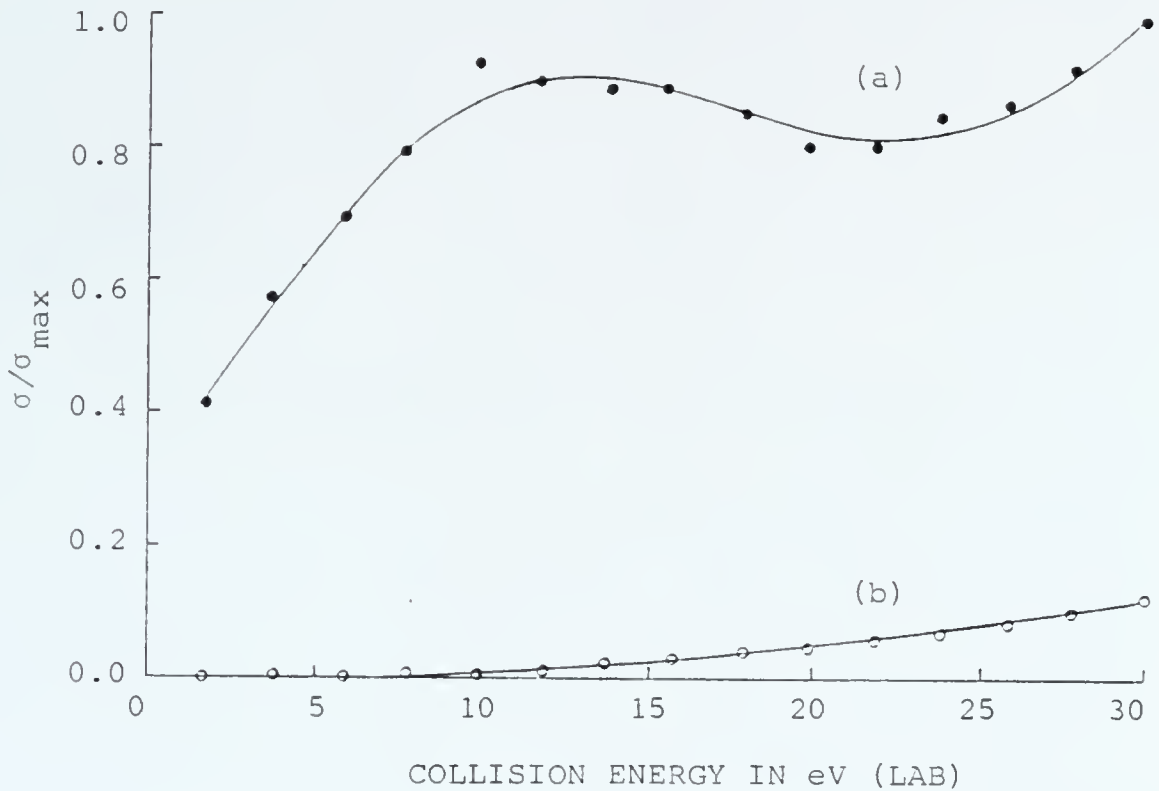
Figure 24. Yield variation (σ/σ_{max}) with collision energy for the protonated aldicarb molecular ion formed in methane CI incident on residual methane reagent gas in the collision cell vs the collision energy (LAB). The lower line (b) shows the m/z 89 ion's cross section for formation vs the maximum total cross section, while the upper line (a) shows the yield variation for the total cross section.
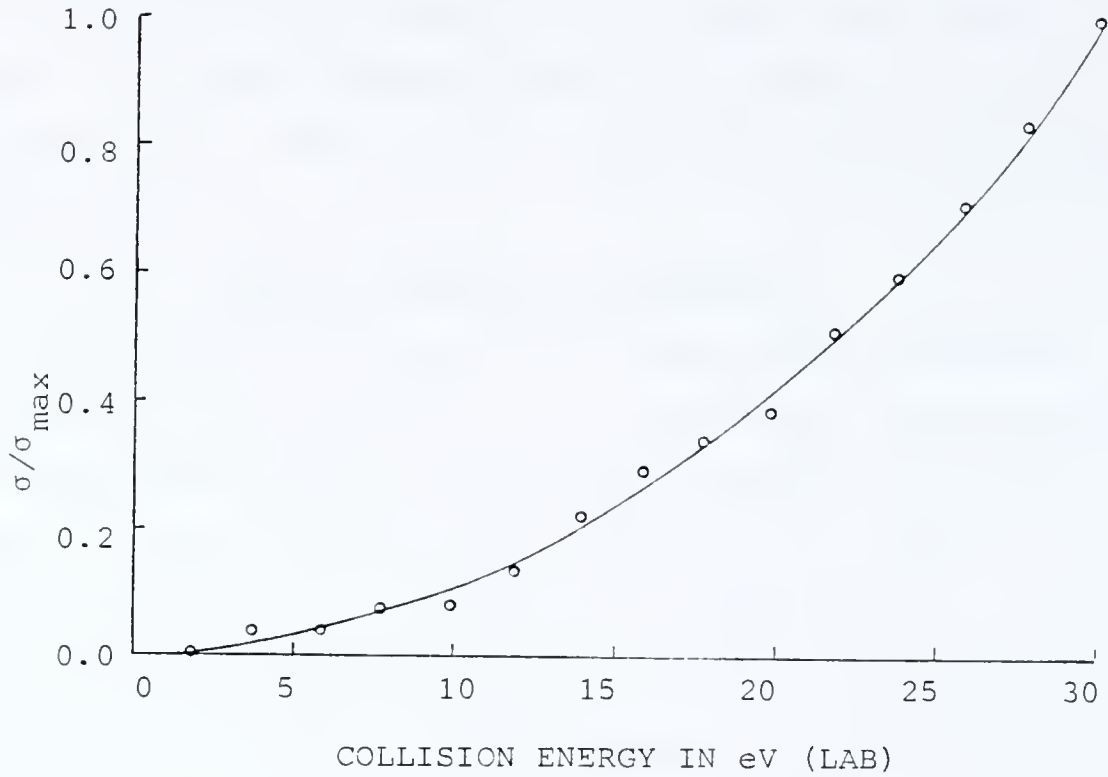
Figure 25.   Yield variation (σ/σ_{max}) with collision energy for the protonated aldicarb nitrile ion formed in methane CI incident on the residual methane reagent gas in the collision cell.

aldicarb nitrile is considerably greater than the 7.9 x 10^{-16} cm^2/molecule determined from the slope of ln(P/Po) vs target gas density with collision energy of 1.1 eV (LAB) for ions generated at a source temperature of 180 $^{\circ}$C. The similarity of the effective cross sections for CID for aldicarb reflects the greater extent which the aldicarb ions retain the internal energy gained in the source while the aldicarb nitrile ions have to a large extent lost the excess energy gained in the source.

Effect of Multiple Collisions

High target gas densities have been used to increase fragmentation of the parent ion in tandem mass spectrometry. At these higher target gas densities, multiple collisions occur, and the weighted average number of collisions encountered by an ion increases. In tandem mass spectrometry of ions with 3-10 keV energy, the daughter ion intensities observed in the CID spectrum have been shown to be consistent with an increase in energy deposition in the parent ion as the target gas density was increased (75). When the target gas density was increased so that the transmittance of the parent ion decreased from 35% to 8.5%, the resulting fragmentation due to grazing collisions appeared to increase the average energy in the fragmenting ions by a factor of 2.6 (75). Experiments in this study on the fragmentation of ions which encounter low energy collisions also indicate that there is an increase in the average amount of energy deposited in the parent ion as the

weighted average number of collisions per ion detected is increased. However, the change in the fragmentation pattern was much less than expected from the collision frequency.

In order to evaluate the effects of multiple collisions in the absence of significant metastable ion contributions, the CID fragmentation of cyclohexene was investigated. In Figure 26 the CID efficiency (sum of daughter ion intensities at a given collision pressure divided by the parent ion intensity in the absence of CID) and weighted average number of collisions per ion is shown vs the the precursor ion transmittance. The attenuation of the parent ion beam with increasing target gas density, and the corresponding increase in the daughter ion intensities, indicate that approximately 75% of the parent ions which encounter a single collision are scattered and lost. Thus, when multiple collisions occur, the number of ions detected is rapidly attenuated. For example, the signal intensity due to daughter ions which encounter one, two and three collisions can be estimated to be 25%, 6.25%, and 1.6% of the parent ion intensity, respectively. Thus, multiple collisions do result in greater fragmentation; however, the intensity of ions formed by multiple collisions is greatly attenuated. The experimentally determined values for CID efficiency vs the transmission efficiency of the parent ion are shown in Figure 26. A first order differential rate equations model (76) was used to calculate the expected CID efficiency vs the transmitted parent ion. The solid line
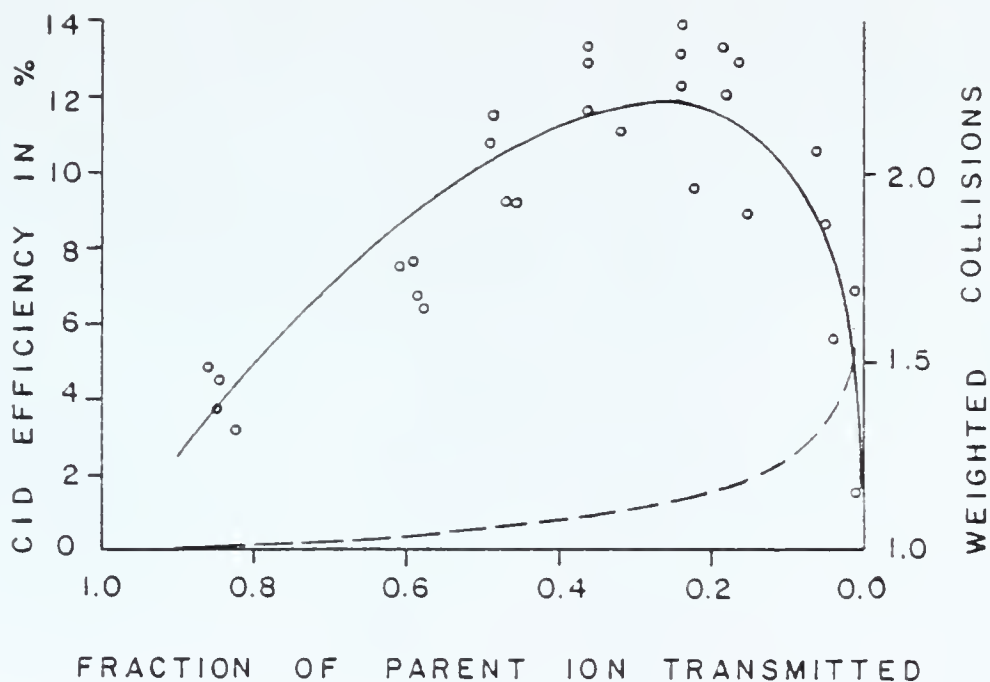
Figure 26. CID efficiency in % (solid line) vs the fraction of the precursor ion transmitted. The weighted average number of collisions encountered by ions which have at least one collision and are detected is shown by the dashed line. The data points, o, indicate the experimentally determined CID efficiency.

was computed for a CID cross section of 4.2×10^{-15} cm^2/molecule, 75% of the parent ions scattered in each collision and a daughter ion collision diameter 70% of that of the parent ion. The weighted average number of collisions per precursor ion (dashed line) is only 1.5 when the transmittance of the parent ion has decreased to 1% of its original intensity, if those ions which are lost are not counted in the weighted average. The maximum daughter ion intensity occurs when the target gas pressure reduces the parent ion intensity by 75%. The experimentally determined values for the CID efficiency are also shown. Calculations of the weighted number of collisions assuming mutually-exclusive collision probabilities (75) in tandem quadrupoles overestimates the contribution of multiple collisions to the observed fragmentation pattern, since the ions which encounter multiple collisions are more likely to be lost due to scattering. For example, assuming mutually-exclusive collision probabilities, the weighted average number of collisions for ions which encounter at least one collision is 1.9 when the parent ion transmittance is 35%, while for the same transmittance, the weighted average number of collisions for ions which encountered at least one collision and were collected is only 1.1.

In Table 18, the daughter ion intensities for CID of cyclohexene are shown for a collision energy of 14.8 eV with target gas pressures from 0.1 to 2.42 mtorr. As the target gas pressure is increased, ions with higher appearance

Table 18. Relative daughter ion intensities in %
with respect to the most intense daughter ion for
CID of cyclohexene vs target gas pressure with a
collision energy of 14.8 eV.

Pressure in mtorr	Relative daughter ion intensities		
	67+	54+	41+
0.1	100	38	-
0.3	100	46	-
0.5	100	62	12
0.75	100	50	9
1.05	100	53	9
1.25	100	52	7
1.75	100	57	10
2.42	100	42	7

potentials and those ions formed by fragmentation of
fragment ions are detected. The 41^+ ion is detected
when the target gas pressure reaches 0.5 mtorr. However,
further increases in the target gas pressure do not result
in a significant change in the daughter ion ratios. At the
higher target gas pressures, those ions formed in multiple
collisions are greatly attenuated by scattering.

Collision-Energy Effects

The collision energy can be increased to 30 eV in the
Finnigan TSQ45 mass spectrometer. At higher collision
energies, greater fragmentation occurs as fragmentation
pathways with higher threshold energies become accessible.
In Table 19, the variation in daughter ion intensities for
the cyclohexene molecular ion, 82^+, formed by EI is
shown as the collision energy is varied from 4.8 eV to 30 eV
in steps of 5 eV with a target gas pressure of 0.5 mtorr
nitrogen. As the collision energy is increased, the
relative intensity of the 54^+ ion with respect to the
67^+ ion increases. A threshold collision energy of 15
eV is necessary to form the 41^+ ion.

Internal-energy effects. The daughter ion ratios
for aldicarb do not show significant internal-energy effects
when daughter ions formed by unimolecular dissociation are
excluded. The ratio of $89^+/70^+$ daughter ions are
shown in Table 20 for collision energies from 1.8 eV to 30
eV with the parent ion fromed at 140 $^{\circ}$C and 180 $^{\circ}$C.
Even in the case of the CID of aldicarb, which undergoes

Table 19. Relative daughter ion intensities in %
with respect to the most intense daughter for CID
of cyclohexene vs collision energy with a target
gas pressure of 0.5 mtorr nitrogen.

Collision	Relative Daughter Ion Intensities		
Energy in eV	67+	54+	41+
4.9	100	10	-
9.8	100	33	-
14.8	100	62	12
19.8	100	71	20
24.8	100	86	38
30.0	87	100	36

Table 20. Ratio of the intensity of the daughter ion m/z 89 to the daughter ion m/z 70 formed on CID of aldicarb vs collision energy with nitrogen collision gas (pressure 1.4 mtorr).

Collision Energy eV (Lab)	Source Temperature in $^{\circ}C$	
	180	140
1.8	14.5	17.6
3.7	12.9	11.9
5.9	8.0	8.4
7.7	7.1	7.1
9.9	6.7	6.6
11.8	6.9	6.8
13.9	7.7	7.4
15.8	7.8	7.6
17.9	8.3	8.3
19.8	8.7	8.7
21.9	9.4	9.2
23.8	9.7	9.6
25.9	10.3	10.3
27.8	11.4	11.2
30.0	11.6	11.7

significant unimolecular dissociation, the CID spectra are
essentially equivalent with respect to daughter ion ratios
at these two source temperatures.

The transmittance of the parent ion as well as the
intensity of the daughter ions formed in CID are influenced
by the accelerating potential. In Table 21, the variation
in the daughter ion intensities for CID of the cyclohexene
82^+ ion formed in EI vs the target gas density is shown.
The parent ion intensities for the aldicarb nitrile MH^+
ion in positive methane CI were 0.816, 13.1, 73.6, 154, and
171 in thousands of counts, for accelerating potentials of
4.9, 9.9, 14.8, 19.8, and 24.8 eV, respectively. Higher
accelerating potentials both increase the intensity of the
parent ion for CID and provide sufficient collision energy
to form daughter ions. At collision energies below 15 eV
(LAB), with nitrogen as the target gas, the aldicarb nitrile
parent ion does not fragment significantly.

Target gases heavier than nitrogen such as argon result
in greater energy transfer in the collisions. The maximum
collision energy which can be transfered to the ion (77) is
given by:

$$E_{CM} = E_{LAB} \; m_g/(m_p + m_g) \tag{5-4}$$

where E_{CM} is the energy in center of mass coordinates,
E_{LAB} is the collision energy in the laboratory frame of
reference, m_g is the mass of the target gas and m_p
is the mass of the parent ion. The greater the mass of the

Table 21. Daughter ion intensities for the MH$^+$ m/z 116 ion of aldicarb nitrile formed in positive methane CI vs nitrogen target gas density (molecules/ion path length) with a path length of 15 cm.

Target gas Density	Pressure mtorr	Daughter Ion Intensities at Specified Collision Energies in eV				
		4.9	9.9	14.8	19.8	24.8
0.11	0.05	-	15	259	1790	4100
0.23	0.10	4	16	256	2300	5370
0.58	0.25	3	8	256	2820	7420
1.39	0.60	3	4	256	2690	6850
2.4	1.05	-	-	40	1790	4900
5.3	2.3	-	-	-	7	156

target gas, the greater the energy transfered in each collision. In Table 22 the daughter ion intensities for CID of the 82^+ ion formed by EI ionization of cyclohexene are shown with nitrogen and with argon vs the collision energy in the laboratory frame of reference. The collision energy necessary to fragment cyclohexene to form the 39^+ and 41^+ daughter ions occurs with lower accelerating potentials when argon is the target gas, as predicted by equation 5-4. Collisions with heavier target gases and greater collision energies result in greater fragmentation, and increase the information available in CID spectra.

Library matching capabilities. The CID spectrum of the cyclohexene 82^+ ion is shown in Figure 27 (a-h) determined at 30 eV with nitrogen target gas pressures ranging from 0.1 to 2.7 mtorr. For comparison, the National Bureau of Standards EI library spectrum for cyclohexene is shown in Figure 27 (i). Currently there are not any commercially available CID library spectra available for the Finnigan TSQ45 mass spectrometer data system. However, in order to demonstrate the feasability of identifying unknowns by matching CID spectra, the CID spectrum for cyclohexene was evaluated by the INCOS library matching algorithm. The INCOS data system matched the CID spectrum for cyclohexene's 82^+ parent ion with the EI spectrum of cyclohexene from approximately 30 thousand compounds in the reference library.

Table 22. Daughter ion intensities in counts for CID of the cyclohexene 82^+ parent ion vs collision energy in the laboratory frame of reference.

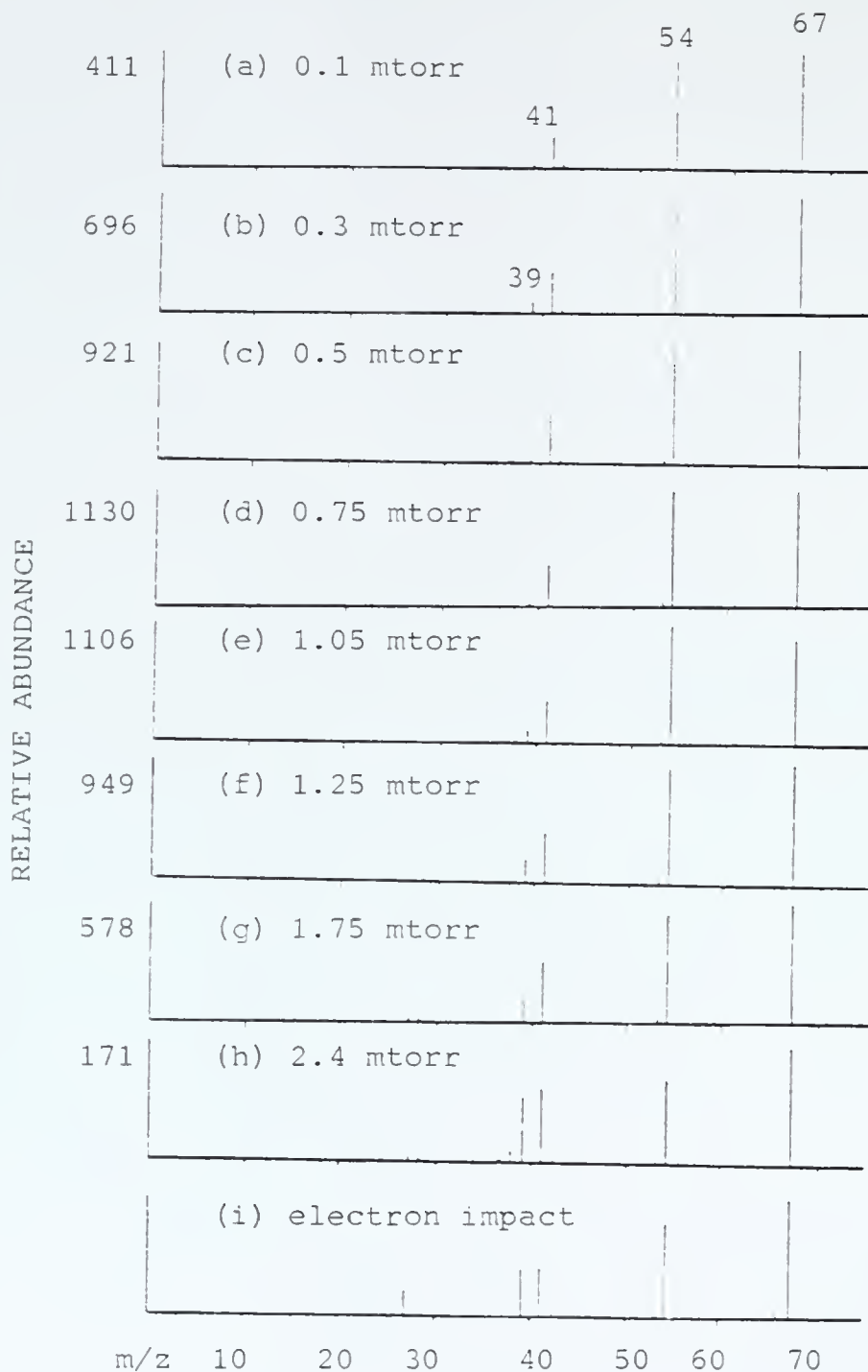| Collision Energy in eV	Argon at 0.7 mtorr Daughter Ion Intensities				Nitrogen at 0.7 mtorr Daughter Ion Intensities			
	39+	41+	54+	67+	39+	41+	54+	67+
4.9	-	-	318	1480	-	-	209	1590
9.9	-	144	865	1550	-	-	805	2320
14.9	-	244	1078	1070	-	211	1150	2290
19.8	79	275	919	799	-	349	1480	1420
24.8	172	317	788	696	-	444	1090	1280
30.0	245	308	493	627	73	361	1140	1100

Figure 27. Effect of nitrogen gas pressure in the collision cell on CID spectra. The daughter spectra obtained for CID of the cyclohexene m/z 82 ion with nitrogen collision gas pressures from 0.1 mtorr to 2.4 mtorr are shown in (a) through (h) and can be compared with the electron impact spectrum for cyclohexene shown in (i).

The intensity of the 39^+ ion relative to the 41^+ ion increases slowly, and does not become comparable to that in the EI spectra until the target gas pressure is 2.7 mtorr, suggesting that it is formed only by multiple collisions. At this pressure, the daughter ion intensities have been reduced by a factor of about 10 from the maximum intensity observed when the collision pressure was 0.75 mtorr. For the identification of trace components, CID library spectra should be made at lower target gas pressures to avoid this loss in sensitivity.

Collision diameter vs target gas. The effective collision diameter for CID of cyclohexene with nitrogen and argon target gases is shown in Table 23. Cyclohexene has a collision diameter 36% larger with argon than with nitrogen. In addition, the collision diameter is not as strongly dependent on collision energy with argon as is the case with nitrogen. The increase in collision diameter for cyclohexene with the heavier target gas also results in an increase in the fraction of ions which are lost due to scattering. Approximately 90% of the parent ions were lost due to scattering with argon, while only approximately 75% were lost when nitrogen was used as the target gas at approximately the same pressure.

Conclusion

The probability of matching CID library spectra with an unknown CID spectrum is increased as the degree of fragmentation in the CID spectra is increased. Thus, higher

Table 23. Effective collision diameter vs
collision energy for nitrogen and argon
target gases.

Collision Energy in eV	Nitrogen $cm^2 \times 10^{-16}$	Argon $cm^2 \times 10^{-16}$
4.8	17.5	43.1
9.8	28.1	50.9
14.8	35.0	53.5
19.8	39.3	54.0
24.8	40.2	55.9
30.0	41.9	56.9

collisions energies and heavier target gases are
more suitable for the development of library spectra. The
Finnigan TSQ45 mass spectrometer is currently limited to a
maximum collision energy of 30 eV (LAB). Increasing the
maximum available collision energy to 100 eV would be likely
to increase fragmentation, and therefore would be useful for
the development of CID library spectra. Although argon,
when used as the target gas, results in greater
fragmentation (which improves the informing power of the
spectrum), there is also greater scattering of the parent
ions, so that sensitivity is decreased by approximately a
factor of 2.

The internal energy of the parent ions does not appear
to significantly influence the CID spectra, possibly due to
the loss of the more energetic ions prior to reaching the
collision cell. However, CID spectra of parent ions
generated by different ionization processes need to be
evaluated. For example, the internal energy of parent ions
generated by fast atom bombardment may greatly differ from
that of parent ions generated by electron impact or chemical
ionization, and different CID spectra might be observed.

The ability of selected reaction monitoring (SRM) to
discriminate between the analyte and the background is best
accomplished when a minimum of fragmentation of the parent
occurs. Thus, SRM will be most effective when the CID
conditions are selected so that the minimum energy necessary
to fragment the parent ion is employed. Nitrogen could be

used as the target gas in most applications, while the optimum collision energy necessary to bring about fragmentation would have to be experimentally determined. The optimum target gas pressure will be that pressure which attenuates the parent ion signal by approximately 75%, when SRM for a daughter ion formed in a single collision from the parent ion is used.

CHAPTER 6
CONCLUSIONS AND FUTURE WORK

Summary of Results

In Chapter 4, the increase in the speed of analysis was demonstrated for short capillary columns operated with the outlet connected to a vacuum. Approximately 6 samples per hour could be analyzed when the 2 m capillary column was used. Short capillary columns not only increase the speed of analysis, but also make possible the determination of thermally labile compounds such as the pesticide aldicarb. The analysis for the intact molecule greatly improves the reliability of the analysis. Prior to the development of this technique, all GC methods had determined aldicarb by quantitating aldicarb nitrile formed from aldicarb in the injection port. If aldicarb nitrile was only formed by thermal degradation of aldicarb in the injection port, then the analysis might be accurate. However, in the degradation experiments (Chapter 2), it was shown that aldicarb can, in the presence of microorganisms anaerobically degrade to aldicarb nitrile. Since aldicarb nitrile is likely to be present in environmental samples, the standard GC methods employed must employ a florisil clean-up procedure or risk a positive interference.

The increase in the speed of analysis that occurs with capillary columns when the outlet is connected to a vacuum was discussed in Chapter 3 in relationship to the fundamental gas chromatographic equations. Analysis time was shown to decrease, not only due to the smaller retention volume with short capillary columns, but also due to the increase in the optimum gas velocity. The increase in sensitivity obtained with these columns is advantageous for analysis by MS/MS, while the added selectivity of MS/MS compensates for the chromatographic resolution lost with shorter columns.

The apparent decrease in the HETP observed on dividing capillary columns was also explained. Since greater inlet pressures are necessary for longer columns compared to shorter columns for the same carrier gas velocity, the gas diffusion coefficient for the longer column will be less. The mass-transfer term in the Golay plot is inversely proportional to the gas diffusion coefficient. Thus, as the column length is reduced, the lower column pressure results in a decrease in the slope of the Golay plot, and the HETP decreases with the column length when measured in the region beyond the optimum gas velocity.

The effects of instrumental parameters on CID spectra were evaluated in Chapter 5. Due to the loss of the ion's internal energy by collisions in the source, radiative losses, and unimolecular dissociation prior to reaching the collision cell, CID spectra do not appear to be greatly

influenced by the source temperature. Multiple collisions were found to result in greater fragmentation of the parent ion. However, since approximately 75% of the ions are lost in each collision due to scattering, the greater fragmentation that occurs at higher target gas densities results in a considerable loss in sensitivity. Higher collision energies, rather than higher target gas densities, appear to offer a more useful means for generating CID library spectra.

Future Work

On-column Injection

Rapid analysis for the less-volatile oxidation by-products of aldicarb was not possible by GC/MS, due to thermal instability. However, future work may involve the introduction of the sample by on-column injection. This method of sample introduction should avoid the need to expose the analytes to high temperatures in the injection port, and a wider range of compounds could be determined. Another difficulty associated with relatively cool injection port temperatures is the likelihood for differential introduction of analytes into the column due to variations in their volatilities. This problem would also be avoided by on-column injection.

Chemical Ionization

The precision of the analysis for aldicarb was found to be influenced by the fluctuation in the CI reagent gas pressure. Feedback control of the CI reagent gas pressure

would counteract the slow drifts observed in the CI signal. Since the CI pressure is already converted to an analog signal by the Pirrani gauge, computer control would require the addition of an analog to-digital converter, a microcomputer and interface, a digital to analog converter, and an analog driven valve operator. This system would be expected to improve the precision possible with CI to that now obtainable with EI.

Tandem Mass Spectrometry

Microwave enhanced CID. A difficulty encountered on occasion in MS/MS is that some ions do not fragment readily. Microwave enhanced/CID (MW/CID) could provide an additional means for introducing energy into the ions immediately prior to their entering the collision cell. The large dipole moment of the ions could result in a very large cross section for the absorption of microwave energy. For the MW/CID technique to be successful, the ions will have to absorb approximately 5 to 10 quanta of microwave energy during their exposure. This is quite feasible, since the ions will experience thousands of microwave cycles while travelling a distance of only a few mm. The additional internal energy is expected to cause many of the ions which are already in a highly energetic state to fragment, and these fragment ions will then be available for further fragmentation. The MW/CID spectrum is expected to have a greater information content due to the formation of a greater variety of more abundant ions.

LITERATURE CITED

1. "Growers ready to use Temik as ban expires" Gainesville Sun, Bl, January 2, 1984.

2. Guerrera, A.A., J. Am. Water Works Assoc., 73(4), 190 (1981).

3. Andrawes, N.R.; Bagley, W.P.; Herrett, R.A., J. Agric. Food Chem., 19(4), 727 (1971).

4. Richey, F.A. Jr.; Bartley, W.J.; Sheets, K.P., J. Agric. Food Chem., 25, 47 (1977).

5. Galoux, M.; Van Damme; J.-C.; Bernes, A.; Potvin, J., J. Chromatogr., 177, 245 (1979).

6. Andrawes, N.R.; Bagley, W.P.; Herrett, R.A., J. Agric. Food Chem., 19(4), 731 (1971).

7. Rouchaud, J.; Moons, C.; Meyer, J.A., Pestic. Sci., 11, 483 (1980).

8. Knaak, J.B.; Tallant, M.J.; Sullivan, L.J., J. Agric. Food Chem., 14, 573 (1966).

9. Metcalf, R.L.; Fukuto, T.R.; Collins, C.; Borck, K.; Burk, J.; Reynolds, H.T.; Osman, M.F., J. Agric. Food Chem., 14(6), 579 (1966).

10. Bartley, W.J.; Andrawes, N.R.; Chancey, E.L.; Bagley, W.P.; Spurr, H.W., J. Agric. Food Chem., 18, 446 (1970).

11. Jones, A.S., J. Agric. Food Chem., 24(1), 115 (1976).

12. Wright, L.H.; Jackson, M.D.; Lewis, R.G., Bull. Environ. Contam. Toxicol., 28, 740 (1982).

13. Sparacino, C.M.; Hines, J.M., J. Chromatogr. Sci., 14, 549 (1976).

14. Moye, H.A.; Scherer, S.J.; St. John, P.A., Anal. Lett., 10, 1049 (1977).

15. Krause, R.T., J. Chromatogr., 185, 615 (1979).

16. Muszkat, L.; Aharonson, N., Int. J. Mass Spectrom. Ion Phys., 48, 323 (1983).

17. Moye, H.A., J. Agric. Food Chem., 23(3), 415 (1975).

18. Hishta, C.; Messerly, J.P.; Reschke, R.F.; Fredericks, D.H.; Cooke, W.D., Anal. Chem., 32, 880 (1960).

19. Gouw, T.H.; Whittemore, I.M.; Jentoft, R.E., Anal. Chem., 42, 256 (1977).

20. Gaspar, G.; Arpino, P.; Guichon, G., J. Chromatog., 15, 256 (1977).

21. Gaspar, G.; Olivo, J.; Guichon, G., Chromatographia, 11, 321 (1978).

22. Hatch, F.W.; Parrish, M.E., Anal. Chem., 50, 1164 (1978).

23. Rose, K., Bairoch, A.; Offord, R.E., J. Chromatog., 268, 197 (1983).

24. Schutjes, C.P.M.; Cramers, C.A.; Vidal-Madjar, C.; Guichon, G., J. Chromatog., 279, 269 (1983).

25. Yost, R.A.; Fetterolf, D.D.; Hass, J.R.; Harvan, D.J.; Weston, A.F.; Skotnicki, P.A.; Simon, N.A., Anal. Chem., 56(12), 2223 (1984).

26. Riva, M.; Carisano, A., J. Chromatogr., 42, 464 (1969).

27. Trehy, M.L.; Yost, R.A., Anal. Chem., 56, 1281 (1984).

28. United States Food and Drug Administration Pesticide Analytical Manual, Volume II, Pesticide Reg. Section 120.269 Aldicarb, GPO, Washington, DC (1970).

29. Cheng, M.T.; Kruppa, G.H.; McLafferty, F.W.; Cooper, D.A., Anal. Chem., 54, 2204 (1982).

30. Bozorgzadeh, M.H.; Morgan, R.P.; Beynon, J.H., Analyst, 103, 613 (1978).

31. Cheng, M.T.; Kruppa, G.H.; McLafferty, F.W.; Cooper, D.A., Anal. Chem., 54, 2204 (1982)

32. Perchalski, R.J.; Yost, R.A.; Wilder, B.J., Anal. Chem., 54(9), 1466 (1982).

33. Schlunger, U.P.; Hirter, P.; von Felten, H., Helv. Chim. Acta., 59, 406 (1976).

34. Hunt, D.F.; Bone, W.M.; Shabanowitz, J.; Rhodes, J.; Ballard, J.M., Anal. Chem., 53, 1704 (1981).

35. Hunt, D.F.; Buko, A.M.; Ballard, J.M.; Shabanowitz, J.; Giordani, A.B., Biomed. Mass Spectrom., 8, 397 (1981).

36. Bradley, C.V.; Howe, I.; Beynon, J.H., Biomed. Mass Spectrom., 8, 85 (1981).

37. van de Sande, C.C.; McLafferty, F.W., J. Am. Chem. Soc., 97, 4617 (1975).

38. Rollgen, F.W.; Borchers, F.; Giessmann, U.; Levsen, K., Org. Mass Spectrom., 12, 541 (1977).

39. Levsen, K., Org. Mass Spectrom., 10, 43 (1975).

40. Dawson, P.H.; Wing-Fung Sun, Int. J. Mass Spectrom. Ion Processes, 55, 155 (1984).

41. Shushan, B.; Fulford, J.E.; Thomson, B.A.; Tanner, S.D. Davidson, W.R. American Society for Mass Spectrometry Extended Abstracts, 32, 7 (1984).

42. McLafferty, F.W.; Hirota, A.; Barbalas, M.P., Org. Mass Spectrom., 15, 327 (1980).

43. McLafferty, F.W.; Kornfield, R.; Haddon, W.F.; Levsen, K.; Sahai, I.; Bente III, P.F.; Tsai, S.C.; Schuddenage, H.D.R., J. Am. Chem. Soc., 95, 3886 (1973).

44. Dawson, P.H.; French, J.B.; Buckley, J.A.; Douglas, D.J.; Simmons, D., Org. Mass Spectrom., 17 205 (1982).

45. Dawson, P.H.; French, J.B.; Buckley, J.A.; Douglas, D.J.; Simmons, D., Org. Mass Spectrom., 17, 212 (1982).

46. Dawson, P.H.; Douglas, D.J., Int. J. Mass Spectrom. Ion Phys., 47, 121 (1983).

47. Fetterolf, D.D.; Yost, R.A., Int. J. Mass Spectrom. Ion Phys., 44, 37 (1982).

48. Owen, W.F.; Stuckey, D.C.; Healey Jr., J.B.; Young, L.Y.; McCarty, P.L., Water Research, 13, 485 (1979).

49. Union Carbide, "Answers to recent questions concerning the use of TEMIK aldicarb and its effect on health and the environment" (flier). Union Carbide, South Charleston, West Virginia (1983).

50. Giddings, J.C., Anal. Chem., 34, 314 (1962).

51. Golay, M.J.E., Nature, 182, 1146 (1958).

52. Desty, D.H., Nature, 181, 604 (1958).

53. Daniels, F.; Alberty, R.A., Physical Chemistry. John Wiley & Sons, Inc., New York (1966).

54. Desty, D.H.; Goldup, A.; Whyman, B.H.F., J. Inst. Petrol., 45, 287 (1959).

55. Holland, J.F.; Enke, C.G.; Allison, J.; Stults, J.T.; Pinkston, J.D.; Newcombe, B.; Watson, J.T., Anal. Chem., 55, 997A (1983).

56. Harris, W.E., J. Chromatogr. Sci., 11, 184 (1973).

57. Grob, K.; Grob, G., Chromatographia, 5, 3 (1972).

58. Grob Jr., K., J. Chromatog., 253, 17 (1982).

59. Cramers, C.A.; Scherpenzeel, G.J.; Leclercq, P.A., J. Chromatog., 203, 207 (1981).

60. James, A.T.; Martin, A.J.P., J. Biochem., 50, 679 (1952).

61. Scott, R.P.W., in Gas Chromatography, ed. R.P.W. Scott, Butterworth, London (1960).

62. Grob, K.; Grob, G., J. Chromatog. Sci., 7, 515 (1969).

63. Yabumoto, K.; Vandenheuvel, W.J.A., J. Chromatog., 140, 197 (1977).

64. Gudzinowicz, B.J., Gudzinwicz, M.J., Martin, H.F. Fundamentals of Integrated GC-MS Part I: Gas Chromatography. Marcel Dekker, Inc., New York (1976).

65. Yost, R.A., Spectra, 9(4), 5 (1983).

66. Payne, L.K.; Stansbury Jr., H.A.; Weiden, M.H.J., J. Agric. Food Chem., (1966), 14(4), 356-365.

67. Millard, B.J., Quantitative Mass Spectrometry. Heydon & Son Ltd., London (1978).
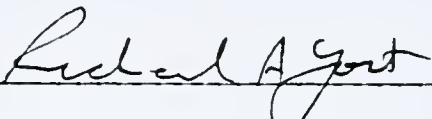
68. Freund, J.E. Modern Elementary Statistics. Prentice-Hall, Inc., Englewood Cliffs, New Jersey (1967).

69. NASA Technical Note TND 5285 by Summers, R.L., Lewis Research Center, National Aeronautics and Space Administration.

70. Todd, P.J.; McLafferty, F.W., in Tandem Mass Spectrometry, ed. F.W. McLafferty, Wiley Interscience, New York (1983).

71. Dawson, P.H.; French, J.B.; Buckley, J.A.; Douglas, D.J.; Simmons, D., Org. Mass Spectrom., 17(5), 212 (1982).

72. Meot-Ner, M.; Field, F.H., J. Amer. Chem. Soc., 95, 7207 (1973).

73. Denbigh, K.G., Trans. Faraday Soc., 40, 352 (1944).

74. Cooks, R.G.; Beynon, J.H.; Caprioli, R.M.; Lester, G.R., Metastable Ions. Elsevier Scientific Publishing Co., New York (1973).

75. Todd, P.J.; McLafferty, F.W., Int. J. Mass Spectrom. Ion Phys. 38, 371 (1981).

76. Ouwerkerk, C.E.D.; McLuckey, S.A.; Kistemaker, P.G.; Boerboom, A.J.H., Int. J. Mass Spectrom. Ion Phys., 56, 11 (1984).

77. Bernstein, R.B.; Levine, R.D., Molecular Reaction Dynamics. Clarendon Press, Oxford (1974).

BIOGRAPHICAL SKETCH

Michael L. Trehy was born on January 10, 1948, in Lakeland, Florida. He attended elementary and high school in St. Petersburg, Florida. He received his B.S. in chemistry from Eckerd College in 1970, while participating in the intercollegiate basketball program. While working for the City of West Palm Beach Water Department, he completed his M.S. in chemistry from Florida Atlantic University under the supervision of Theodore I. Bieber on "The Formation of Dihaloacetonitriles by Chlorination of Natural Water." In 1984, while working under the direction of Richard A. Yost, he received his Ph.D. with a specialization in analytical chemistry from the University of Florida.
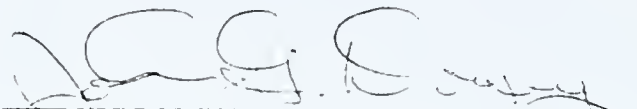
He married Nancy L. Breier on December 27, 1968, and they have two children, Daniel and Benjamin.

I certify that I have read this study and that in my
opinion it conforms to acceptable standards of scholarly
presentation and is fully adequate, in scope and quality,
as a dissertation for the degree of Doctor of Philosophy.
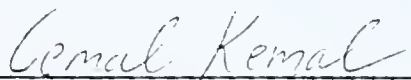

Richard A. Yost

Richard A. Yost, Chairman
Associate Professor of Chemistry

I certify that I have read this study and that in my
opinion it conforms to acceptable standards of scholarly
presentation and is fully adequate, in scope and quality,
as a dissertation for the degree of Doctor of Philosophy.

John G. Dorsey

John G. Dorsey
Assistant Professor of Chemistry

I certify that I have read this study and that in my
opinion it conforms to acceptable standards of scholarly
presentation and is fully adequate, in scope and quality,
as a dissertation for the degree of Doctor of Philosophy.

Cemal Kemal

Cemal Kemal
Assistant Professor of Chemistry

I certify that I have read this study and that in my
opinion it conforms to acceptable standards of scholarly
presentation and is fully adequate, in scope and quality,
as a dissertation for the degree of Doctor of Philosophy.

J. Edward Singley

J. Edward Singley
Professor Environmental
Engineering Sciences

I certify that I have read this study and that in my opinion it conforms to acceptable standards of scholarly presentation and is fully adequate, in scope and quality, as a dissertation for the degree of Doctor of Philosophy.

Anna Brajter-Toth
Assistant Professor of Chemistry

This dissertation was submitted to the Graduate Faculty of the Department of Chemistry in the College of Liberal Arts and Sciences and to the Graduate School, and was accepted as partial fulfillment of the requirements for the degree of Doctor of Philosophy.

December, 1984

Dean for Graduate Studies and Research